RÉPUBLIQUE FRANÇAISE
Liberté
Égalité
Fraternité

ONERA
THE FRENCH AEROSPACE LAB

TECHNICAL REPORT

THERMOCITY Project

Authors : A. Michel ; L. Roupioz

OPTICS AND ASSOCIATED TECHNIQUES DEPARTMENT

RT 1/31221 DOTA - November 2021

ref: 4500067714

OPTICS AND ASSOCIATED TECHNIQUES DEPARTMENT

Technical Report N° RT 1/31221 DOTA

ref: 4500067714

November 2021

THERMOCITY Project

Written by :
A. Michel
L. Roupioz

Verified by :
X. Briottet, Chargé de Mission Télédétection Optique Passive et Active

Approved by :
Director
Optics and Associated Techniques Department
A. Roblin

BP 4025 - 2, avenue Edouard Belin
31055 Toulouse Cedex - FRANCE
Tél. : 05 62 25 25 25 - Fax : 05 62 25 25 50

ONERA
THE FRENCH AEROSPACE LAB

Abstract :
The THERMOCITY project, led by CNES/Eolab and federating ONERA, MétéoFrance and CSTB as well as the metropolises of Montpellier, Strasbourg and Toulouse, aims at studying urban heat islands and heat loss in the current context of climate change through the development of an urban thermography analysis tool based on satellite images. In the framework of this project, the task of ONERA is to provide LST (Land Surface Temperature) maps from available satellite imagery acquired in the thermal infrared (TIR) at native and enhanced spatial resolution domain using state-of-the-art methods developed specifically for urban areas. This work consisted in identifying and improving existing TIR spatial data products over five study areas by generating updated LST maps from ASTER and ECOSTRESS images processed with a TES algorithm accounting for the specificities of urban materials. Along with the updated LST maps, a Quality Assessment (QA) layer is produced based on current knowledge on LST estimation over urban areas to inform users on the reliability of the retrieved values and facilitate data interpretations. For ASTER products, LST maps at a higher resolution are also generated based on validated empirical disaggregation methods. This report constitutes the technical synthesis of the first phase of the THERMOCITY project.

Key words :
THERMAL ; SCO ; URBAN SETTINGS ; SATELLITE

BP 4025 - 2, avenue Edouard Belin
31055 Toulouse Cedex - FRANCE
Tél. : 05 62 25 25 25 - Fax : 05 62 25 25 50

BP 4025 - 2, avenue Edouard Belin
31055 Toulouse Cedex - FRANCE
Tél. : 05 62 25 25 25 - Fax : 05 62 25 25 50

TABLE DES MATIERES

1. INTRODUCTION

The THERMOCITY project, led by CNES/Eolab and federating ONERA, MétéoFrance and CSTB as well as the metropolises of Montpellier, Strasbourg and Toulouse, aims at studying urban heat islands and heat loss in the current context of climate change through the development of an urban thermography analysis tool based on satellite images.

In the framework of this project, the task of ONERA is to provide LST (Land Surface Temperature) maps from available satellite imagery acquired in the thermal infrared (TIR) at native and enhanced spatial resolution domain using state-of-the-art methods developed specifically for urban areas. This work consisted in identifying and improving existing TIR spatial data products over five study areas by generating updated LST maps from ASTER and ECOSTRESS images processed with a TES (Temperature-Emissivity Separation) algorithm [6] accounting for the specificities of urban materials. Along with the updated LST maps, a Quality Assessment (QA) layer is produced based on current knowledge on LST estimation over urban areas to inform users on the reliability of the retrieved values and facilitate data interpretations. For ASTER products, LST maps at a higher resolution are also generated based on validated empirical disaggregation methods. This report constitutes the technical synthesis of the first phase of the THERMOCITY project.

The subsequent sections of this report provide more details on the implementation of the methods and the produced THERMOCITY TIR data. Section 2 presents the study areas and satellite missions selected for this project. Section 3 describes the methods used to estimate LST and disaggregated products and Section 4 shows and evaluates the generated products. Finally, Section 5 provides some conclusions and perspectives. A bibliography is available at the end of the report.

Appendices A, B, and C provide additional details of the products for each date and study areas.

2. DATA

2.1. Study areas

Five metropolises have been identified:

- Aix-Marseille located in the South of France along the Mediterranean Sea: 92 municipalities over 3173 km^2, 1 895 600 inhabitants (2018)
- Montpellier, located also along the Southern coast: 31 municipalities, 422 km^2, 457 839 inhabitants (2018)
- Paris: 131 municipalities over 814 km², 7 026 765 inhabitants (2016)
- Strasbourg, in the North-eastern part of France, between the German border and the Vosges mountains: 33 municipalities over 337 km^2, 500 510 inhabitants (2018)
- Toulouse in the South-western part of France: 37 municipalities over 460 km^2, 747 000 inhabitants (2014)

These five metropolises are very diverse regarding their climate, number of inhabitants, population density, local economy or historical development. To get a global picture of the urban areas and its rural surroundings required to analyse the SUHI (Surface Urban Heat Island) effect, 100 km square study areas centered on the city of interest were considered for each metropolis. They are illustrated on Figure 1 showing rural areas and urban areas with Sentinel-2 data.

Among those five metropolises, three are involved in this project: Montpellier, Strasbourg and Toulouse.

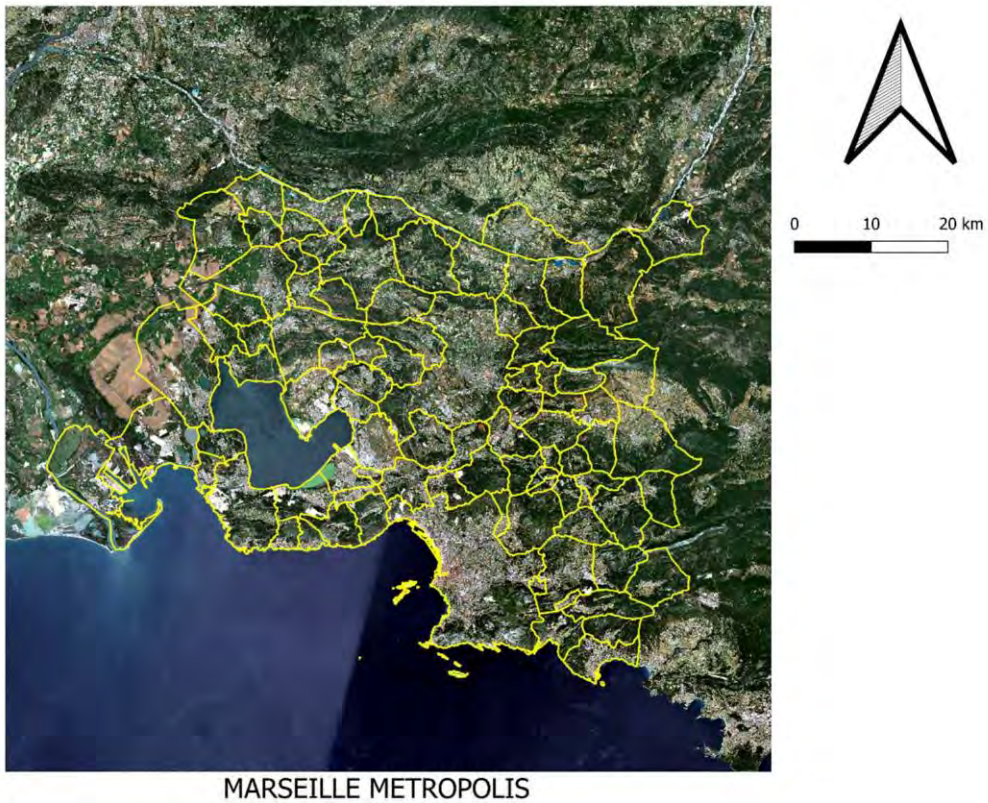

MARSEILLE METROPOLIS

MONTPELLIER METROPOLIS

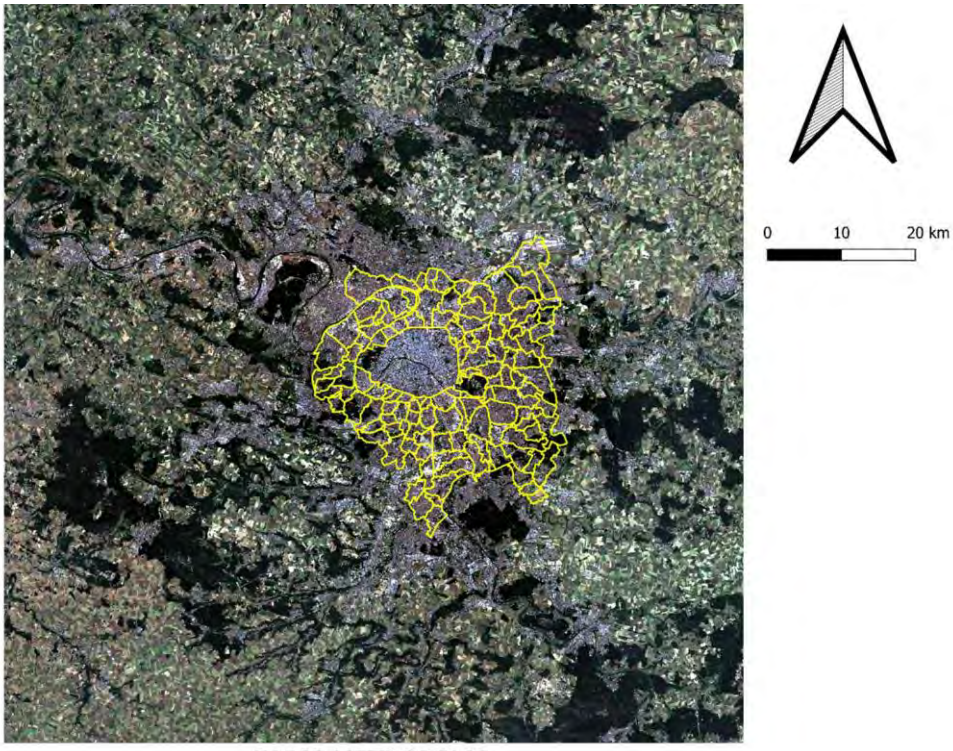

PARIS METROPOLIS

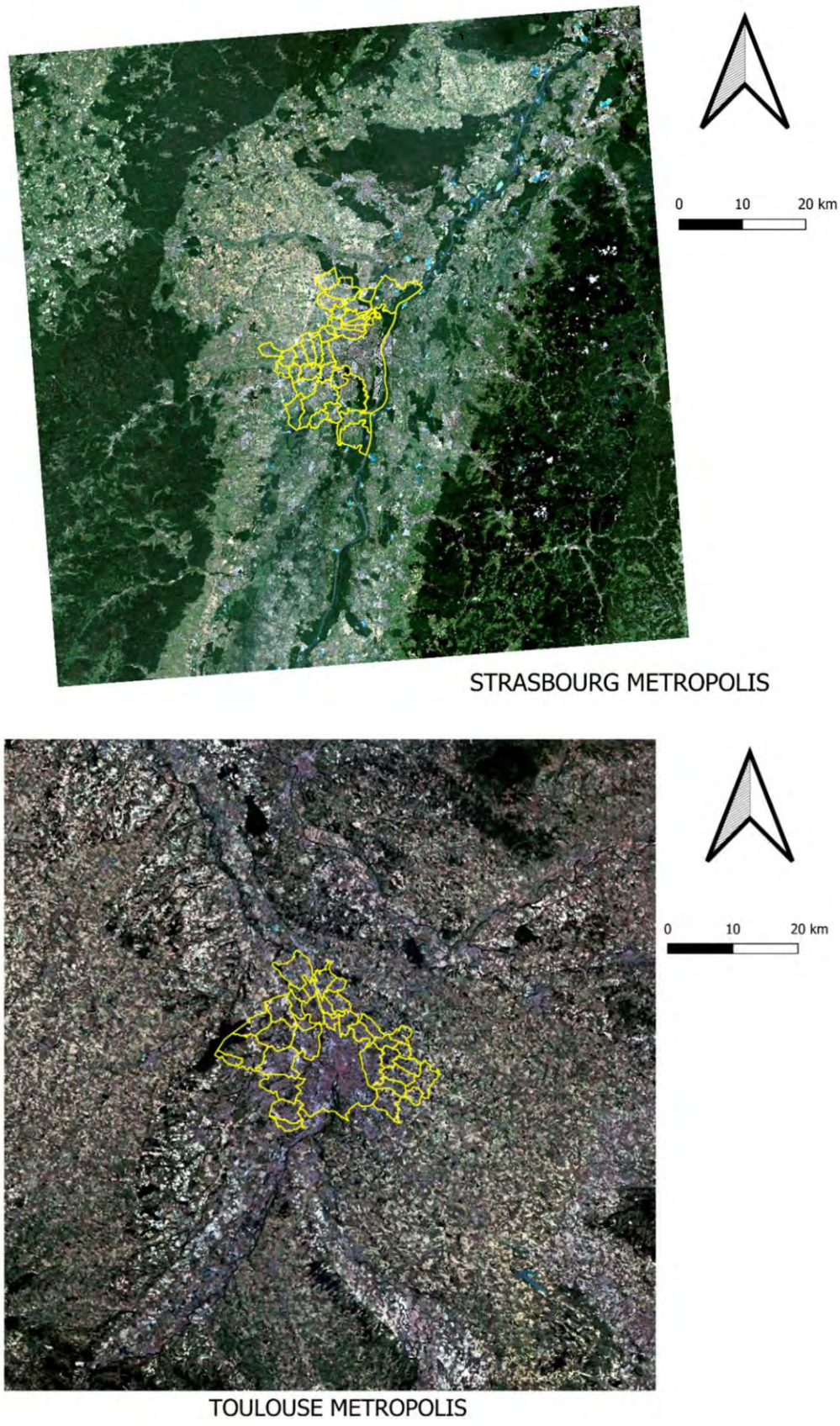

Figure 1: THERMOCITY study areas: Aix-Marseille, Montpellier, Paris, Strasbourg and Toulouse

2.2. Satellite data: ASTER and ECOSTRESS

Currently, two spaceborne sensors provide TIR data in at least three thermal bands which allows to estimate LST with a decametric spatial resolution using the TES algorithm: ASTER and ECOSTRESS. Their main characteristics, i.e. the spatial, temporal and spectral resolutions in the TIR are given in Table 1.

	ASTER	**ECOSTRESS**
Spatial resolution in the TIR (m)	90	70
Revisit	Heliocentric orbit : 15 days	ISS Orbit (not heliocentric)
Number of TIR spectral bands	5	5 / 3 (since 2018)
Website (for more information)	asterweb.jpl.nasa.gov	ecostress.jpl.nasa.gov

Table 1: Main characteristics for the TIR sensors on-board ASTER and ESCOSTRESS

Among the satellite images available via the NASA data portals, the data used in THERMOCITY were selected based on several criteria according to their availability:

- Pairs of day and night-time images
- One pair acquired in winter
- One pair acquired in summer
- No clouds
- Close dates between study areas for comparison purposes

Further details on each satellite mission, its products and imagery selection are given in the following subsections.

2.2.1. ASTER

ASTER (Advanced Spaceborne Thermal Emission and Reflection Radiometer) is a NASA satellite multispectral mission launched in 1999. The spatial resolution is 90 meters in the TIR with five spectral bands, 30 meters in the SWIR with 6 spectral bands and 15 meters in the VNIR with 3 spectral bands. The SWIR sensor has been out of service since 2008. ASTER is jointly managed by the United States (US) and Japan: JPL (Jet Propulsion Laboratory) and J-Spacesystems respectively. The Science Team has a US and a Japanese component gathering 40 researchers. Different levels of products are generated and are freely available.

For ASTER, 3 to 5 dates have been selected over each study area following the aforementioned criteria. Several data products, listed below, were downloaded from the NASA data portal service for processing and comparison. The links for further information on each product are also provided.

- AST_05: LSE (Land Surface Emissivity) in the five TIR bands : https://lpdaac.usgs.gov/products/ast_05v003/
- AST_07XT: VNIR (3 bands) and SWIR (6 bands, when available) reflectance: https://lpdaac.usgs.gov/products/ast_07xtv003/
- AST_08: LST : https://lpdaac.usgs.gov/products/ast_08v003/
- AST_09T: TIR surface radiance (5 bands), also called the BOA (Bottom of Atmosphere) radiance and the sky irradiance in the five TIR bands: https://lpdaac.usgs.gov/products/ast_09tv003/

The selected dates and products are summarized in Table 2. The acquisitions times are in UTC (Coordinated Universal Time).

Study Area	Date	Acquisition time (UTC)	AST_05	AST_07XT	AST_08	AST_09T
Aix-Marseille	12/08/2003	10:40:31	x	x	x	x
	30/01/2005	10:34:25	x	x	x	x
	14/01/2019	21:35:51	x		x	x
Montpellier	02/11/2007	10:47:02	x	x	x	x
	29/08/2015	10:42:08	x	x	x	x
	29/08/2015	21:49:08	x		x	x
	01/11/2015	21:48:48	x		x	x
Paris	01/08/2003	10:57:21	x	x	x	x
	22/10/2004	10:57:11	x	x	x	x
	01/11/2015	21:50:07	x		x	x
	01/11/2015	21:50:16	x		x	x
	03/08/2018	10:53:34	x	x	x	x
	03/08/2018	10:53:43	x	x	x	x
	05/08/2018	21:51:00	x		x	x
	05/08/2018	21:51:09	x		x	x
Strasbourg	17/02/2003	10:40:41	x	x	x	x
	12/08/2003	10:38:54	x	x	x	x
	26/01/2017	21:24:47	x		x	x
	22/06/2018	21:26:19	x		x	x
Toulouse	14/01/2003	10:54:28	x	x	x	x
	10/08/2003	10:52:42	x	x	x	x
	28/12/2016	21:54:33	x		x	x
	23/06/2018	11:01:15	x	x	x	x

Table 2: ASTER NASA products used in THERMOCTY

2.2.2. ECOSTRESS

ECOSTRESS (Ecosystem Spaceborne Thermal Radiometer Experiment on Space Station) is an ongoing scientific experiment measuring TIR radiance from the International Space Station since mid-2018. The sensor is a multispectral radiometer acquiring data in five TIR spectral bands spread between 8 and 12 microns, with a spatial resolution of 70 m. Several products are generated from the ECOSTRESS data, among which a LST product. Those products are available via various NASA data portals and are free of charge. In THERMOCITY, the following data products are used:

- ECOSTRESS_L1B_MAP_RAD: mapped radiance product, combining Top Of Atmosphere (TOA) TIR radiance and geolocation products to supply registered TIR radiance data
- ECOSTRESS_L2_CLOUD : cloud mask
- ECOSTRESS_L2_LSTE : LST and LSE products

For ECOSTRESS, 5 dates have been selected over each city following the aforementioned criteria. Foreach date, several data products were downloaded from the NASA data portal service for processing and comparison. The selected dates and products are summarized in Table 3 The acquisitions times are in UTC.

.

Study Area	Date	Acquisition time (UTC)	MAPRAD	CLOUD	LSTE
Aix-Marseille	27/08/2018	11:25:30	x	x	x
	27/02/2019	10:13:14	x	x	x
	15/07/2019	21:56:27	x	x	x
	05/01/2020	01:21:31	x	x	x
	07/08/2020	12:01:37	x	x	x
Montpellier	27/08/2018	11:25:30	x	x	x
	27/02/2019	10:13:14	x	x	x
	15/07/2019	21:56:27	x	x	x
	05/01/2020	01:21:31	x	x	x
	11/01/2020	22:59:17	x	x	x
	07/08/2020	12:01:37	x	x	x
Paris	28/08/2018	10:33:02	x	x	x
	15/02/2019	10:49:09	x	x	x
	15/07/2019	23:33:19	x	x	x
	21/01/2020	23:03:59	x	x	x
	07/08/2020	13:38:46	x	x	x
Strasbourg	22/08/2018	12:32:48	x	x	x
	17/09/2018	22:47:10	x	x	x
	15/02/2019	10:50:01	x	x	x
	08/08/2020	12:52:13	x	x	x
Toulouse	20/08/2018	09:24:48	x	x	x
	13/02/2019	10:54:26	x	x	x
	15/07/2019	21:55:35	x	x	x
	11/01/2020	22:59:17	x	x	x
	07/08/2020	12:00:45	x	x	x

Table 3: ECOSTRESS NASA products used in THERMOCITY

2.3. Ancillary Data

2.3.1. Imperviousness density

The TES algorithm used in THERMOCITY (detailed in 3.2) requires as input a classification to differentiate natural from artificial land cover. After evaluating different data sources, we selected the Imperviousness Density product from Copernicus [1]. This dataset, available at 10 m resolution, was resampled at the resolution of the TIR satellite data acquired by ECOSTRESS and ASTER, respectively 70 m and 90 m. This pre-processing step was performed by the Eolab team at CNES.

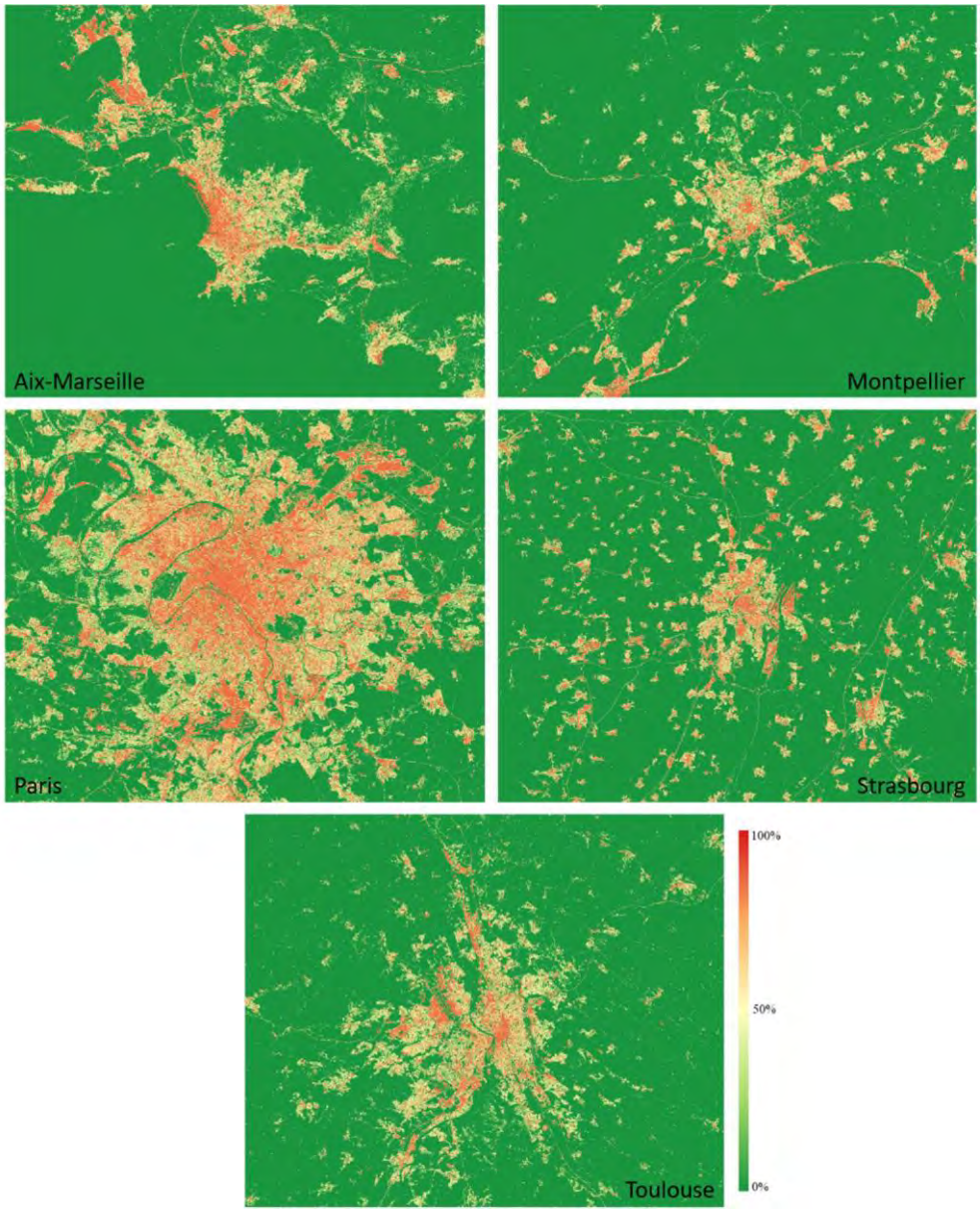

Figure 2: Imperviousness density maps at 10 m spatial resolution for each metropolis

2.3.2. Atmospheric profiles and cloud cover

Unlike for ASTER, there is no at-surface TIR radiance product available for ECOSTRESS. Before applying the TES algorithm, an atmospheric correction step is then required to convert ECOSTRESS TOA radiance to BOA radiance values. To do so, we used a precise description of the atmosphere provided by vertical atmospheric profiles produced by MétéoFrance for each acquisition time of selected ECOSTRESS images. Those profiles consist in temperature, relative humidity and air pressure values at 50 geopotential altitude levels starting from ground height above sea level to 50 km high. They were generated by two models: AROME[1] below 10 000 Pa and ARPEGE[2] above 10 000 Pa. Above 50 km, the values are interpolated from atmospheric databases. The values are also horizontally interpolated to fit the requested profile location and correspond to the closest hour to the image acquisition time.

2.3.3. Sky View Factor

The Sky View Factor (SVF) used in the construction of the QA layer was computed from the BD topo [2] rasterized at 1 m spatial resolution, using a tool developed by CNES (for more information please, contact the LOT team at CNES). The parameters used for the SVF computation are defined according to the recommendations given in [3] for urban areas: a calculation radius of 100 m and 16 search directions. An example of SVF map is presented in Figure 3.

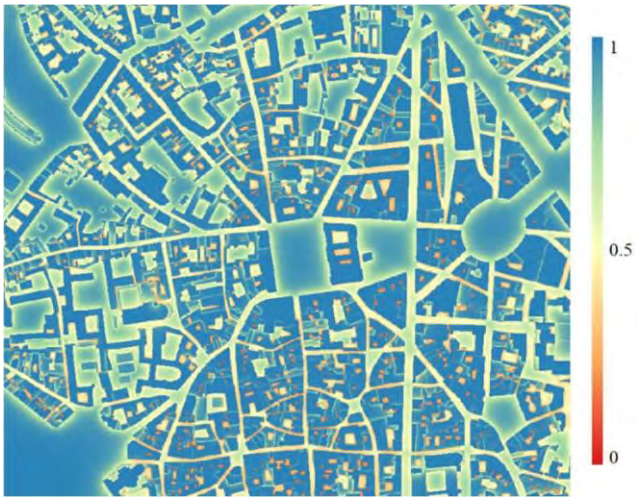

Figure 3: Example of Sky View Factor maps at 1 m spatial resolution over the city centre of Toulouse

The SVF at 1 m spatial resolution was aggregated at 70 and 90 m, the resolutions of ECOSTRESS and ASTER respectively. When aggregated, the dense areas with narrow streets showed high SVF values because most of the pixels consist of roofs with SVF value close to 1. By averaging, the high values on the roofs pull the pixel average up, leading to a loss of the urban canyon contribution. To compensate for this effect, we weighted the aggregated SVF values at 70 m and 90 m by the percentage of build-up area in each pixel of 70 m and 90 m respectively. This weighting allowed compensating for the fact that the SVF are almost 1 on the roofs and thus masking the low values observed in the urban canyons in case of dense buildings.

[1] https://www.umr-cnrm.fr/spip.php?article120&lang=en
[2] https://www.umr-cnrm.fr/spip.php?article121

The weighting is only applied on pixels with maximum 95% of build-up area in order to avoid SVF of 0 in case of pixels fully covered by buildings. The SVF values obtained after weighting are consistent with recent works on the subject [10, 11].

3. METHODS

Prior to being processed, all the data have been geometrically corrected to fit Copernicus Sentinel-2 mission geolocalization and to ensure perfect overlapping between the different spectral bands and the various data products. This pre-processing step was performed by the Eolab team at CNES [4].

3.1. Atmospheric correction of ECOSTRESS TOA radiance

The level 1B MAP_RAD ECOSTRESS data product provides geometrically corrected radiance values at the top of the atmosphere. It is then necessary to apply an atmospheric correction to retrieve the bottom of atmosphere radiance values required as input of the TES algorithm.

The atmospheric correction was performed using COMANCHE [5]. This code, computing the incoming spectral radiance at the sensor level for instruments operating in the VIS - LWIR spectral range, was used to estimate the atmospheric transmittance and path radiance values required to convert TOA to BOA radiance according to the following equation:

$$L_{B0Æ,} = \frac{L_{T0Æ,} - L_{est,}}{T_{est,}}$$

With: $L_{B0Æ,}$: Bottom Of Atmosphere thermal radiance in band λ
$L_{T0Æ,}$: Top Of Atmosphere thermal radiance in band λ
$L_{est,}$: Atmospheric radiance estimated by COMANCHE in band λ
$T_{est,}$: Atmospheric transmittance estimated by COMANCHE in band λ

COMANCHE simulations also provided the atmospheric irradiance value, which is the second input required by the TES algorithm to estimate the LSE and LST.

The properties of the atmosphere provided as input to COMANCHE were derived from atmospheric profiles computed by MétéoFrance for each product acquisition time. Those profiles were generated over the city centre and applied to the entire study area.

The parameterization of COMANCHE used in THERMOCITY is detailed in Table 4. The same parameters are set for all study sites except when the metropolis' first letter name is specified.

Parameters	Summer day	Summer night	Winter day	Winter night
Temperature min (°c)	20	10	-5 (P, S, T) 0 (AM, M)	-5 (P, S, T) 0 (AM, M)
Temperature max (°c)	80	70	60	60
Number of temperature steps between the min and max values	13	13	14 (P, S, T) 13 (AM, M)	14 (P, S, T) 13 (AM, M)
Default model	2 Mid-Latitude Summer	2 Mid-Latitude Summer	3 Mid-Latitude Winter	3 Mid-Latitude Winter
CO_2 Particule content (ppmv)	400	400	400	400
Aerosols model (MODTRAN code)	5 URBAN (P, S, T) 4 MARITIME (AM, M)	5 URBAN (P, S, T) 4 MARITIME (AM, M)	5 URBAN (P, S, T) 4 MARITIME (AM, M)	5 URBAN (P, S, T) 4 MARITIME (AM, M)
Visibility (km)	23	23	23	23
Number flux disort	2 fluxes model	2 fluxes model	2 fluxes model	2 fluxes model
Spectral resolution (cm^{-1})	1	1	1	1

Table 4: Parameters set in COMANCHE for atmospheric correction. The same parameters are set for all study sites except when the metropolis' first letter name is specified (AM = Aix-Marseille, M = Montpellier, P = Paris, S = Strasbourg, T = Toulouse)

3.2. LST retrieval: the TES algorithm

The TES algorithm was originally developed for ASTER data [6]. It retrieves jointly the land surface temperature and the land surface emissivity from the TIR BOA radiance and the TIR irradiance thanks to four steps:

1. The NEM (Normalized Emissivity Method), which uses an initial emissivity value (here 0.99) and iteratively corrects for the downwelling radiance. A maximum number of iterations is required (here 13) and a flag is raised if there is no convergence, meaning the algorithm failed. The outputs of the NEM step are : the emissivity spectrum, the Quality Assessment (QA) layer of the NEM module and the preliminary values of the LST.

2. The RATIO module, which normalizes the emissivity spectrum by the emissivity average value over the spectrum. It allows the algorithm to be less sensitive to errors in temperature and preserves the shape of the spectrum. The output of the RATIO step is the normalized emissivity spectrum.

3. The MMD (Minimum Maximum Difference) module, which converts normalized emissivities into actual emissivities using the empirical MMD relationship. The MMD relationship is a non-linear regression between the minimum emissivity and the spectral contrast defined as the minimum-maximum difference and is expressed as:

$$s_{min} = a + b.MMD^{c}$$

4. Once the minimum emissivity is computed, the LST is retrieved with the inverse Planck's law. If the LST is complex, a flag is raised to show that the MMD module failed.

The outputs of the TES algorithm are:

- LST,
- LSE in each processed TIR band,
- Quality Assessment (QA) layer of the NEM module,
- QA layer of the MMD module,
- Map of the minimum emissivity value used as an input for the NEM module.

To apply the TES algorithm, the parameters of the MMD relationship need to be estimated according to the number and spectral responses of the considered TIR bands using an emissivity spectral database. Usually, the MMD relationship is constructed from a database in which artificial materials are under-represented leading to potential LST estimation errors over those types of materials, especially in urban areas. Thus, an urban- oriented database was developed comprising 47% of manmade materials and 53% of natural, to be representative for both urban and rural areas. Furthermore, a study based on airborne and spaceborne data acquired over the city of Madrid found that separating this urban-oriented database into one manmade-surface-oriented database and one natural-surface-oriented database to construct two MMD relationships led to LST retrieval accuracy improvement [7]. In THERMOCITY, we followed this approach and separated the manmade and the natural materials into two distinct databases, each one split into two for calibration and validation of two MMD relationships. To use this version of the TES, it is then necessary to know which material type is covered by each pixel, natural or artificial, in order to choose which MMD relationship to apply. Further information on the TESalgorithm can be found in [8, 9].

3.2.1. Calibration and validation of the TES algorithm for ASTER

Figure 4 illustrates the MMD relationship for the manmade-surface-oriented database for calibration and validation as well as the MMD relationship for the natural-surface-oriented database for calibration and validation. The Pearson linear correlation coefficients between the observed data and the retrieved data are given.

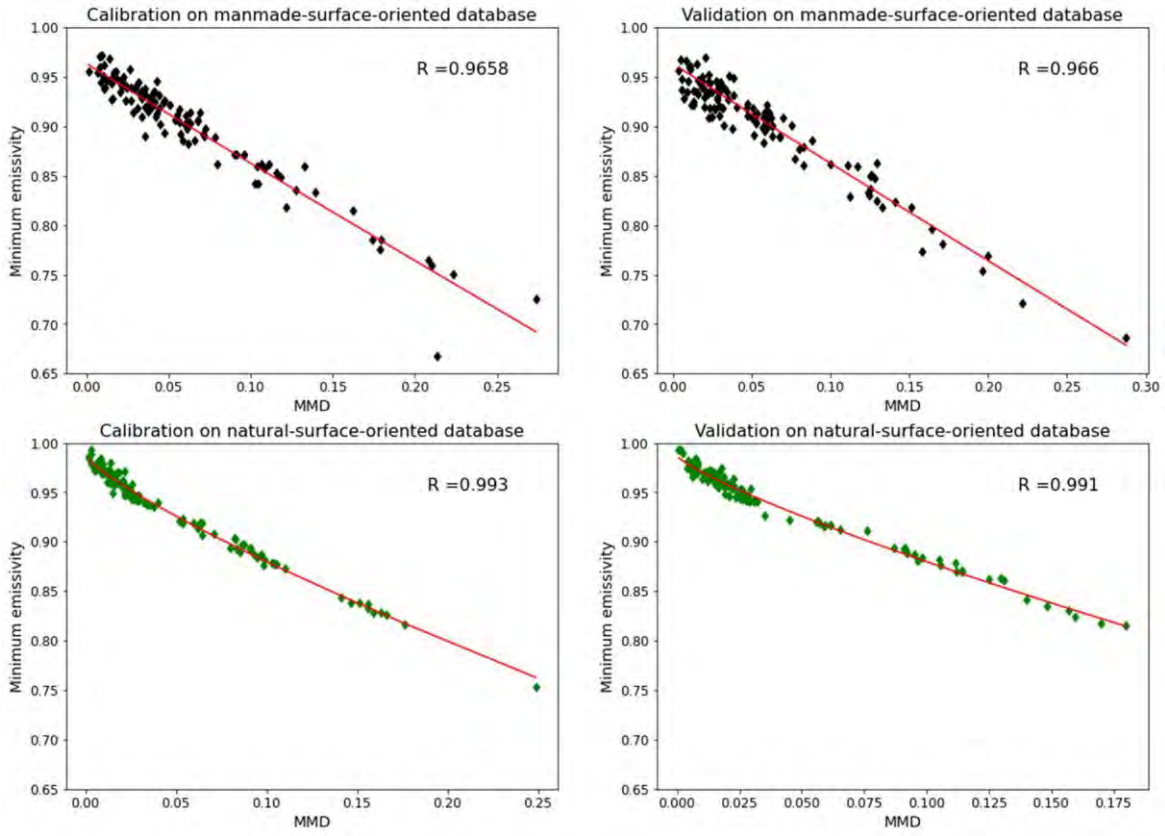

Figure 4: MMD relationship for ASTER

Table 5 gives the RMSE (Root Mean Square Error) and the parameters a, b, c of the MMD relationship.

Database	**a**	**b**	**c**	**RMSE calibration**	**RMSE validation**
Natural-surface-oriented	0.987	0.692	0.811	0.0052	0.0050
Manmade-surface-oriented	0.964	0.969	0.982	0.0139	0.0137

Table 5: Parameter values and RMSE for calibration and validation of the TES algorithm for ASTER

3.2.2. Calibration and validation of the TES algorithm for ECOSTRESS

Figure 5 illustrates the MMD relationship for the manmade-surface-oriented database for calibration and validation as well as the MMD relationship for the natural-surface-oriented database for calibration and validation. The Pearson linear correlation coefficients between the observed data and the retrieved data are given.

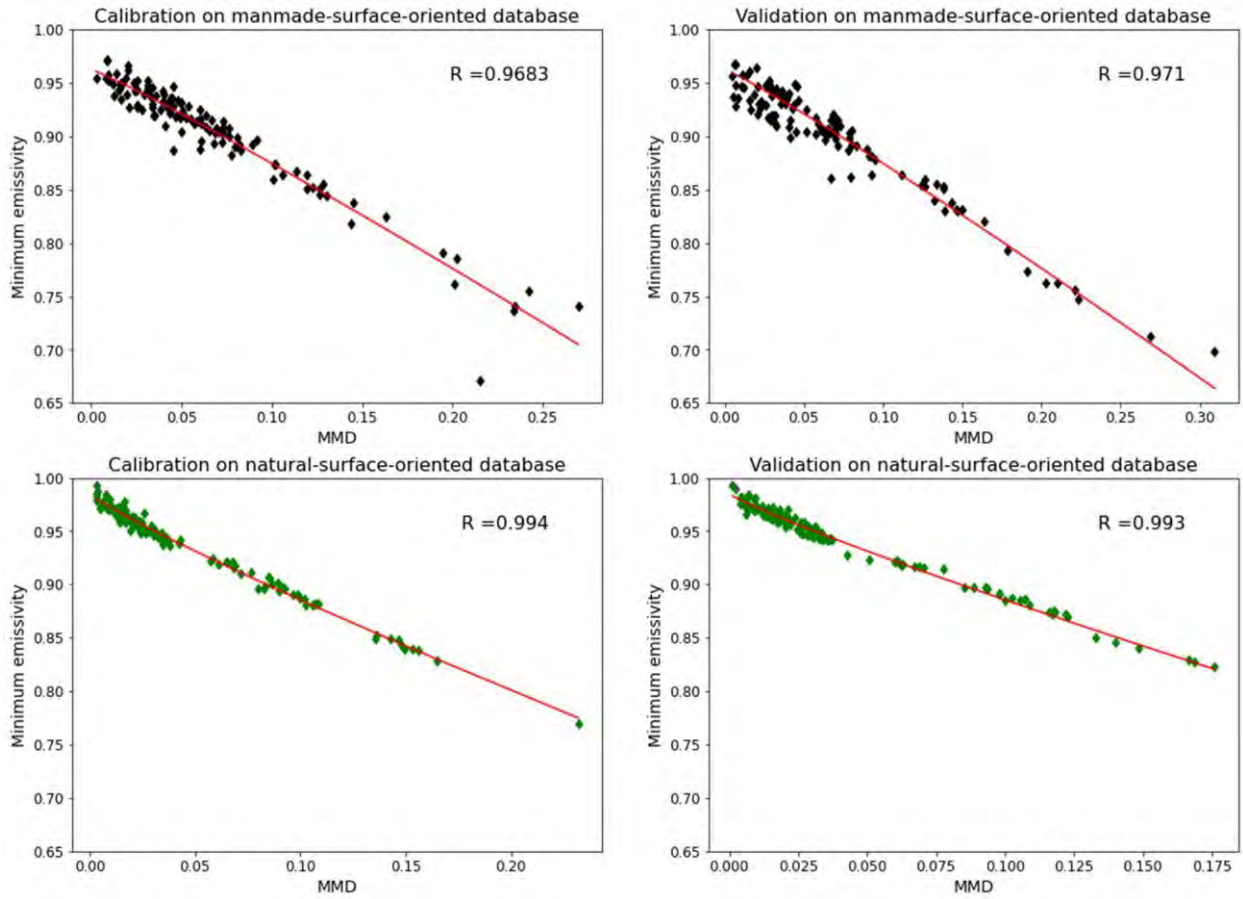

Figure 5: MMD relationship for ECOSTRESS with 5 TIR bands

Table 6 gives the RMSEs and the parameters a, b, c of the MMD relationship with five bands.

Database	**a**	**b**	**c**	**RMSE calibration**	**RMSE validation**
Natural-surface-oriented	0.985	0.771	0.890	0.0045	0.0045
Manmade-surface-oriented	0.962	1.063	1.082	0.0134	0.0132

Table 6: Parameter values and RMSE for calibration and validation of the TES algorithm for ECOSTRESS with 5 TIR bands

Figure 6 illustrates the MMD relationship for the manmade-surface-oriented database for calibration and validation as well as the MMD relationship for the natural-surface-oriented database for calibration and validation when only three thermal bands are used because two TIR bands of ECOTRESS are out of service since May 2019. The Pearson linear correlation coefficients between the observed data and the retrieved data are given.

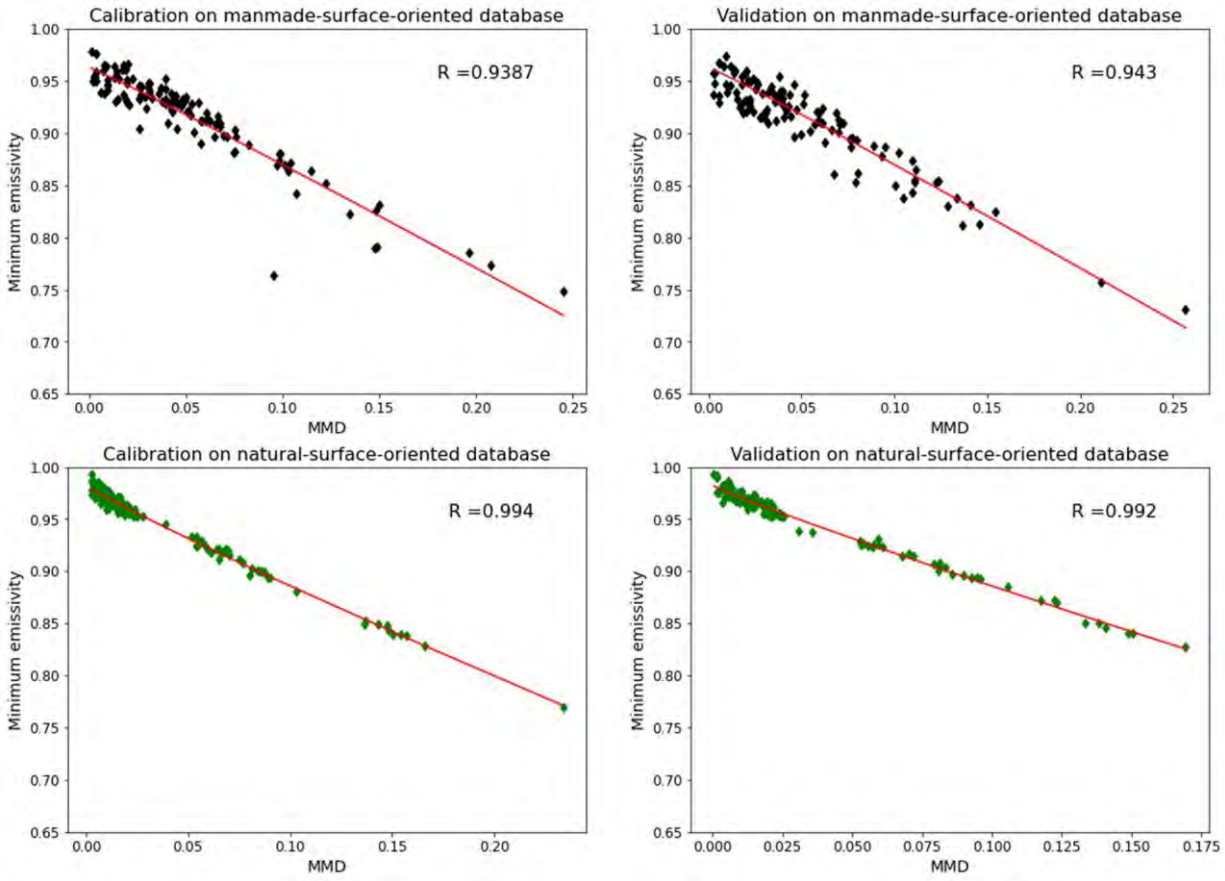

Figure 6: MMD relationship for ECOSTRESS with 3 TIR bands

Table 7 gives the RMSEs and the parameters a, b, c of the MMD relationship for three bands.

Database	**a**	**b**	**c**	**RMSE calibration**	**RMSE validation**
Natural-surface-oriented	0.981	0.924	0.961	0.0045	0.0047
Manmade-surface-oriented	0.962	1.263	1.093	0.017	0.015

Table 7: Parameters and RMSE for calibration and validation of the TES algorithm for ECOSTRESS with 3 TIR bands

3.2.3. Imperviousness density for natural/artificial classification

To apply the right MMD relationship to the considered pixel, it is necessary to define whether the pixel material is manmade or natural. To this end, imperviousness density products (section 2.3.1) were analysed visually over the five selected cities and thresholds were set empirically by photo-interpretation. Thresholds are different for wintertime and summertime data to take into account the temporal variability of the trees that are often deciduous in cities. The fact that this approach does not consider pixels as mixed but pure can be mentioned as a limitation.

The thresholds used by city and season to retrieve the LST from ASTER data are given in Table 8. The threshold indicates the minimum imperviousness density value required to consider a pixel as artificial. Below, the pixel is considered as natural.

Study Area	Summer threshold (%)	Winter threshold (%)
Aix-Marseille	20	10 for 20050130T103425 20 for 20190114T213551
Montpellier	30	20
Paris	30	20
Strasbourg	30	10
Toulouse	50	30

Table 8: Thresholds used for the imperviousness density for ASTER

To retrieve LST from ECOSTRESS data, the same summer and winter thresholds were used for all cities. Those thresholds, given in the Table 9, indicate the minimum imperviousness density values required to consider a pixel as artificial. Below, the pixel is considered as natural. The threshold has been set empirically according to the area and the spatial resolution, which explains why they are different between Table 8 and Table 9.

Study Area	Summer threshold (%)	Winter threshold (%)
All	50	40

Table 9: Thresholds used for the imperviousness density for ECOSTRESS

3.3. Disaggregation of the LST derived from ASTER data

3.3.1. Disaggregation approach

The methods applied in this project rely on the base that images are acquired at a better resolution in the reflective domain than in the TIR domain, and consequently, the finer information present in the visible and/or shortwave domain can be used to downscale the TIR images. To do so, a regression between a spectral index retrieved from the VNIR-SWIR at a fine resolution and the LST retrieved at the coarse resolution is used. The regression parameters are estimated at the coarse resolution (here 90 meters) and, under the hypothesis of the scale invariance, are used at the finer resolution (here 30 meters and 15 meters). Mathematically, if the regression is considered linear, the LST at a general resolution l can be expressed as:

$$T_1 = a_1 + b_1 I_1$$

Where T_1 is the LST and I_1 is an index obtained from the VNIR-SWIR, both at resolution l.

The second hypothesis is that the linear relationship between the surface temperature and the index is the same at any resolution, which is the scale invariance hypothesis. Then, the linear parameters a_1 (intercept) and b_1 (slope) do not depend on the scale and they can be noted a and b.

$$T_1 = a + bI_1 \ \forall 1$$

Where l indicates a generic resolution l.

First, using the TIR spectral bands of the image, the LST TL_{xL} is obtained at a given coarse resolution L. At the same time, using the VNIR-SWIR spectral bands, an index I is obtained at a finer resolution h (Ih_{xh}). By aggregating (spatially averaging) the VNIR-SWIR spectral bands, this index is also obtained at the coarse resolution L (IL_{xL}). Both, LST and the index are function of the pixel locations x (xL at the coarse scale and xh at the fine scale).

Second, the linear parameters a and b are obtained by linear regression at the coarse resolution L.

$$TL_{xL} = a + bIL_{xL}$$

Third, this linear relationship is applied pixel by pixel to deduce the temperature eTh at the fine scale.

$$\mathrm{e}Th_{xh} = a + bIh_{xh}$$

Fourth, the residuals DTh of the unmixed LST (Th) are estimated and used to correct eTh.

$$Th_{xh} = \mathrm{e}Th_{xh} + DTh_{xh}$$

The different methods based on this approach mainly differ on the index that is used, or in the residuals estimation. [9] studied the downscaling of the LST retrieved from satellite data over urban areas from 100 meters to 20 meters, comparing fourteen indices and seven methods. They showed that the ATPRK (Area-To-Point Regression Kriging) and the AATPRK (Adaptive Area-To-Point Regression Kriging) methods provided the best results when comparing with a LST reference map retrieved from airborne data. The ATPRK method was the most efficient method for downscaling daytime data and the AATPRK method was the most efficient for nighttime data with similar performances between the use of the NDVI (Normalized Differential Vegetation Index) or the NDBI (Normalized Differential Built Index). For nighttime data, the NDVI or the NDBI were retrieved from daytime data acquired at a close date. Both ATPRK and AATPRK rely on a regression that is assumed as linear. A description of each method and of the methodology is provided in the following subsections. Description of ATPRK and AATPRK is provided in [9].

3.3.2. Methods and indices used for the disaggregation

The NDVI and NDBI indices are derived from the reflectance in the VNIR-SWIR bands. The formula to derive those indices from ASTER data are:

$$NDVI = \frac{VNIR_3 - VNIR_2}{VNIR_3 + VNIR_2}$$

With $VNIR_2$ and $VNIR_3$ the second band and the third band in the VNIR domain respectively.

$$NDBI = \frac{SWIR_1 - VNIR_3}{SWIR_1 + VNIR_3}$$

With $VNIR_3$ the third band in the VNIR domain and $SWIR_1$ the first band in the SWIR domain.

To perform the disaggregation, the VNIR surface radiances at 15 m were undersampled at 30 and 90 m and the SWIR surface radiances at 30 m were undersampled at 90 m by spatial averaging. NDVI is then retrieved from the reflectance at the three different spatial resolutions.

Table 10 summarizes the index and disaggregation method used for each disaggregation level, 30 or 15 m, for each date. The acquisitions times are in UTC.

Study Area	Date	Acq. time (UTC)	Downscaled to 30 m	Downscaled to 15 m
Aix-Marseille	12/08/2003	10:40:31	ATPRK+NDVI / ATPRK+NDBI	ATPRK+NDVI
	30/01/2005	10:34:25	ATPRK+NDVI / ATPRK+NDBI	ATPRK+NDVI
	14/01/2019	21:35:51	x	x
Montpellier	02/11/2007	10:47:02	ATPRK+NDVI / ATPRK+NDBI	ATPRK+NDVI
	29/08/2015	10:42:08	ATPRK+NDVI	ATPRK+NDVI
	29/08/2015	21:49:08	AATPRK+NDVI	AATPRK+NDVI
	01/11/2015	21:48:48	x	x
Paris	01/08/2003	10:57:21	ATPRK+NDVI / ATPRK+NDBI	ATPRK+NDVI
	22/10/2004	10:57:11	ATPRK+NDVI / ATPRK+NDBI	ATPRK+NDVI
	01/11/2015	21:50:07	x	x
	01/11/2015	21:50:16	x	x
	03/08/2018	10:53:34	ATPRK+NDVI	ATPRK+NDVI
	03/08/2018	10:53:43	ATPRK+NDVI	ATPRK+NDVI
	05/08/2018	21:51:00	AATPRK+NDVI	AATPRK+NDVI
	05/08/2018	21:51:09	AATPRK+NDVI	AATPRK+NDVI
Strasbourg	17/02/2003	10:40:41	ATPRK+NDVI / ATPRK+NDBI	ATPRK+NDVI
	12/08/2003	10:38:54	ATPRK+NDVI / ATPRK+NDBI	ATPRK+NDVI
	26/01/2017	21:24:47	x	x
	22/06/2018	21:26:19	x	x
Toulouse	14/01/2003	10:54:28	ATPRK+NDVI / ATPRK+NDBI	ATPRK+NDVI
	10/08/2003	10:52:42	ATPRK+NDVI / ATPRK+NDBI	ATPRK+NDVI
	28/12/2016	21:54:33	x	x
	23/06/2018	11:01:15	ATPRK+NDVI	ATPRK+NDVI

Table 10: Method and index used for downscaling according to the study area and the acquisition time

3.4. Quality Assessment

A quality assessment (QA) layer was defined to inform users about the reliability of the LST products by flagging pixels for which higher uncertainties can be expected due to several factors impacting the estimations. In this QA, there is no calculation of uncertainty values, the idea is to indicate where the LST is expected with a high accuracy or where caution with the result interpretation is required. On top ofuncertainties linked to the radiometric quality of the input data, the presence of clouds or the TES algorithm itself, this QA considers sources of uncertainties specific to urban areas where LST errors can be induced by the adjacency effect and 3D structure.

In order to consider a large range of potential sources of errors, we gathered information from the data products itself and ancillary datasets such as input radiance quality planes and cloud masks, Sky View Factor (SVF) and output from the TES to evaluate the reliability of the retrieved values. The criteria and thresholds are defined based on knowledge derived from recent studies on LST estimation in urban areas [10, 11].

No filtering or data filling was applied to remove bad or suspect values from the LST products. Data considered as “bad” may not be bad for all users or may still contain some scientifically useful information. The user thus has access to the original values provided by the TES and can choose to filter themusing the QA layer to mask out pixels according to one or several sources of uncertainty or to generate his own mask.

A pixel is flagged as suspect in the QA according to the following criteria:

- Physically grounded LST: in case of unrealistic values, out of a given valid range
- Physically grounded LSE: if one of the spectral emissivities shows an unrealistic value, out of a given valid range
- TES algorithm: if the NEM module from the TES did not converge
- Input BOA radiance: if the quality flag associated with the radiance data used as input in the TES is different from 0 (including cloud mask information if available). In case of ECOSTRESS, the cloud mask information was available for only 14 dates out of 25; the images without cloud mask are detailed in the readme file associated with the products
- Surface roughness: according to the Sky View Factor (SVF) value as a proxy of surface roughness based on several studies using this metric to evaluate the impact of the city 3D structure on LST estimation. Low SVF values are related to higher impacts on LST retrieval

The QA layer has a common structure for all LST products. A binary code is attributed to each pixel allowing to quickly identify which source of error could potentially affect the retrieved LST value. A pixel with a QA value of “0” is highly reliable. If the QA value is superior to 0, it is advised to check the QA code to evaluate LST uncertainty. The QA code is made of five bits to which is attributed a specific source of errors. The structure of the QA layer and the applied thresholds are detailed in Table 11.

Bit	Criteria	Source of error	Threshold (flagged if…)
1	LST	Algorithm	Below -10°C or above 100°C
2	LSE	Algorithm	Below 0.4 or above 1
3	Module NEM	Algorithm	Non convergence flag = 1
4	BOA radiance	Input data	QA input data > 0
5	SVF	Surface 3D	Below 0.3

Table 11: Bit code and associated criteria used in the QA layer

4. THERMOCITY PRODUCTS

The LST maps generated in the project are compared with the LST products from NASA at the spatial resolutions of 90 m for ASTER and 70 m for ECOSTRESS. To highlight the differences and the similarities between both products, several metrics are considered:

- For each product:
  - LST mean value over the entire study area
  - LST spatial variability (standard deviation) over the entire study area

- From the difference between the two products:
  - Mean Bias Error (MBE)
  - Root Mean Square Error (RMSE)
  - Pearson linear correlation coefficient (R^2)

To compute those metrics, only pixels fulfilling the following conditions are taken into account:

- Input radiance in each band is not equal to 0
- Not flagged in the QAmap and QAmmd layers generated by the TES
- LST is not a NaN value and comprised between 250 and 360K (the percentage of pixels out of this range is provided in the scatterplots in Appendix A and C)
- LST NASA is not a dummy filling value

In addition, the LST distribution is studied through the production of histograms and difference scatterplots. Those figures, along with LST and LST difference maps are provided for each dates and study areas in Appendix A for ASTER and Appendix C for ECOSTRESS.

For the downscaled ASTER LST maps at 30 m and 15 m, the mean and spatial variability (standard deviation) of the LST are provided with the corresponding histograms to compare with the maps at 90 m.

4.1. ASTER

4.1.1. LST at 90 m

Table 11 provides the criteria values to compare the NASA products and the LST maps retrieved from our processing, according to the study area and the acquisition time (in UTC). The LST, LST difference maps, histograms and scatterplot for each date are provided in the Appendix A.

Study Area	Date	Acq. time (UTC)	Mean LST NASA (K)	Mean LST (K)	Stdev LST NASA (K)	Stdev LST (K)	RMSE (K)	MBE (K)	R^2
Aix-Marseille	12/08/2003	10:40:31	305.87	305.62	6.81	7.04	1.65	0.25	0.95
	30/01/2005	10:34:25	281.76	281.83	4.39	4.39	0.84	-0.07	0.96
	14/01/2019	21:35:51	283.56	283.5	4.76	4.67	0.96	0.06	0.96
Montpellier	02/11/2007	10:47:02	290.02	290.08	2.74	2.57	0.73	-0.06	0.93
	29/08/2015	10:42:08	306.85	306.56	3.55	3.38	0.96	0.28	0.93
	29/08/2015	21:49:08	291.96	291.36	2.23	1.9	1.18	0.59	0.79
	01/11/2015	21:48:48	281.58	281.42	2.08	1.84	1.14	0.16	0.71
Paris	01/08/2003	10:57:21	307.42	307.38	5.60	5.63	1.97	0.04	0.88
	22/10/2004	10:57:11	290.96	291.02	1.84	1.82	1.34	-0.06	0.53
	01/11/2015	21:50:07	282.10	281.87	1.79	1.87	1.06	0.23	0.70
	01/11/2015	21:50:16	282.32	281.96	1.61	1.67	1.05	0.41	0.69
	03/08/2018	10:53:34	313.76	313.69	5.48	5.41	1.97	0.07	0.87
	03/08/2018	10:53:43	314.54	314.53	5.51	5.43	2.13	0.013	0.85
	05/08/2018	21:51:00	292.48	292.27	3.04	3.28	1.2	0.21	0.87
	05/08/2018	21:51:09	291.92	291.7	3.18	3.17	1.45	0.23	0.81
Strasbourg	17/02/2003	10:40:41	273.94	273.9	3.07	3.08	0.91	0.04	0.91
	12/08/2003	10:38:54	310.99	310.73	5.3	5.2	1.9	0.26	0.88
	26/01/2017	21:24:47	266.07	265.86	2.22	2.22	0.78	0.21	0.89
	22/06/2018	21:26:19	284.36	284.18	2.55	2.52	1.34	0.19	0.75
Toulouse	14/01/2003	10:54:28	277.50	277.52	1.45	1.38	0.52	-0.02	0.87
	10/08/2003	10:52:42	319.62	318.96	5.4	4.71	2.79	0.66	0.75
	28/12/2016	21:54:33	274.67	274.37	1.48	1.38	0.69	0.3	0.82
	23/06/2018	11:01:15	305.9	305.8	4.31	3.98	1.22	0.1	0.92

Table 12: Evaluation criteria between NASA ASTER LST maps and THERMOCITY LST maps

THERMOCITY LST and NASA LST are in good agreement, with low values of RMSE between 0.5 and 2 K and a maximum value of the RMSE of 2.79K. The spatial variability of the LST is similar between both products with lower nighttime values than daytime, in agreement with the homogenization of the LST at nighttime. Most of the differences are seen over the urban areas, especially for manmade materials. Furthermore, two dates have clouds so the LST values over cloudy pixels are those of the clouds and not of the surface, which also affects the image statistics:

- 01/08/2003 10:57:21 over Paris: cloudy pixel LST value mainly between 280 and 290 K
- 17/02/2003 10:40:41 over Strasbourg: cloudy pixel LST value mainly between 260 and 270 K

The LST values of cloudy pixels can be masked with the QA layer taking into account the cloud mask.

4.1.2. Downscaled LST at 30 m

Table 13 gives the mean LST and its spatial variability at 30 m when the NDVI is used with the ATPRK method (only daytime images).

Study Area	Date	Acq. time (UTC)	Mean LST at 90 m (K)	Mean LST (K)	Stdev LST (K)
Aix-Marseille	12/08/2003	10:40:31	305.62	305.46	7.73
	30/01/2005	10:34:25	281.83	281.74	5.44
Montpellier	02/11/2007	10:47:02	290.08	289.90	5.09
	29/08/2015	10:42:08	306.56	306.44	4.86
Paris	01/08/2003	10:57:21	307.38	307.31	6.59
	22/10/2004	10:57:11	291.02	290.94	3.49
	03/08/2018	10:53:34	313.69	313.64	6.11
	03/08/2018	10:53:43	314.53	314.52	5.93
Strasbourg	17/02/2003	10:40:41	273.9	273.85	3.76
	12/08/2003	10:38:54	310.73	310.64	6.27
Toulouse	14/01/2003	10:54:28	277.52	277.44	3.36
	10/08/2003	10:52:42	318.96	318.92	10.06
	23/06/2018	11:01:15	305.8	305.63	5.91

Table 13: Mean and standard deviation for the downscaled LST maps with ATPRK and NDVI

For nighttime images, the AATPRK method can be used if a pair of daytime and nighttime images is available. Two dates meet this criterion:

- Montpellier 29/08/2015 with a daytime image from 29/08/2015,
- Paris 5/08/2018 with daytime images from 03/08/2018.

To compare with ATPRK method used with NDVI, Table 14 gives the mean and spatial variability of the LST at 30 m when the NDBI is used (only daytime images before 2008 when SWIR bands are available).

Study Area	Date	Acq. time (UTC)	Mean LST (K)	Stdev LST (K)
Aix-Marseille	12/08/2003	10:40:31	305.43	7.91
	30/01/2005	10:34:25	281.74	5.48
Montpellier	02/11/2007	10:47:02	289.90	5.12
Paris	01/08/2003	10:57:21	307.34	6.61
	22/10/2004	10:57:11	290.95	3.49
Strasbourg	17/02/2003	10:40:41	273.86	3.78
	12/08/2003	10:38:54	310.66	6.32
Toulouse	14/01/2003	10:54:28	277.44	3.37
	10/08/2003	10:52:42	318.97	10.08

Table 14: Mean and standard deviation for the downscaled LST maps with ATPRK and NDBI

The mean LST and spatial variabilities retrieved with ATPRK+NDVI or ATPRK+NDBI are very similar, in agreement with [9].

Last, Table 15 gives the statistics for nighttime images at 30 m where the AATPRK method is used. Only the NDVI is used because no pairs of nighttime images and daytime images were available before 2008, when SWIR bands were still acquired. The statistics provided for 90 m LST differ between Table 13 and Table 15 as the area used for the disaggregation is smaller nighttime.

Study Area	Date	Acq. time (UTC)	Mean LST at 90 m (K)	Mean LST (K)	Stdev LST at 90 m(K)	Stdev LST (K)
Montpellier	29/08/2015	21:49:08	291.64	291.82	4.42	2.12
Paris	05/08/2018	21:51:00	292.32	292.39	4.46	3.42
	05/08/2018	21:51:09	292.2	292.30	5.2	4.24

Table 15: Mean and spatial variability of the LST at 30 m with AATPRK and NDVI

4.1.3. Downscaled LST at 15 m

Table 16 gives the mean LST and its spatial variability at 15 m when the NDVI is used with the ATPRK method (only daytime images). The NDBI cannot be used as the NDBI's spatial resolution is 30 m.

Study Area	Date	Acq. time (UTC)	Mean LST at 90 m (K)	Mean LST (K)	Stdev LST (K)
Aix-Marseille	12/08/2003	10:40:31	305.62	305.46	7.77
	30/01/2005	10:34:25	281.83	281.74	5.48
Montpellier	02/11/2007	10:47:02	290.08	289.90	5.14
	29/08/2015	10:42:08	306.56	306.44	4.90
Paris	01/08/2003	10:57:21	307.38	307.32	6.67
	22/10/2004	10:57:11	291.02	290.94	3.54
	03/08/2018	10:53:34	313.69	313.65	6.19
	03/08/2018	10:53:43	314.53	314.53	6.01
Strasbourg	17/02/2003	10:40:41	273.9	273.85	3.79
	12/08/2003	10:38:54	310.73	310.66	6.33
Toulouse	14/01/2003	10:54:28	277.52	277.44	3.42
	10/08/2003	10:52:42	318.96	318.92	10.28
	23/06/2018	11:01:15	305.8	305.64	5.99

Table 16: Mean and standard deviation of the downscaled LST maps at 15 m with the NDVI and ATPRK

Table 17 gives the mean and the spatial variability of the LST at 15 m for the nighttime images.

Study Area	Date	Acq. time (UTC)	Mean LST at 90 m (K)	Mean LST (K)	Stdev LST at 90 m (K)	Stdev LST (K)
Montpellier	29/08/2015	21:49:08	291.64	291.82	4.42	2.17
Paris	05/08/2018	21:51:00	292.32	292.39	4.46	3.45
	05/08/2018	21:51:09	292.2	292.31	5.2	4.28

Table 17: mean and spatial variability of the LST at 15m with AATPRK and NDVI

4.2. ECOSTRESS

Table 18 provides the criteria values to compare the NASA standard products and the THERMOCITY LST maps retrieved from our processing, according to the study area and the acquisition time. The RMSE, MBE and R^2 are missing for some dates due to geometric correction issues preventing to compute the difference maps (refer to [4] for more information). The LST and LST difference maps (when available) for each dates are provided in the Appendix C.

The comparison of the respective LST mean and standard deviation values shows a good agreement between the LST maps produced in THERMOCITY and the NASA ones. This is confirmed by the RMSE and R^2 ranging between 0.37 and 2.07 K and between 0.68 and 0.99 respectively. The lowest R^2 values are observed for LST maps with very low temperature dynamics (see Appendix C). The MBE ranges from -1.97to 0.3, indicating slightly higher LST values in the THERMOCITY products as compared to the NASA LST products with, generally, larger difference observed during daytime. For Aix-Marseille and Montpellier, the large proportion of water in some images can mask out the LST behaviour on continental land. From the analysis of the LST and LST difference maps, there is no general trend in the differences observed between both products. Globally, most of the differences are observed over the urban areas, especially for manmade materials. A brief description of the results date by date is provided in Appendix C.

In the case of ECOSTRESS, the differences between the THERMOCITY and the NASA products are not only resulting from the modification of the TES algorithm. They can also come from the atmospheric correction performed to convert radiance TOA to BOA values. With no ground truth to validate the retrieved LST value, it is not possible to conclude on the benefit brought by our approach. However, we could notice a reduction of extreme values with our method.

Study Area	Date	Acq. time (UTC)	Mean LST NASA (K)	Mean LST (K)	Stdev LST NASA (K)	Stdev LST (K)	RMSE (K)	MBE (K)	R^2
Aix-Marseille	27/08/2018	11:25:30	302.06	303.67	6.76	7.30	-	-	-
	27/02/2019	10:13:14	288.78	290.75	2.60	2.82	2.07	-1.97	0.95
	15/07/2019	21:56:27	291.35	292.11	2.13	2.61	1.02	-0.76	0.96
	05/01/2020	01:21:31	278.06	278.45	5.18	5.44	0.68	-0.39	0.99
	07/08/2020	12:01:37	308.50	309.72	8.74	9.62	-	-	-
Montpellier	27/08/2018	11:25:30	304.17	305.05	6.95	7.02	-	-	-
	27/02/2019	10:13:14	289.75	291.67	3.03	3.20	2.01	-1.91	0.96
	15/07/2019	21:56:27	292.67	293.60	2.39	2.69	1.07	-0.93	0.97
	05/01/2020	01:21:31	277.95	278.51	4.38	4.55	-	-	-
	11/01/2020	22:59:17	273.28	273.84	2.75	2.94	0.75	-0.56	0.97
	07/08/2020	12:01:37	310.37	310.91	9.45	9.70	-	-	-
Paris	28/08/2018	10:33:02	303.23	303.63	4.52	4.67	-	-	-
	15/02/2019	10:49:09	282.77	283.44	1.01	1.20	0.95	-0.67	0.68
	15/07/2019	23:33:19	284.32	285.00	1.94	2.26	0.98	-0.68	0.91
	21/01/2020	23:03:59	269.86	269.95	0.91	0.94	0.51	-0.09	0.73
	07/08/2020	13:38:46	316.34	317.31	3.98	4.34	-	-	-
Strasbourg	22/08/2018	12:32:48	309.87	308.94	7.00	6.88	-	-	-
	17/09/2018	22:47:10	286.54	286.23	2.65	2.77	0.65	0.30	0.96
	15/02/2019	10:50:01	281.43	282.14	1.72	1.76	0.97	-0.70	0.86
	08/08/2020	12:52:13	309.22	310.57	5.15	5.58	-	-	-
Toulouse	20/08/2018	09:24:48	302.29	303.17	2.20	2.39	-	-	-
	13/02/2019	10:54:26	283.69	284.77	0.91	1.05	1.24	-1.08	0.68
	15/07/2019	21:55:35	289.22	289.18	1.72	1.98	0.66	0.04	0.90
	11/01/2020	22:59:17	271.62	271.73	0.82	0.84	0.37	-0.12	0.83
	07/08/2020	12:00:45	317.36	316.50	3.24	3.18	-	-	-

Table 18: Evaluation criteria between NASA ECOSTRESS LST maps and THERMOCITY LST maps

4.3. SUHI

For the SUHI estimation, a rural reference area was identified for each study site. The selection of this reference area is based on the following criteria:

- Not too close to a river or water surface
- Altitude close to that of the city
- Should be more of an agricultural area, not (too) much forest or built-up area
- The reference area should be the same for each date and product over a given metropolis (to allow comparison between dates)

It was difficult to find a suitable reference area around Montpellier and especially around Aix-Marseille that met all these criteria. For Aix-Marseille, the ASTER winter images could not be processed as they do not cover any reliable reference area. The size of the area identified for each city is presented in Table 19.

Study area	Ref area size	Comments
Aix-Marseille	0.44 km²	Few agricultural lands around the city. Different area for ASTER summer image (0.38 km²)
Montpellier	2.34 km²	-
Paris	4.5 km²	-
Strasbourg	3.0 km²	-
Toulouse	3.71 km²	Different area for the ECOSTRESS 07/08/2020 (2.96 km²)

Table 19: Size of the rural area use to compute the SUHI for each metropolis

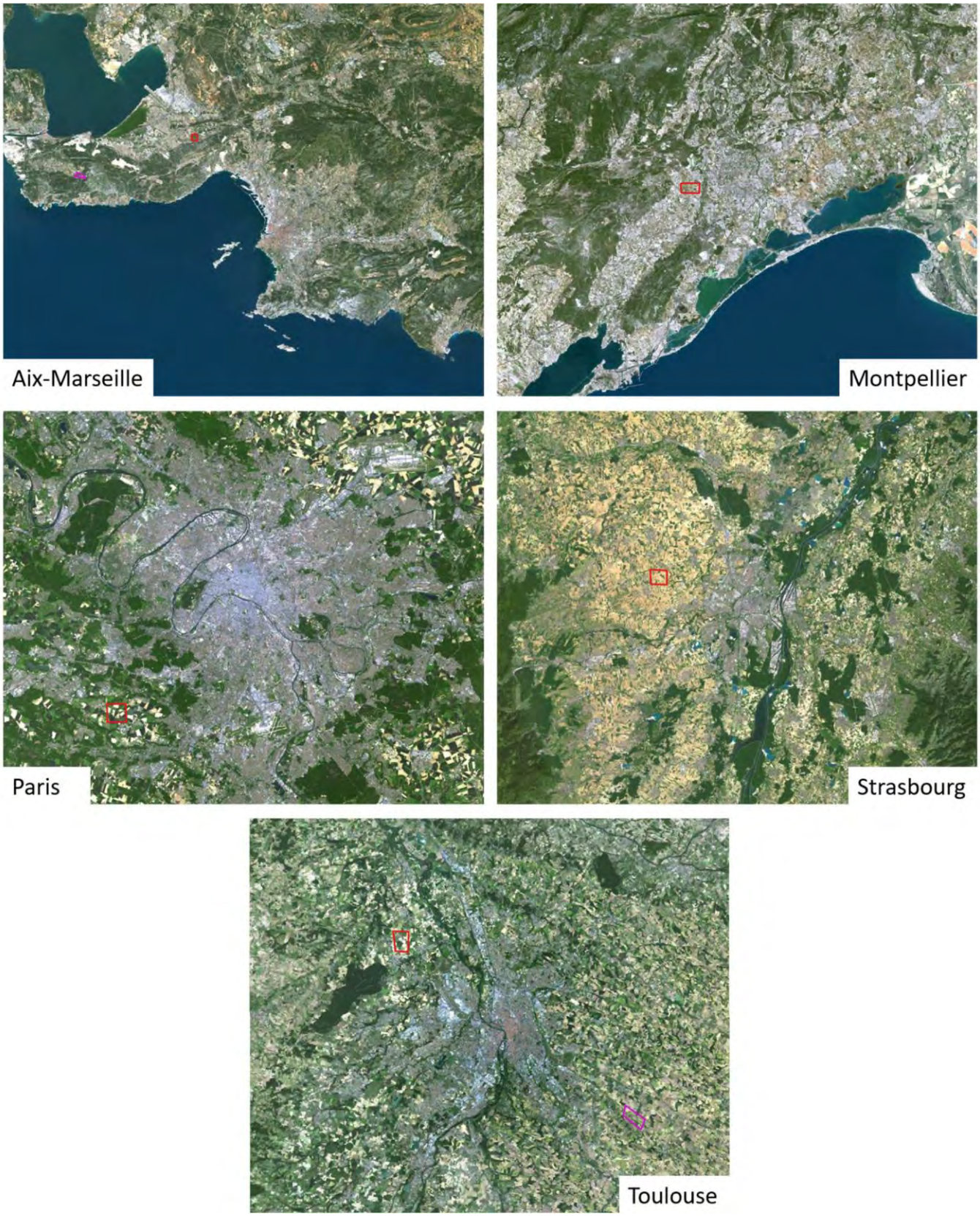

Figure 7: Location of the reference rural areas for each metropolis (red: main reference area, purple: second reference area for Marseille and Toulouse)

The reference LST derived from the reference rural area for each date and image are provided in Table 20 for ASTER and in Table 21 for ECOSTRESS.

Study area	Date	Acq. time (UTC)	LST rural reference (K)	Stdev LST reference (K)
Aix-Marseille	12/08/2003	10:40:31	313.74	1.79
	30/01/2005	10:34:25	-	-
	14/01/2009	21:35:51	-	-
Montpellier	02/11/2007	10:47:02	292.06	1.07
	29/08/2015	10:42:08	307.57	1.22
	29/08/2015	21:49:08	292.68	0.65
	01/11/2015	21:48:48	281.64	0.72
Paris	01/08/2003	10:57:21	308.69	3.68
	22/10/2004	10:57:11	289.86	0.63
	01/11/2015	21:50:07	280.29	1
	01/11/2015	21:50:16	280.29	1
	03/08/2018	10:53:34	313.47	4.8
	03/08/2018	10:53:43	313.47	4.8
	05/08/2018	21:51:00	289.07	1.3
	05/08/2018	21:51:09	289.07	1.3
Strasbourg	17/02/2003	10:40:41	275.42	0.51
	12/08/2003	10:38:54	312.74	3.13
	26/01/2017	21:24:47	264.7	0.37
	22/06/2018	21:26:19	283.28	0.49
Toulouse	14/01/2003	10:54:28	277.77	0.78
	10/08/2003	10:52:42	315.82	6.72
	28/12/2016	21:54:33	273.88	0.72
	23/06/2018	11:01:15	304.71	2.56

Table 20: Reference temperatures in K for each metropolis and date to compute the SUHI using LST from ASTER

Study area	Date	Acq. time (UTC)	LST rural reference	Stdev LST reference
Aix-Marseille	27/08/2018	11:25:30	308.94	0.7
	27/02/2019	10:13:14	292.14	0.47
	15/07/2019	21:56:27	293.34	0.24
	05/01/2020	01:21:31	275.28	0.39
	07/08/2020	12:01:37	318.72	0.69
Montpellier	27/08/2018	11:25:30	311.2	0.93
	27/02/2019	10:13:14	295.06	0.42
	15/07/2019	21:56:27	293.55	0.62
	05/01/2020	01:21:31	275.38	0.71
	11/01/2020	22:59:17	273.27	0.44
	07/08/2020	12:01:37	318.79	1.21
Paris	28/08/2018	10:33:02	305.14	2.37
	15/02/2019	10:49:09	282.08	0.36
	15/07/2019	23:33:19	284.48	0.76
	21/01/2020	23:03:59	269.69	0.66
	07/08/2020	13:38:46	317.3	2.77
Strasbourg	22/08/2018	12:32:48	311.79	1.98
	17/09/2018	22:47:10	283.49	0.56
	15/02/2019	10:50:01	280.57	0.56
	08/08/2020	12:52:13	317.39	2.1
Toulouse	20/08/2018	09:24:48	306.31	1.48
	13/02/2019	10:54:26	283.12	0.53
	15/07/2019	21:55:35	288.73	1.34
	11/01/2020	22:59:17	271.54	0.57
	07/08/2020	12:00:45	315.73	1.94

Table 21: Reference temperatures in K for each metropolis and date to compute the SUHI using LST from ECOSTRESS

After a visual check of the reference temperature and a comparison with the mean LST values computed over the entire area, it appears that the following ones may be overestimated:

- ECOSTRESS image acquired over Aix-Marseille on the 07/08/2020-12:01:37
- ECOSTRESS image acquired over Strasbourg 08/08/2020-12:52:13
- ECOSTRESS image acquired over Toulouse 20/08/2018- 09:24:48

The analysis of produced SUHI maps showed that, overall:

- Winter images, both day and night, do not always show a strong contrast between the city and the rural environment. However, some interesting thermal anomalies show up on some images
- The summer daytime images show high positive LST difference for both built-up and the bare ground surfaces. Wooded areas (forest or parks) generally stand out well in "cool" areas
- The summer night images highlight the urban heat island effect
- A distinct effect of the topography can be seen on some maps

These conclusions remain very general. It is important to deepen the analysis image by image, especially for the results obtained on the city of Strasbourg, which seem difficult to interpret. The resulting SUHI maps strongly depends on the choice of the reference rural area. For now, there is no clear guideline to select this reference area, which can potentially lead to different SUHI maps. It is then important to interpret them carefully, considering the temperature differences more as a trend which can be interpreted at more or less 2 K (observed variability between reference LST values taken from several potential reference areas in the image for some dates), on top of which estimation error may be added (as mentioned in section 3.4). Cross-referencing with other parameters such as relief, wind, concurrent Sentinel-2 backgrounds could help in this interpretation.

5. CONCLUSIONS AND FUTURE WORKS

The first step of the THERMOCITY project was to provide updated LST maps with an improved version of the TES algorithm developed for urban areas and, when possible, finer-scale LST maps based on state-of-the-art empirical disaggregation methods. Five metropolises were investigated: Aix-Marseille, Montpellier, Paris, Strasbourg and Toulouse. Several ASTER and ECOSTRESS standard data products were used along with the Imperviousness Density product from Copernicus, the BD Topo from IGN and atmospheric profiles from MétéoFrance (also part of the THERMOCITY consortium). The updated LST maps were generated using a two MMD relationships TES algorithm applied on ASTER and ECOSTRESS measured TIR radiance, an atmospheric correction being required for ECOSTRESS data. The produced LST have been compared to NASA standard LST products. In the case of ASTER, the simultaneous acquisition in the VNIRand SWIR data allowed to produce downscaled LST at 30 and 15 m when the required data were available. The mains conclusions of this work are:

- The comparison with NASA standard LST product showed a good agreement with the THERMOCITY LST maps, with rather low values obtained for the comparison criteria based on the differences between both products (mainly between 1 and 2 K for the RMSE and -1 and 1 K for the MBE and higher than 0.7 for the Pearson linear correlation coefficient). For ECOSTRESS data, radiometric issues were observed.
- ASTER LST maps were downscaled with a scale factor of 3 and 6 to obtain LST maps at 30 and 15 m with the NDVI, and also NDBI at 30 m. The statistics show a good agreement with the 90 m maps and visual checks showed that fine urban structures could be highlighted thanks to the downscaling.
- For SUHI maps, the choice of the rural reference is crucial. In the end, higher SUHI values were observed over urban district centres, especially during summertime at nighttime.
- The QA layer produced based on expert evaluation and recent literature aims at providing to the users information about the reliability of the LST products by flagging pixels for which higher uncertainties can be expected and thus support better data interpretation.

The LST maps at 90 and 30 m are freely available on the webpage of the THEIA SEC « LST/LSE » and other data is available on request. These products can help institutional users to analyse urban areas or the scientific community to access new datasets.

In the second step of THERMOCITY, these LST maps will be used by CSTB and MétéoFrance, especially for the study of thermal losses or the relationship between SUHI and UHI.

As perspective, different ways of improvements can be considered for this work such as:

- Performing an atmospheric correction adapted to urban areas to improve the accuracy of BOA TIR radiance provided as input of the TES algorithm,
- Investigating the best cost-effective and efficient classification to be used for natural/artificial differentiation to apply the two MMD TES algorithm,
- Deepening the SUHI analysis and investigate a procedure to find the optimal temperature rural reference,
- Changing the disaggregation configuration by downscaling ASTER maps with the Sentinel-2 reflective sensor,
- Establishing a correction factor for the 3D structure impact on LST retrieval in the TES algorithm.

6. BIBLIOGRAPHY

[1] https://land.copernicus.eu/user-corner/technical-library/hrl-imperviousness-technical-document-prod-2015 and
https://land.copernicus.eu/user-corner/technical-library/clms_hrl_imd_validation_report_sc04_1_3.pdf

[2] https://geoservices.ign.fr/sites/default/files/2021-07/DC_BDTOPO_3-0_0.pdf

[3] Dirksen, M.; Ronda, R.J. ; Theeuwes, N.E.; Pagani, G.A. Sky view factor calculations and its application in urban heat island studies. Urban Climate 2019, 30, 100498. doi.org/10.1016/j.uclim.2019.100498

[4] Leturgie, Q.; Mondot, A. Geometric correction of ECOSTRESS and ASTER data in the frame of the THERMOCITY project, Technical Note, DNO/OT/LOT-2021.0013697

[5] Poutier L.; Miesch, C.; Lenot, X.; Achard, V.; Boucher, Y. COMANCHE and COCHISE: two reciprocal atmospheric codes for hyperspectral remote sensing. AVIRIS Earth Science and Applications Workshop Proceedings, 2002.

[6] Gillespie, A.; Rokugawa, S.; Matsunaga, T.; Cothern, J.S.; Hook, S.; Kahle, A.B. A temperature and emissivity separation algorithm for Advanced Spaceborne Thermal Emission and Reflection Radiometer (ASTER) images. IEEE Transactions on Geoscience and Remote Sensing 1998, 36, 1113–1126. doi:10.1109/36.700995

[7] Michel, A.; Granero-Belinchon, C.; Cassante, C.; Boitard, P.; Briottet, X.; Adeline, K.; Poutier, L.; Sobrino, J. A new material-oriented TES for Land Surface Temperature and SUHI Retrieval in urban areas: case study over Madrid in the framework of the future TRISHNA mission. Submitted

[8] Sobrino, J.A.; Jiménez-Muñoz, J.C.; Zarco-Tejada, P.J.; Sepulcre-Cantó, G.; de Miguel, E. Land surface temperature derived from airborne hyperspectral scanner thermal infrared data. Remote Sensing of Environment 2006, 102(1-2), 99 – 115. doi:10.1016/j.rse.2006.02.001

[9] Granero-Belinchon, C.; Michel, A.; Lagouarde, J.P.; Sobrino, J.; Briottet, X. Multi-Resolution Study of Thermal Unmixing Techniques over Madrid Urban Area: Case Study of TRISHNA Mission. Remote Sensing 2019, 11(10), 1251. doi:10.3390/rs11101251

[10] Zheng, X.; Gao, M.; Li, Z.L.; Chen, K.S.; Zhang, X.; Shang, G. Impact of 3-D Structures and Their Radiation on Thermal Infrared Measurements in Urban Areas. IEEE Transactions on Geoscience and Remote Sensing 2020, 58(12), 8412-8426. doi:10.1109/TGRS.2020.2987880

[11] Roupioz, L.; Nerry, F.; Colin, J. Correction for the Impact of the Surface Characteristics on the Estimation of the Effective Emissivity at Fine Resolution in Urban Areas. Remote Sensing 2018, 10(5). doi:10.3390/rs10050746

7. APPENDIX

7.1. Appendix A: Comparison of ASTER LST maps at 90 m with the NASA standard products

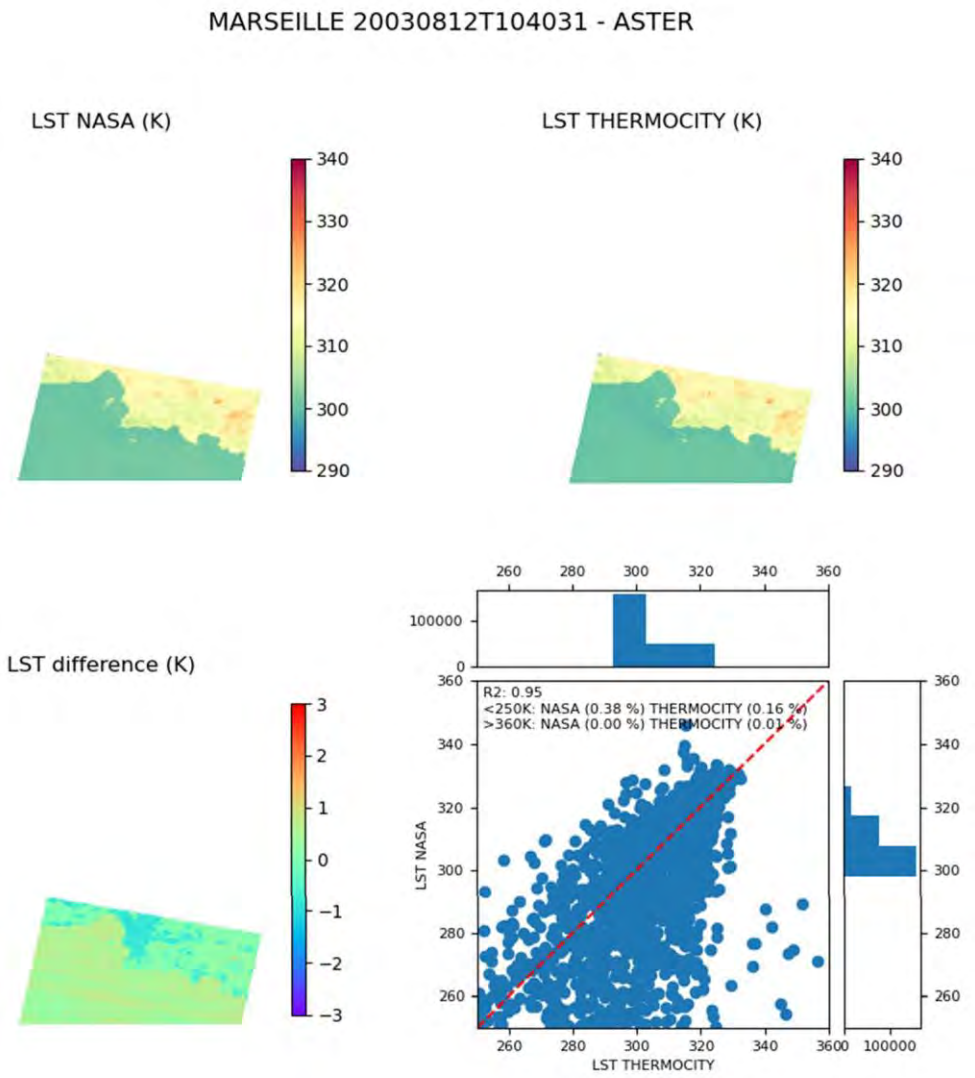

The retrieved temperatures are coherent between the two products. Globally higher temperatures are observed in the THERMOCITY map, as confirmed by the statistics in Table 18 with 1.65 K. These higher temperatures are mainly located on build-up areas. Furthermore, NASA temperatures are higher over water, which can be due to the different TES algorithm or the radiometric quality.

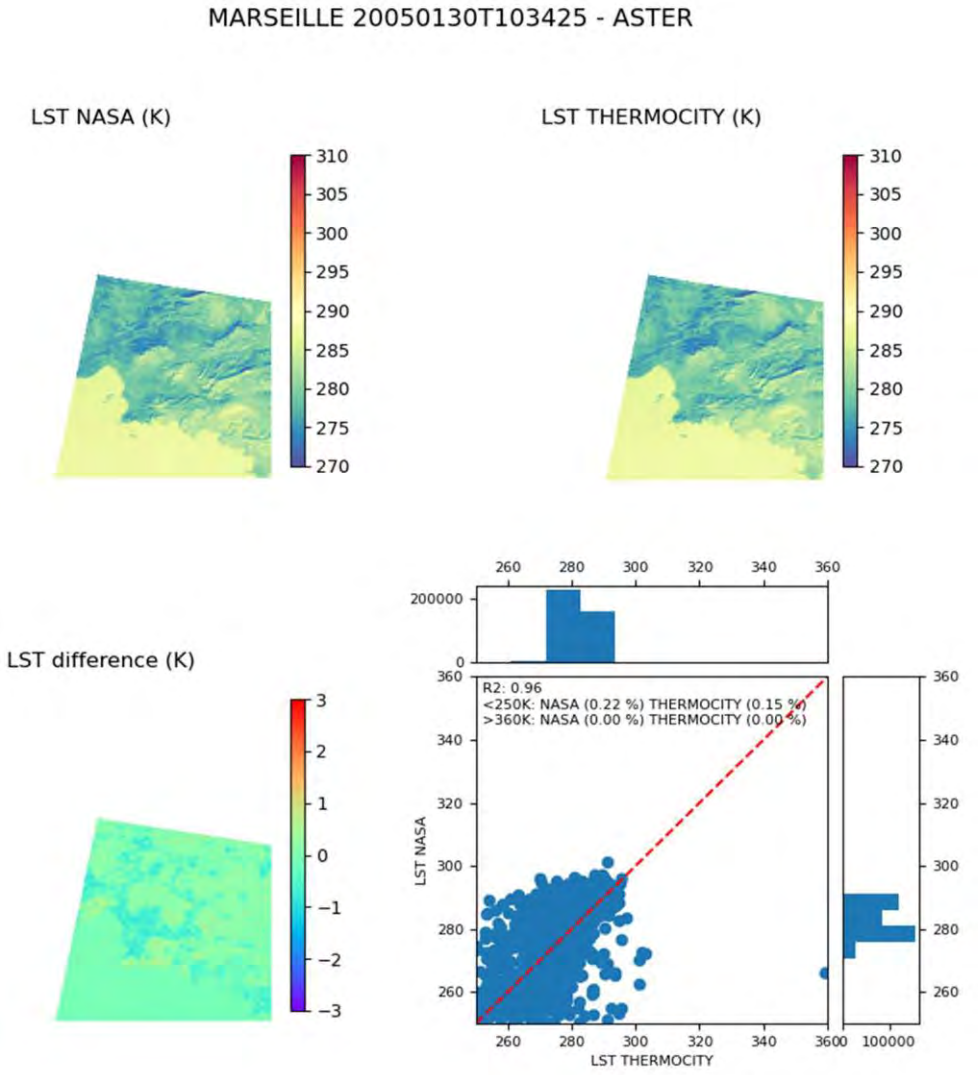

The retrieved temperatures are coherent between the two products. Globally higher temperatures are observed in the THERMOCITY map, as confirmed by the statistics in Table 18 with 0.84 K. These higher temperatures are mainly located on build-up areas and bare ground.

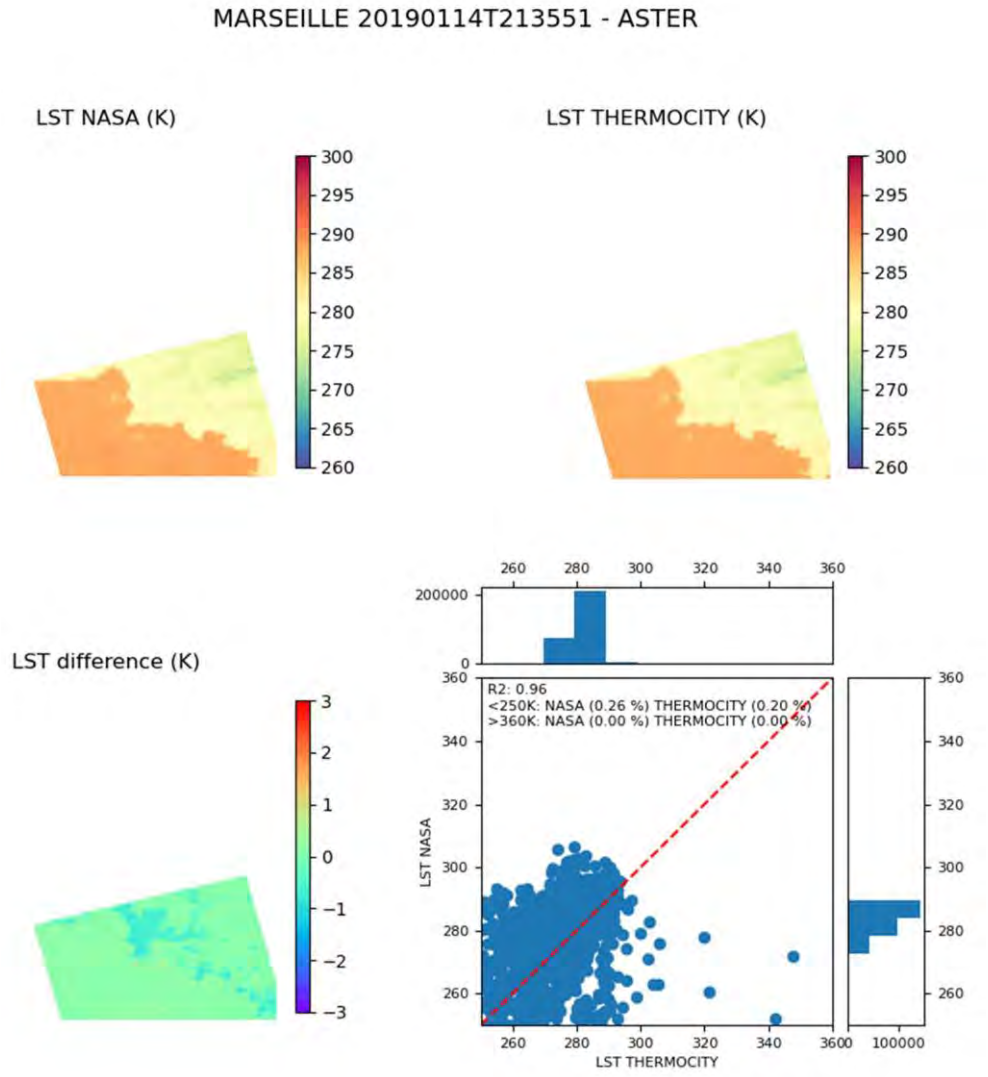

The retrieved temperatures are coherent between the two products. Globally higher temperatures are observed in the THERMOCITY map, as confirmed by the statistics in Table 18 with 0.96 K. These higher temperatures are mainly located on build-up areas and bare ground.

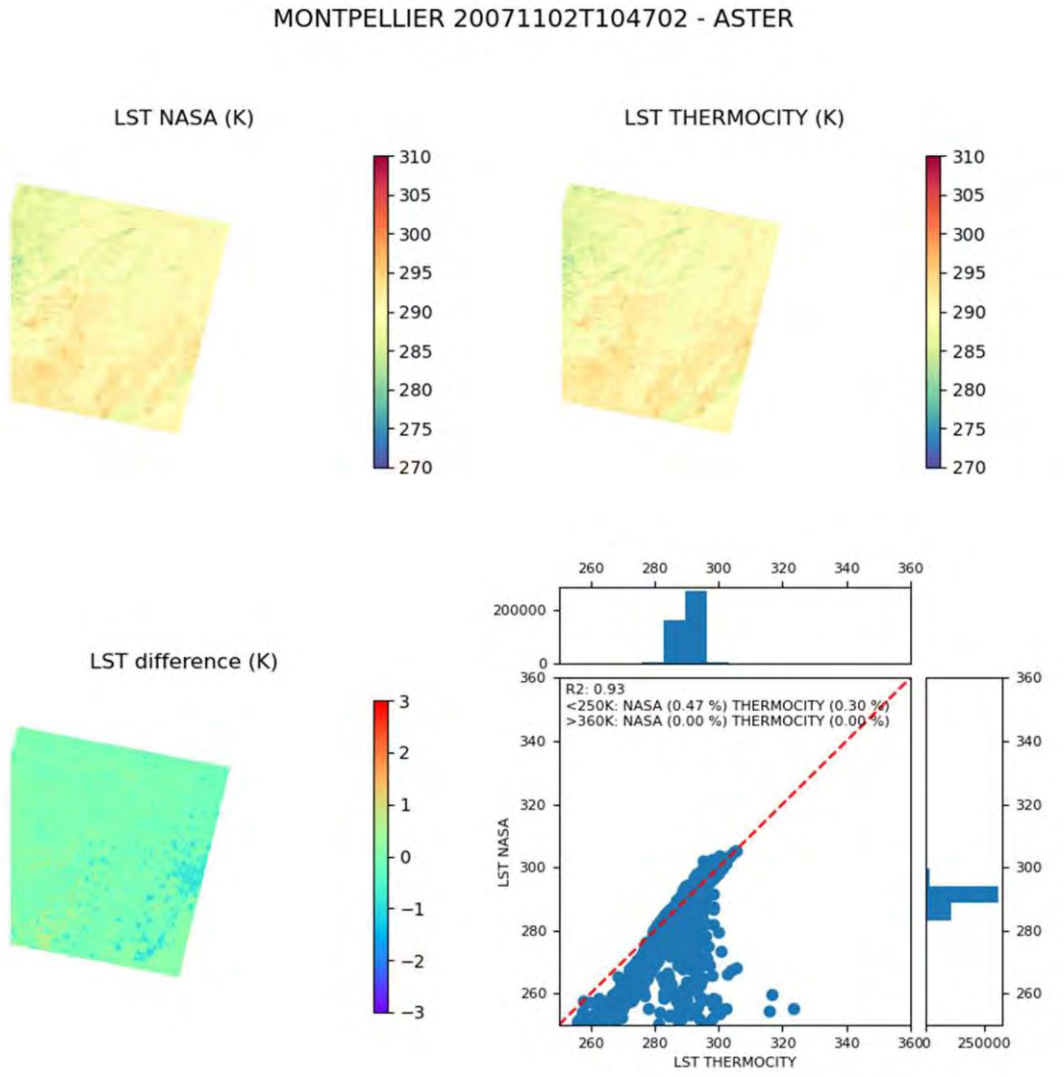

The retrieved temperatures are coherent between the two products. Globally higher temperatures are observed in the THERMOCITY map, as confirmed by the statistics in Table 18 with 0.73 K. These higher temperatures are mainly located on build-up areas and bare ground.

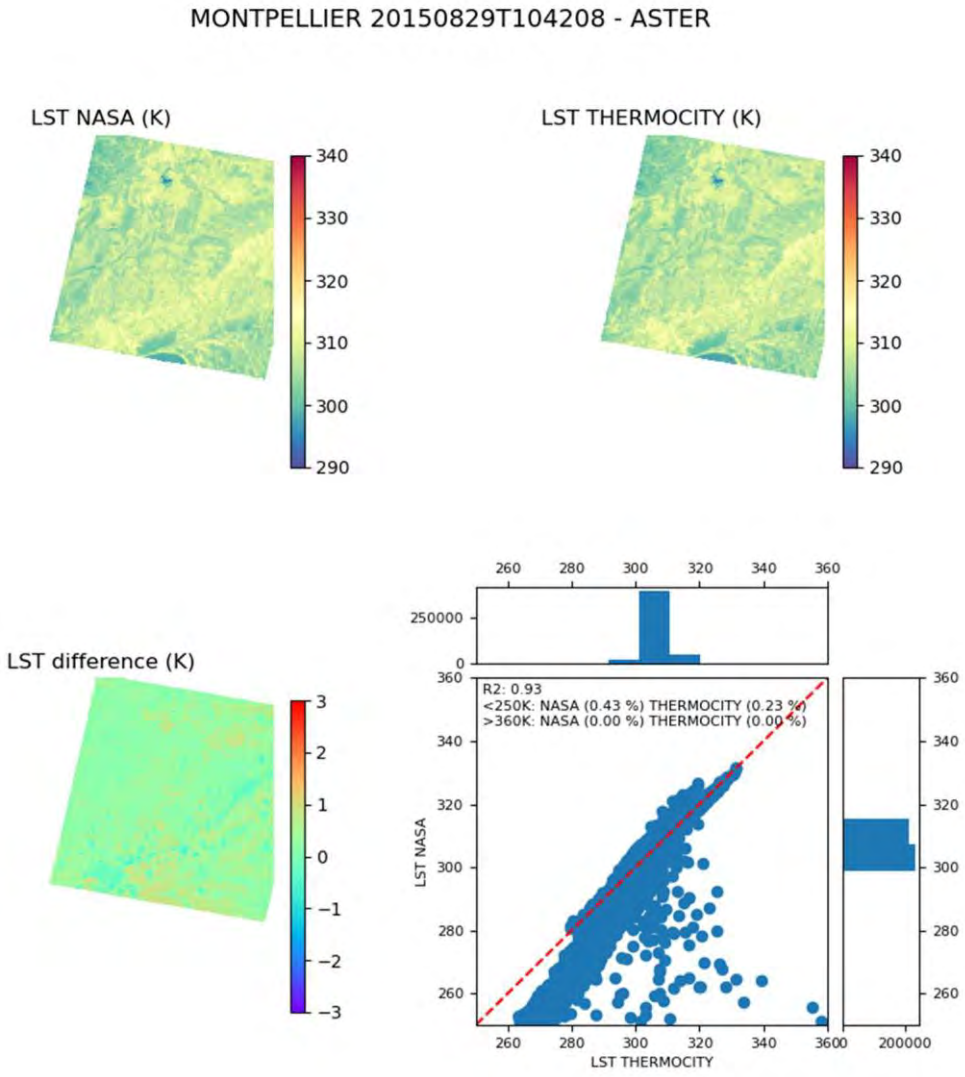

The retrieved temperatures are coherent between the two products. Globally higher temperatures are observed in the THERMOCITY map, as confirmed by the statistics in Table 18 with 0.96 K. These higher temperatures are mainly located on build-up areas and bare ground.

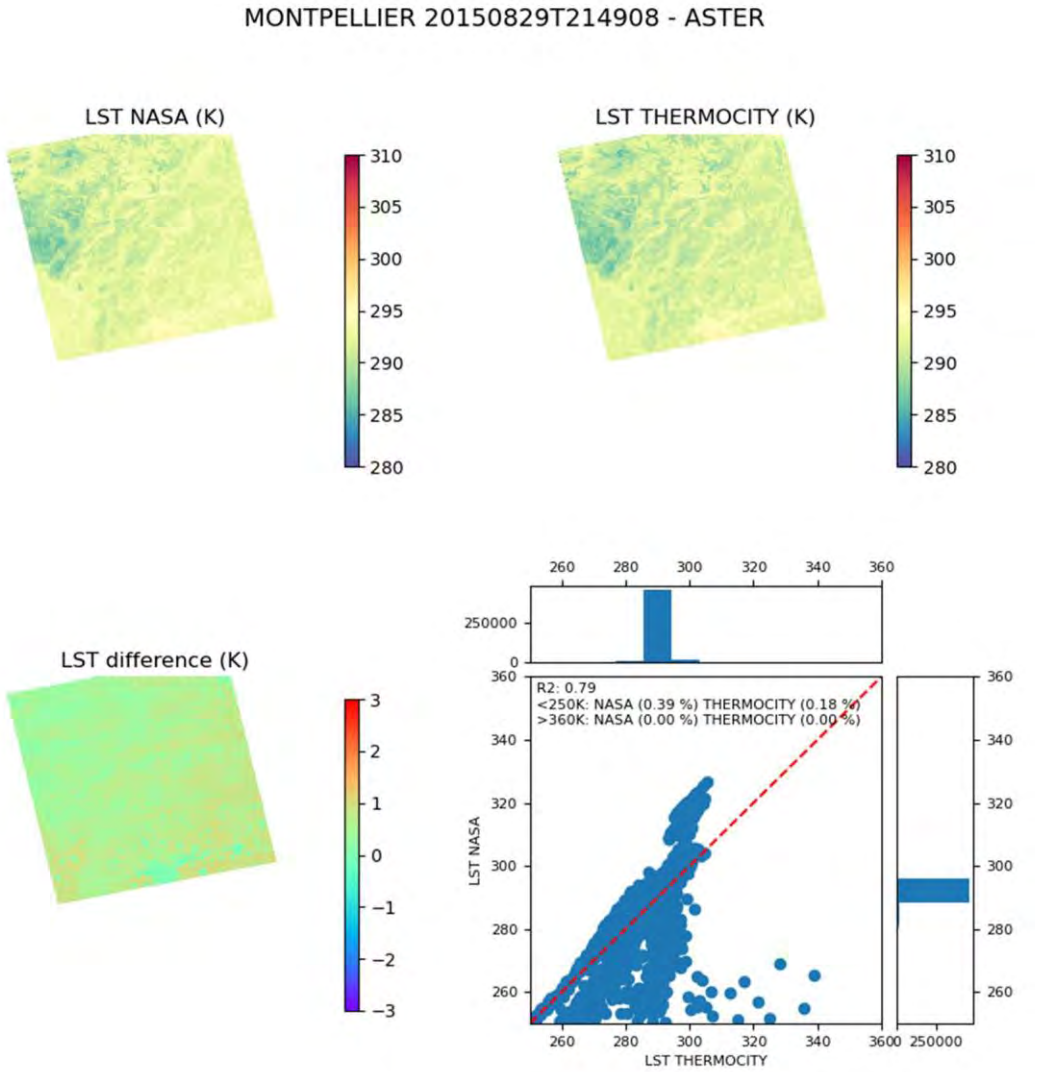

The retrieved temperatures are coherent between the two products. Globally lower temperatures are observed in the THERMOCITY map, as confirmed by the statistics in Table 18 with 1.18 K. These lower temperatures can be due to the radiometric quality (observable stripes in the difference map).

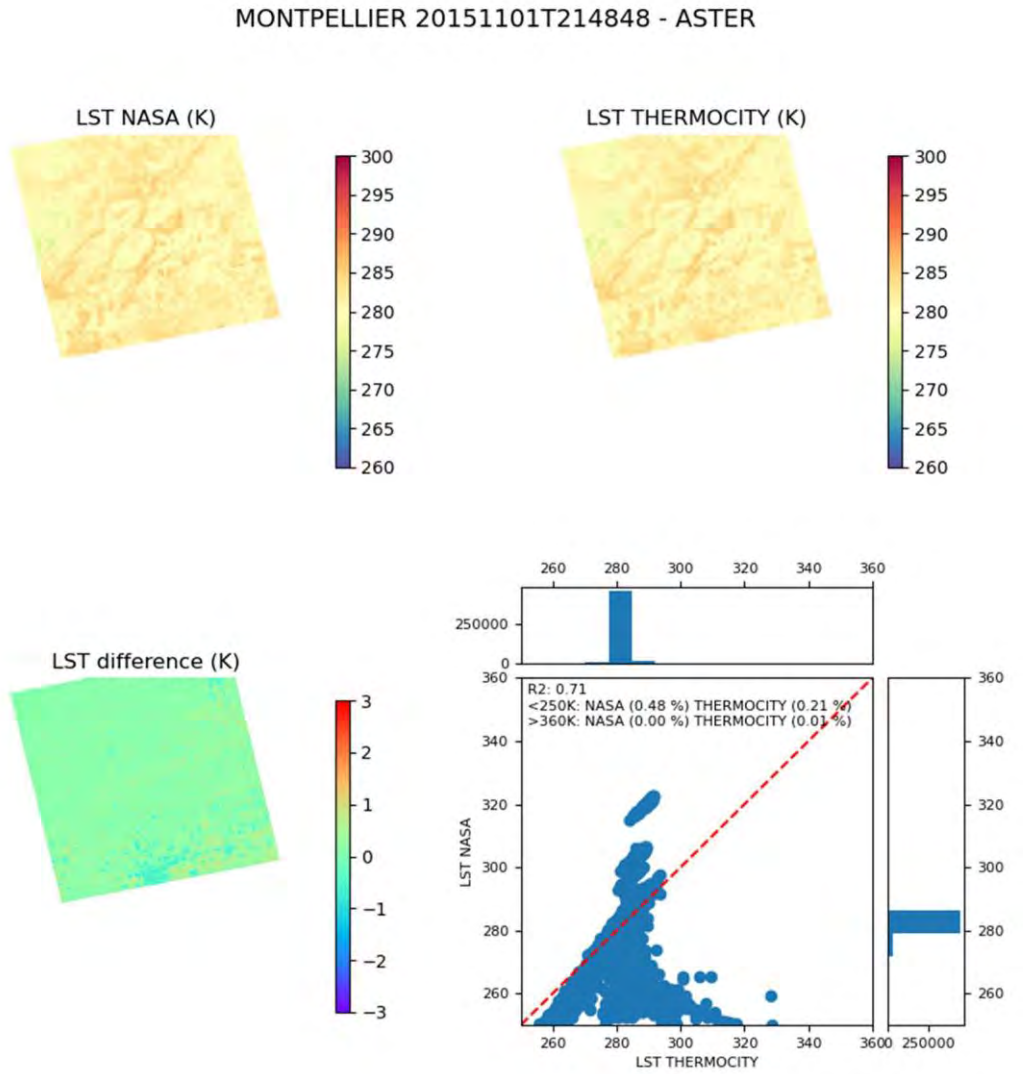

The retrieved temperatures are coherent between the two products. Globally higher temperatures are observed in the THERMOCITY map, as confirmed by the statistics in Table 18 with 1.14 K. These higher temperatures are mainly located on build-up areas and bare ground.

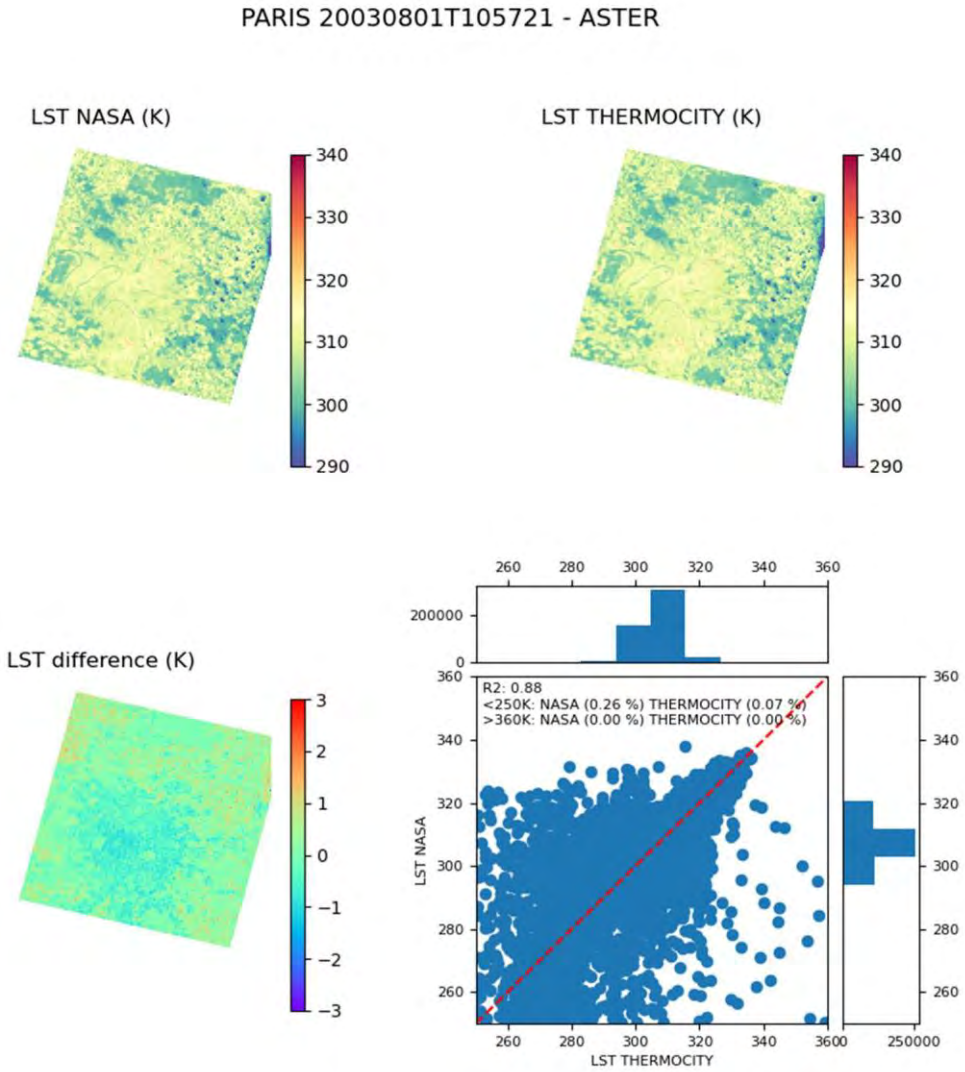

The retrieved temperatures are coherent between the two products. Higher temperatures are observed in the THERMOCITY map, as confirmed by the statistics in Table 18 with 1.97 K. These higher temperatures are mainly located on build-up areas. Lower temperatures are also seen on bare/agricultural grounds and clouds.

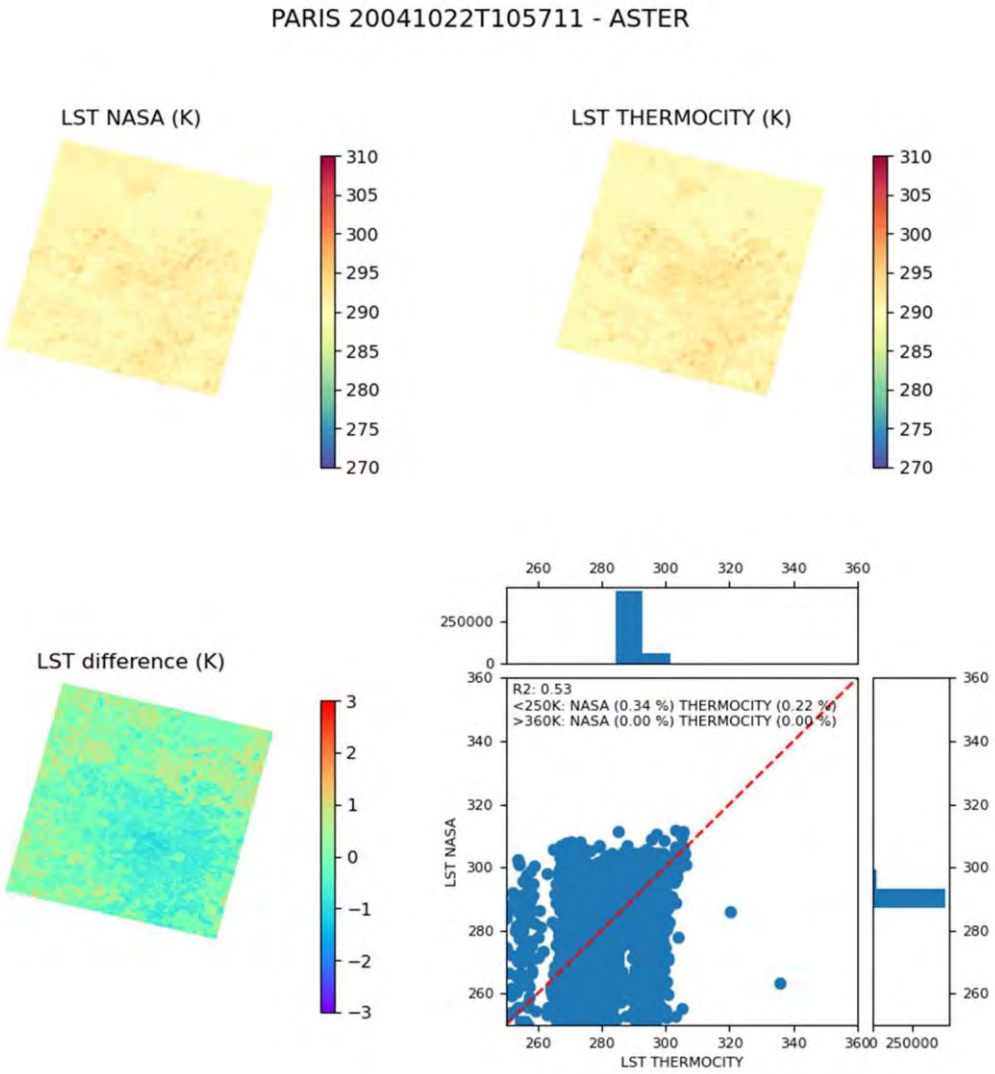

The retrieved temperatures are coherent between the two products. Higher temperatures are observed in the THERMOCITY map, as confirmed by the statistics in Table 18 with 1.34 K. These higher temperatures are mainly located on build-up areas. Lower temperatures are also seen on bare/agricultural grounds. The scatterplot shape might be due to the percentage of outliers.

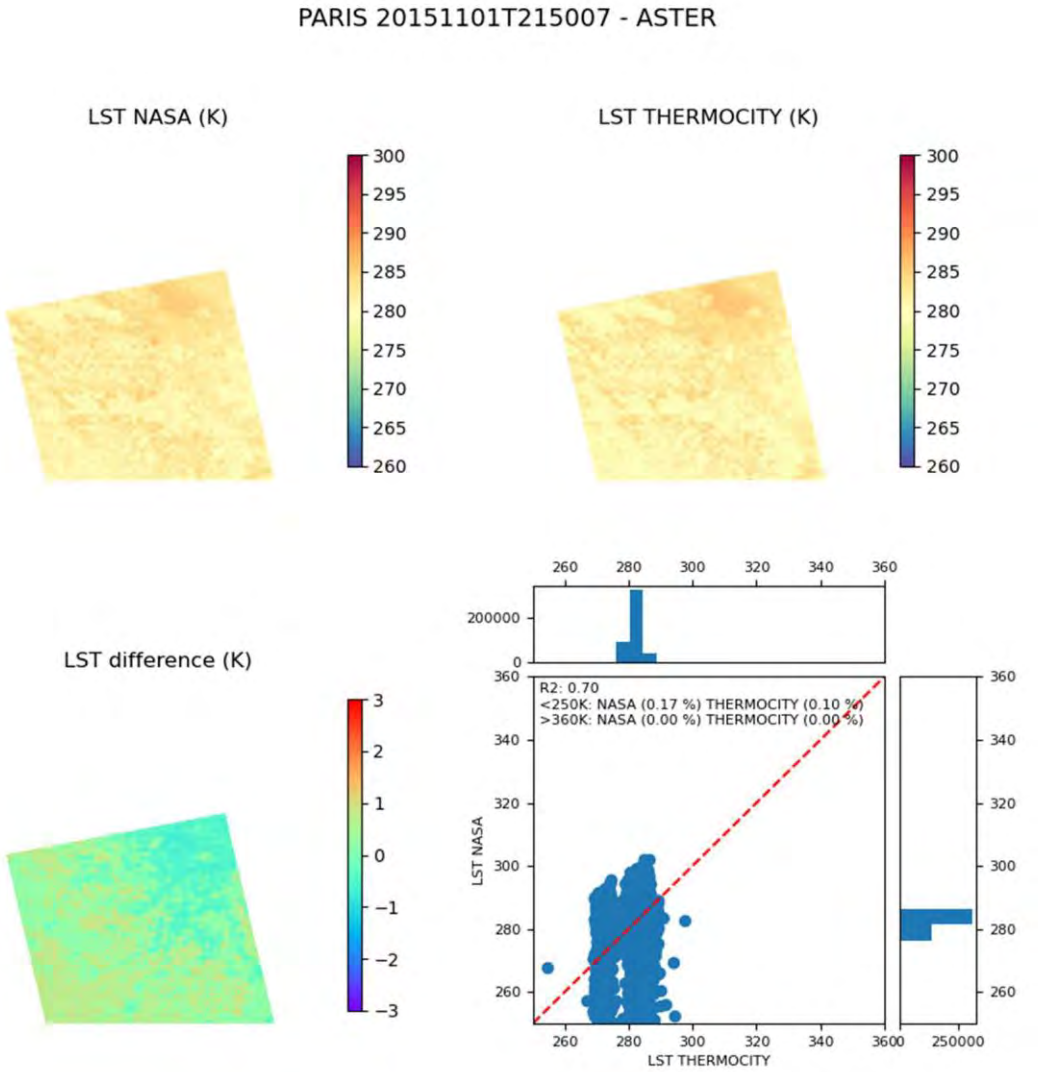

The retrieved temperatures are coherent between the two products. Higher temperatures are observed in the THERMOCITY map, as confirmed by the statistics in Table 18 with 1.06 K. These higher temperatures are mainly located on build-up areas. Lower temperatures are also seen on bare/agricultural grounds.

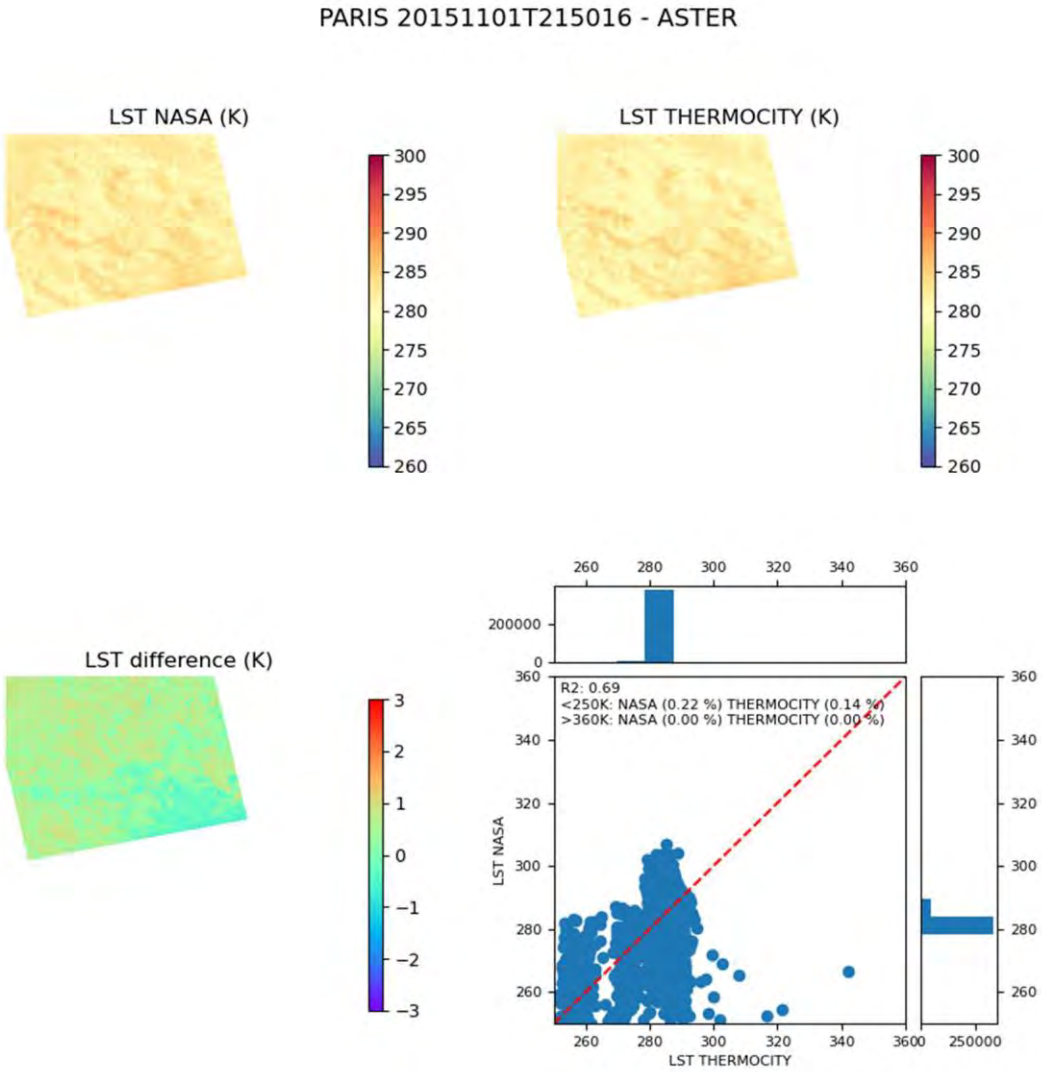

The retrieved temperatures are coherent between the two products. Higher temperatures are observed in the THERMOCITY map, as confirmed by the statistics in Table 18 with 1.05 K. These higher temperatures are mainly located on build-up areas. Lower temperatures are also seen on bare/agricultural grounds.

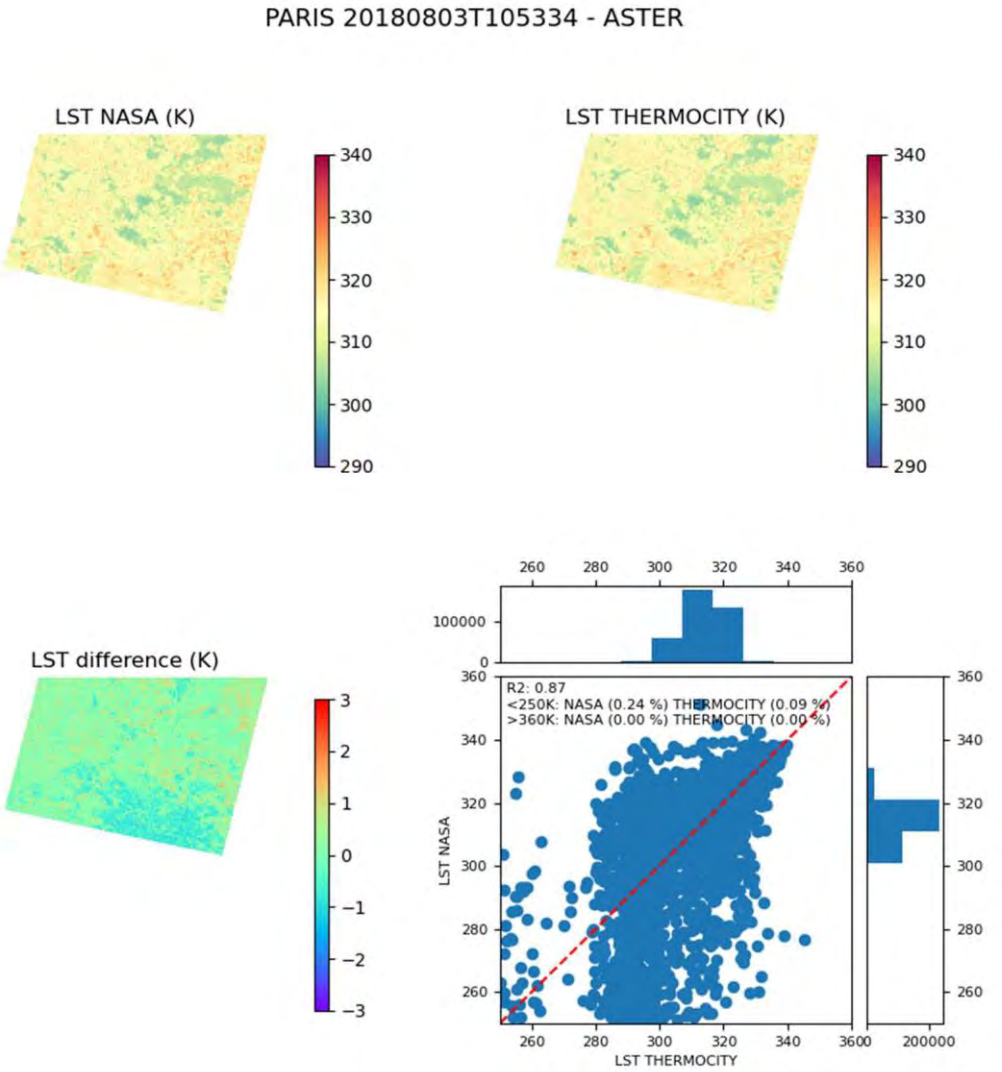

The retrieved temperatures are coherent between the two products. Higher temperatures are observed in the THERMOCITY map, as confirmed by the statistics in Table 18 with 1.97 K. These higher temperatures are mainly located on build-up areas. Lower temperatures are also seen on bare/agricultural grounds.

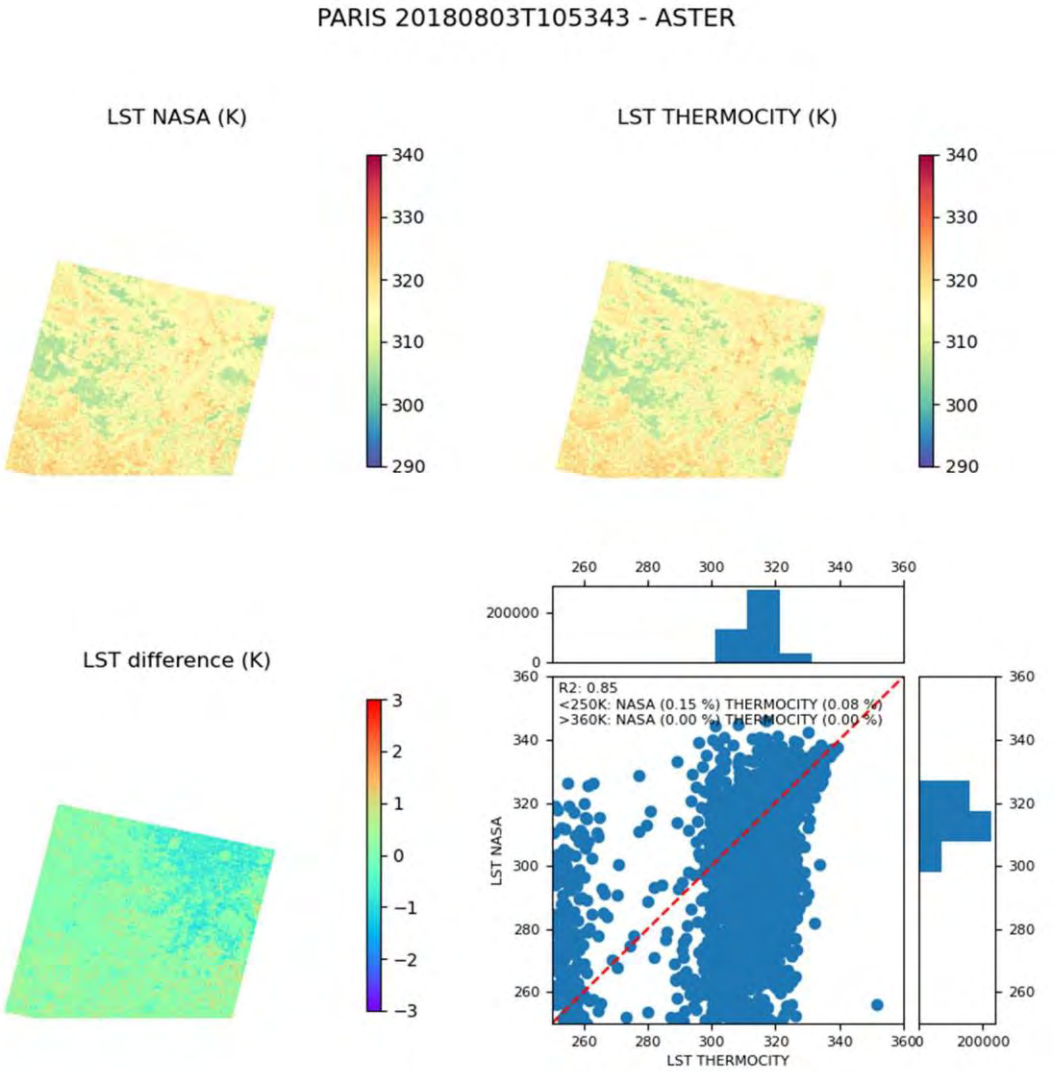

The retrieved temperatures are coherent between the two products. Higher temperatures are observed in the THERMOCITY map, as confirmed by the statistics in Table 18 with 2.13 K. These higher temperatures are mainly located on build-up areas. Lower temperatures are also seen on bare/agricultural grounds.

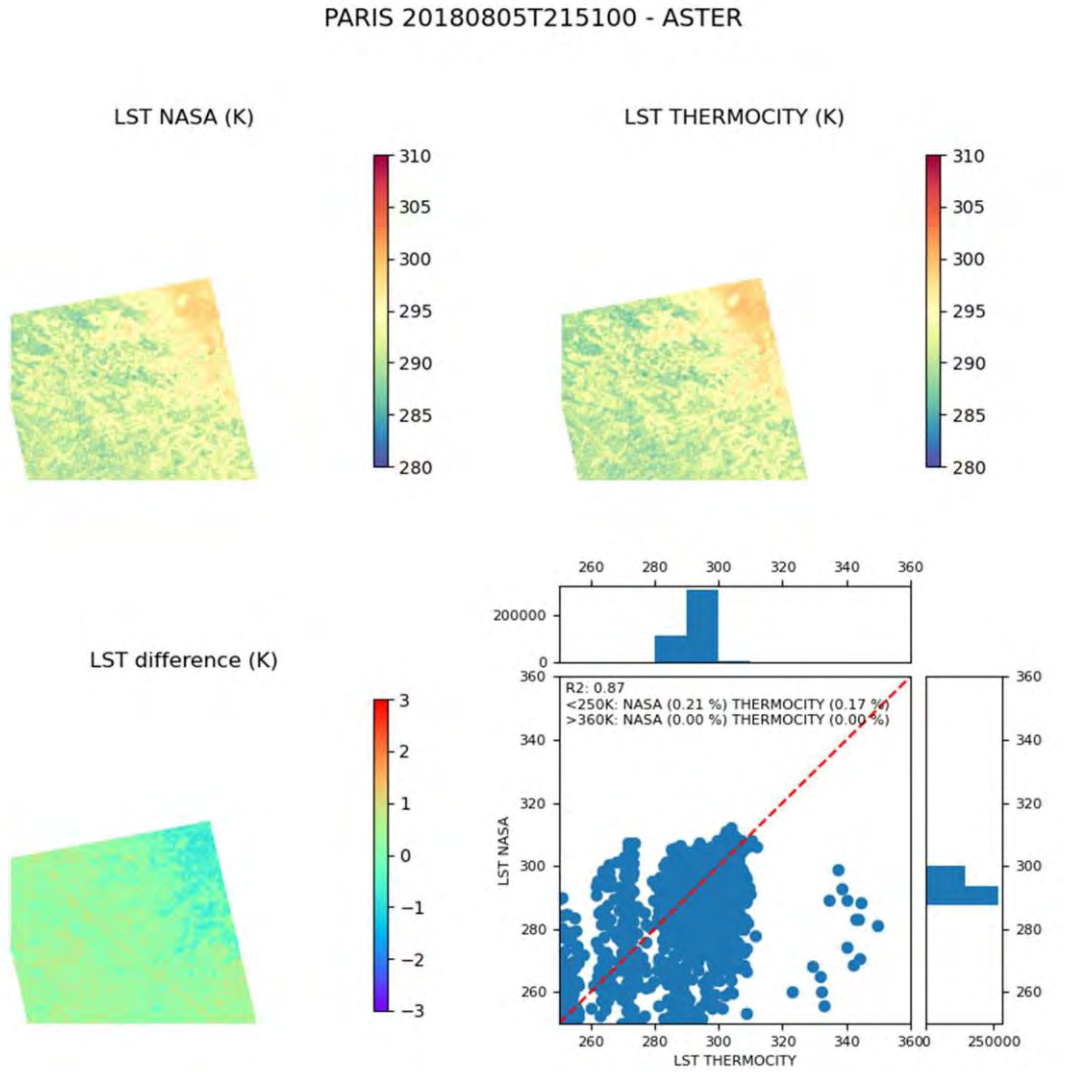

The retrieved temperatures are coherent between the two products. Higher temperatures are observed in the THERMOCITY map, as confirmed by the statistics in Table 18 with 1.2 K. These higher temperatures are mainly located on build-up areas. Lower temperatures are also seen on bare/agricultural grounds.

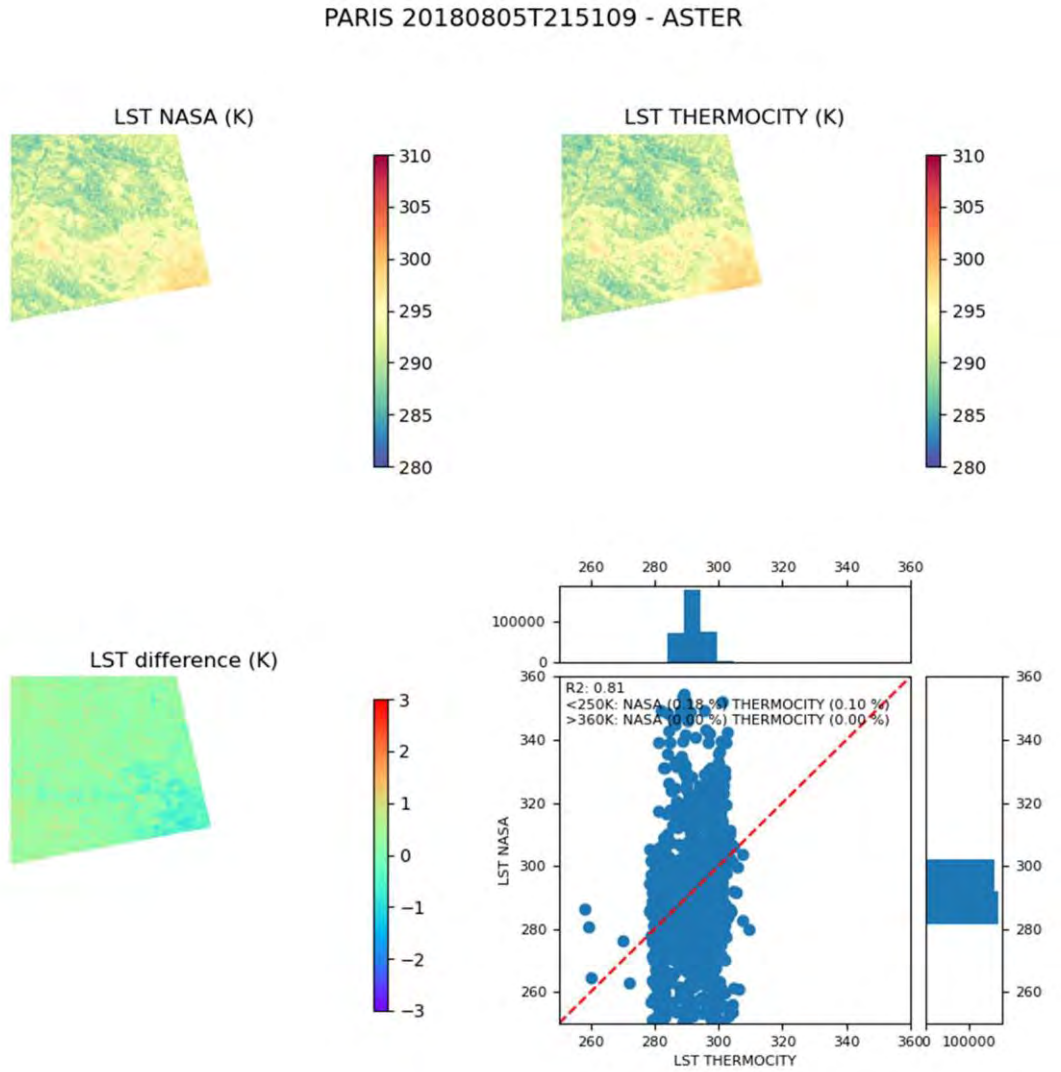

The retrieved temperatures are coherent between the two products. Higher temperatures are observed in the THERMOCITY map, as confirmed by the statistics in Table 18 with 1.45 K. These higher temperatures are mainly located on build-up areas. Lower temperatures are also seen on bare/agricultural grounds.

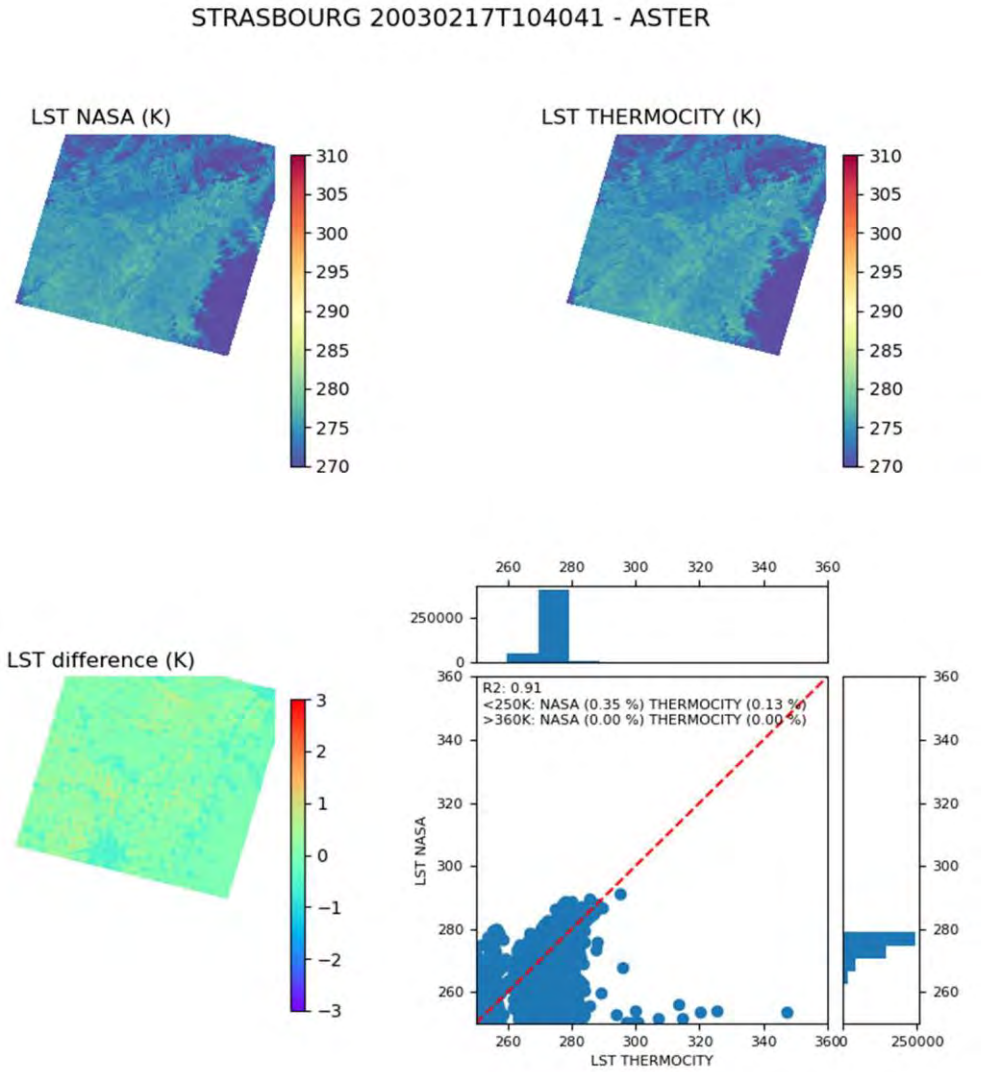

The retrieved temperatures are coherent between the two products. Higher temperatures are observed in the THERMOCITY map, as confirmed by the statistics in Table 18 with 0.91 K. These higher temperatures are mainly located on build-up areas. This image contains clouds.

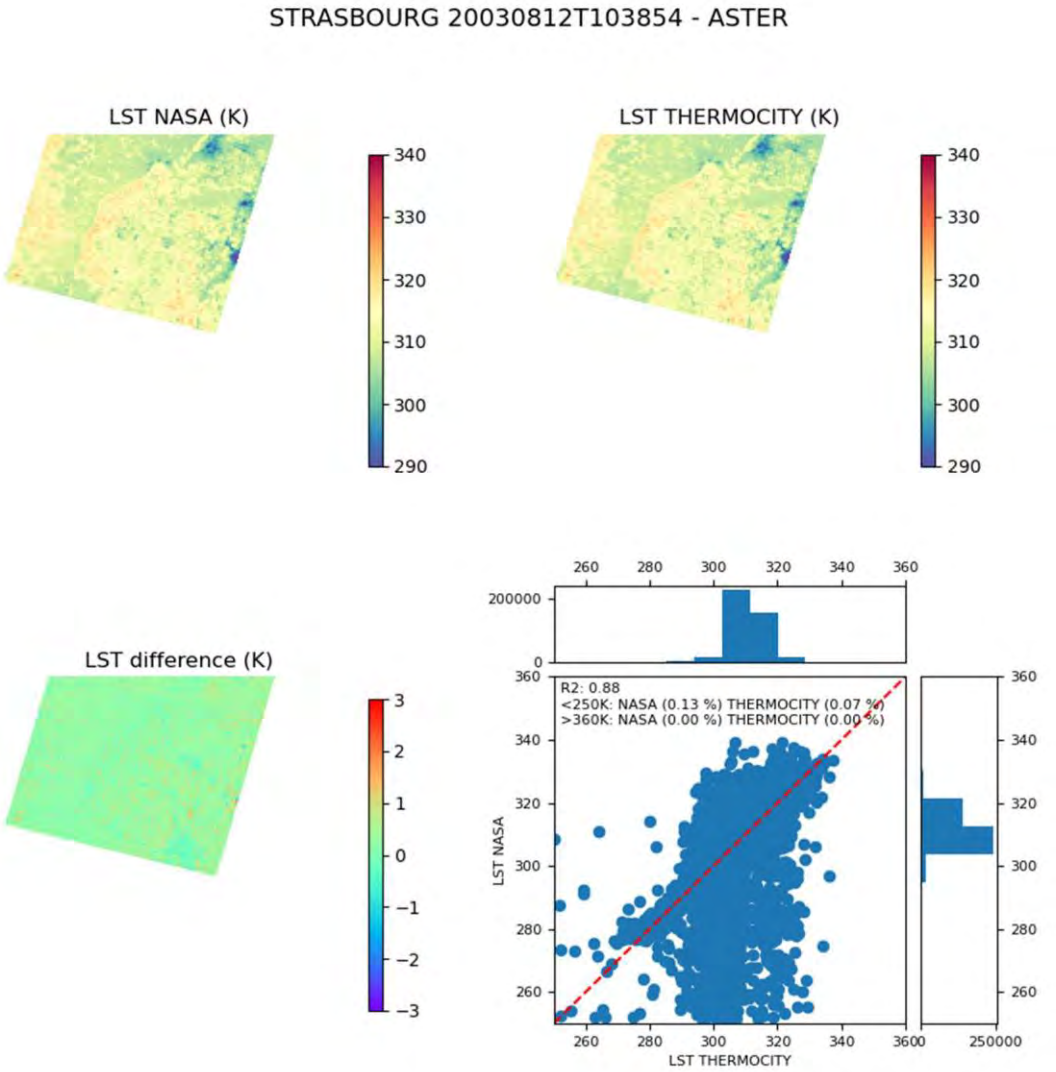

The retrieved temperatures are coherent between the two products. Higher temperatures are observed in the THERMOCITY map, as confirmed by the statistics in Table 18 with 1.9 K. These higher temperatures are mainly located on build-up areas.

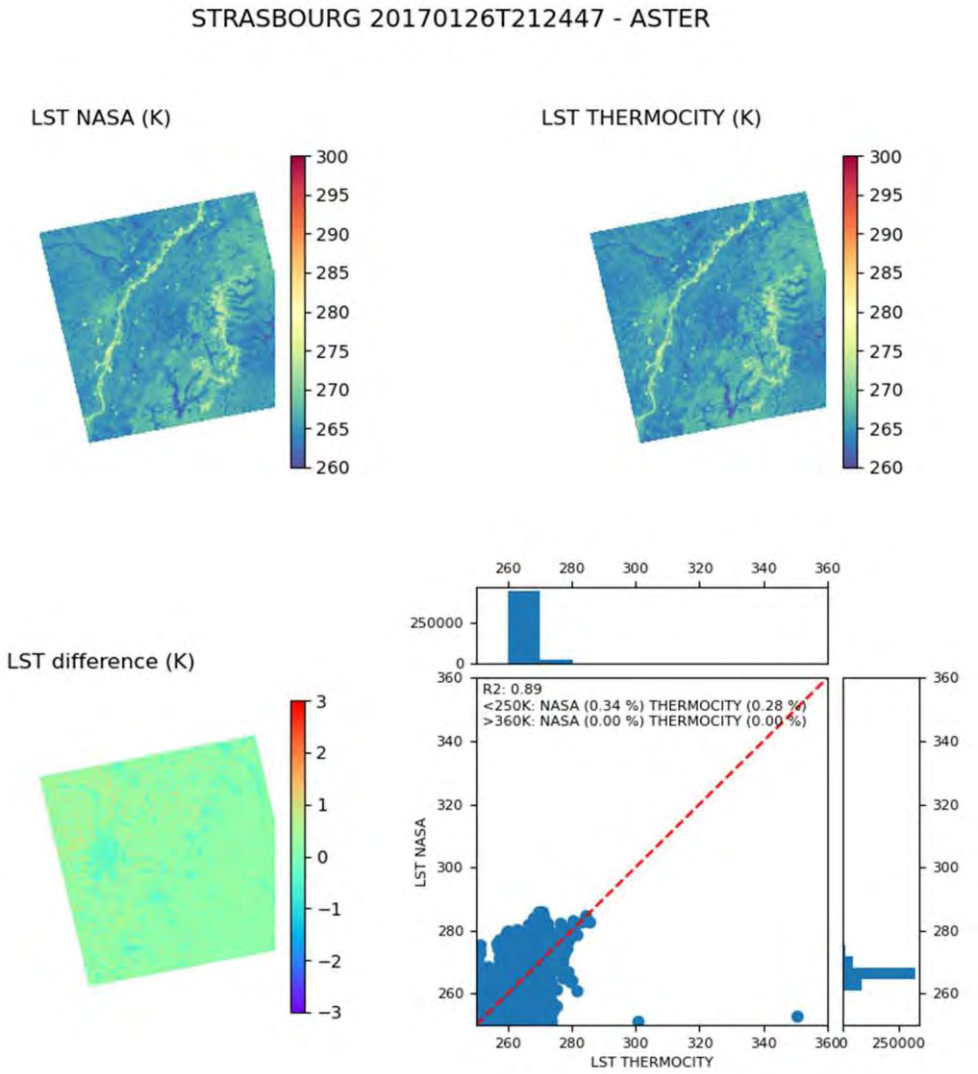

The retrieved temperatures are coherent between the two products. Higher temperatures are observed in the THERMOCITY map, as confirmed by the statistics in Table 18 with 0.78 K. These higher temperatures are mainly located on build-up areas.

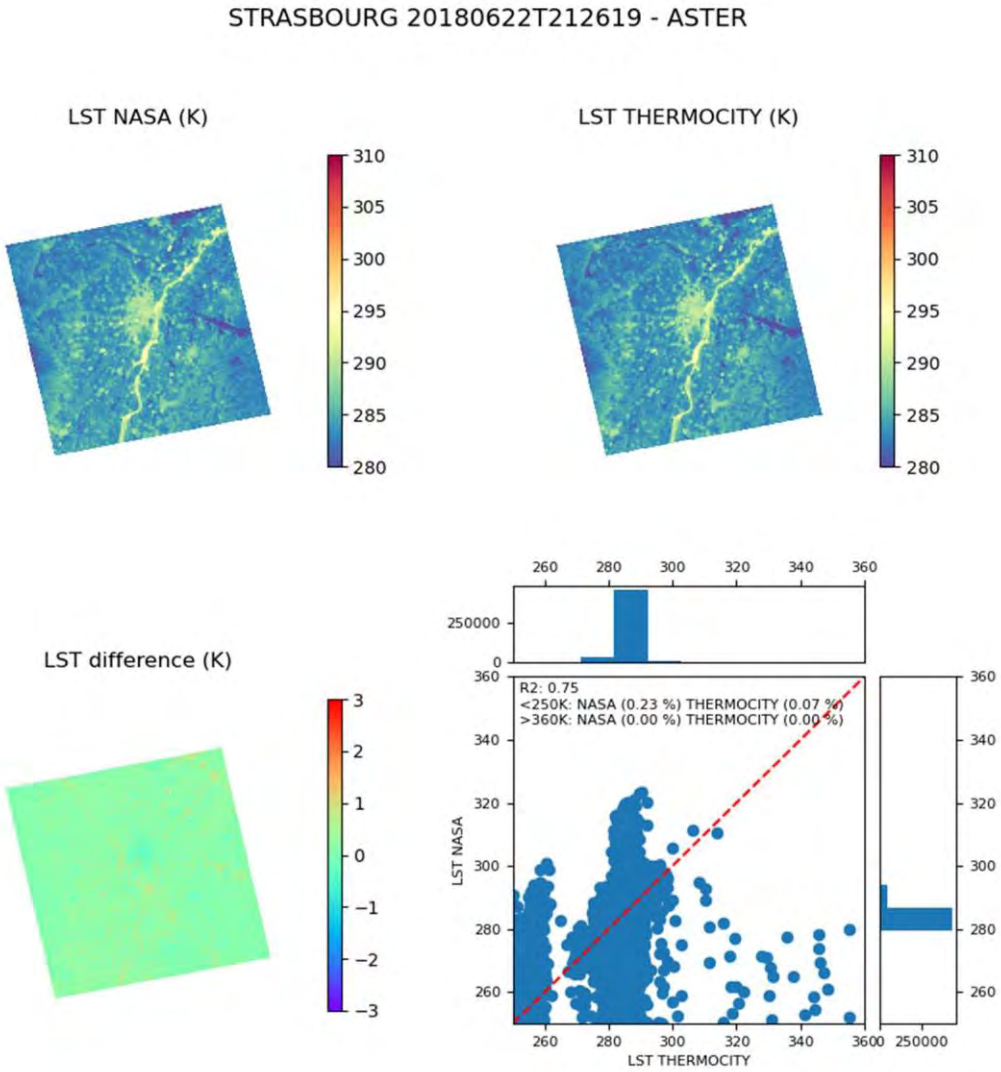

The retrieved temperatures are coherent between the two products. Higher temperatures are observed in the THERMOCITY map, as confirmed by the statistics in Table 18 with 1.34 K. These higher temperatures are mainly located on build-up areas.

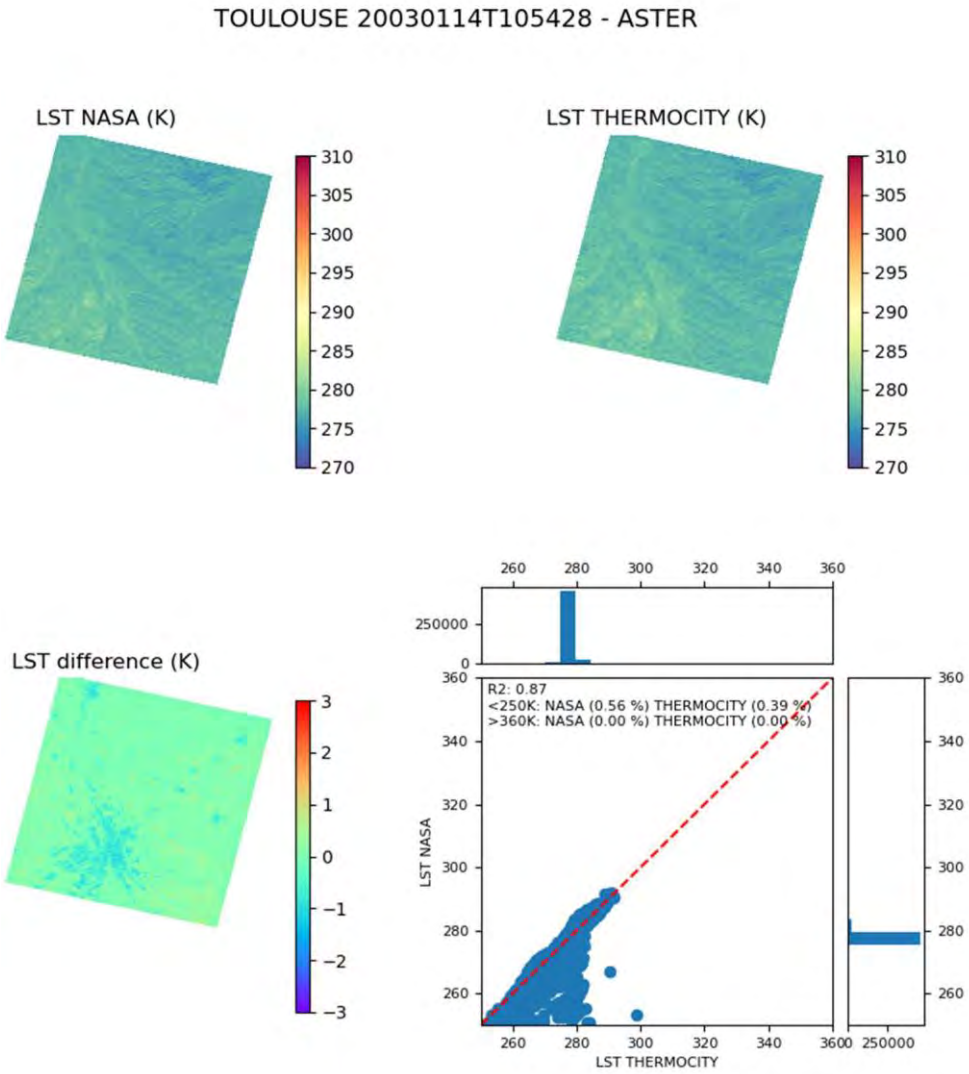

The retrieved temperatures are coherent between the two products. Higher temperatures are observed in the THERMOCITY map, as confirmed by the statistics in Table 18 with 0.52 K. These higher temperatures are mainly located on build-up areas and bare ground.

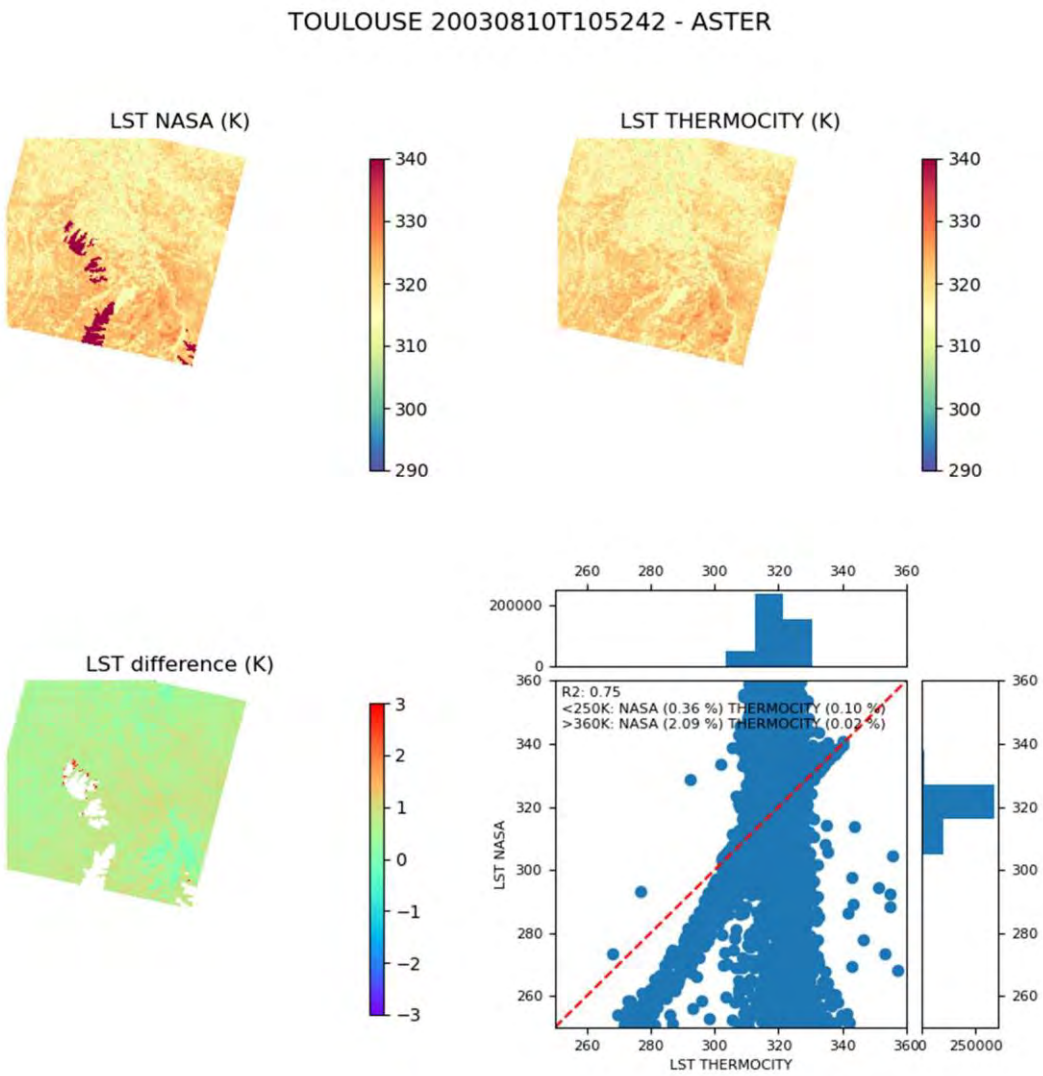

The retrieved temperatures are less coherent between the two products than the other dates as confirmed by the statistics in Table 18 with 2.79 K. This is due to the extreme values (over 250 K) that can be seen. Otherwise, higher temperatures are observed in the THERMOCITY map. These higher temperatures are mainly located on build-up areas.

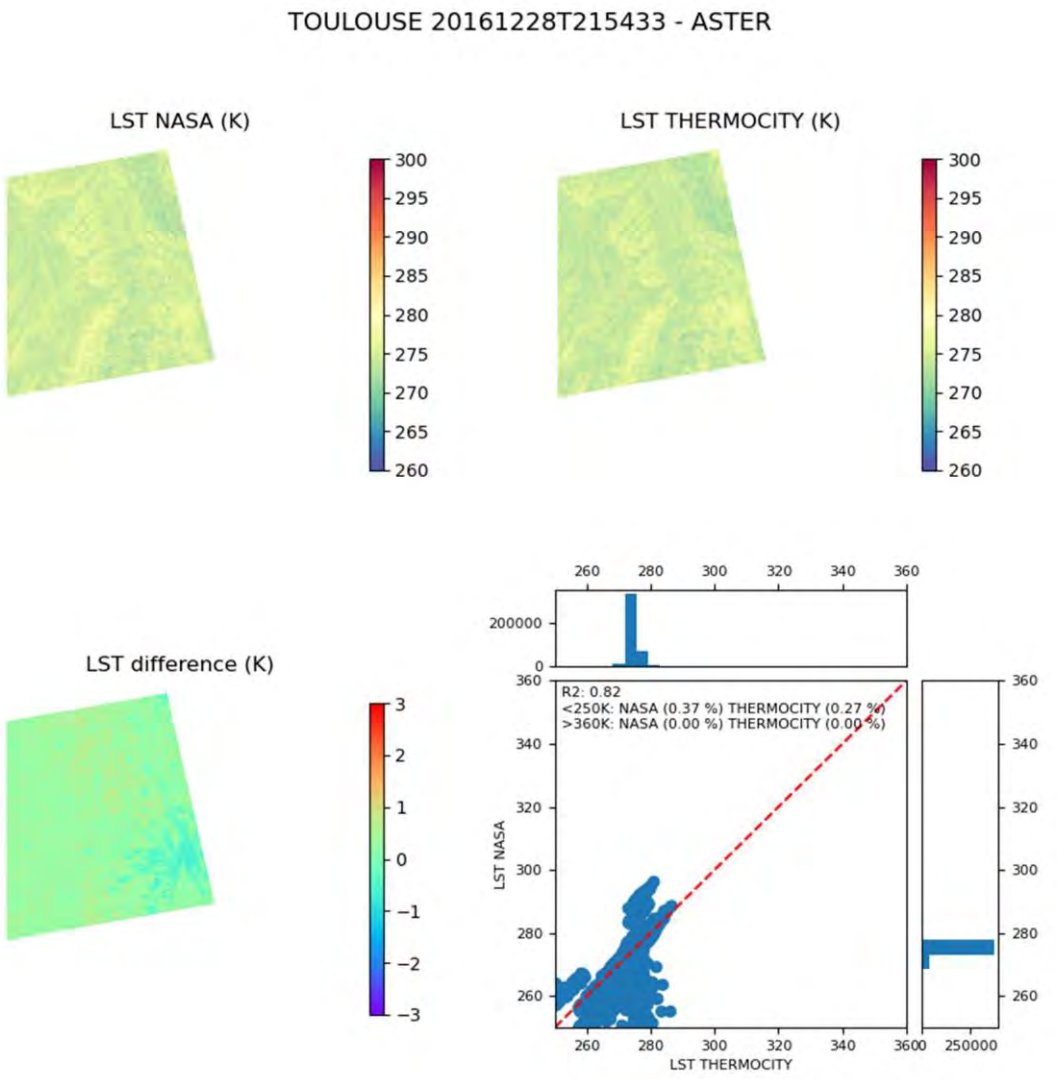

The retrieved temperatures are coherent between the two products. Higher temperatures are observed in the THERMOCITY map, as confirmed by the statistics in Table 18 with 0.69 K. These higher temperatures are mainly located on build-up areas and bare ground.

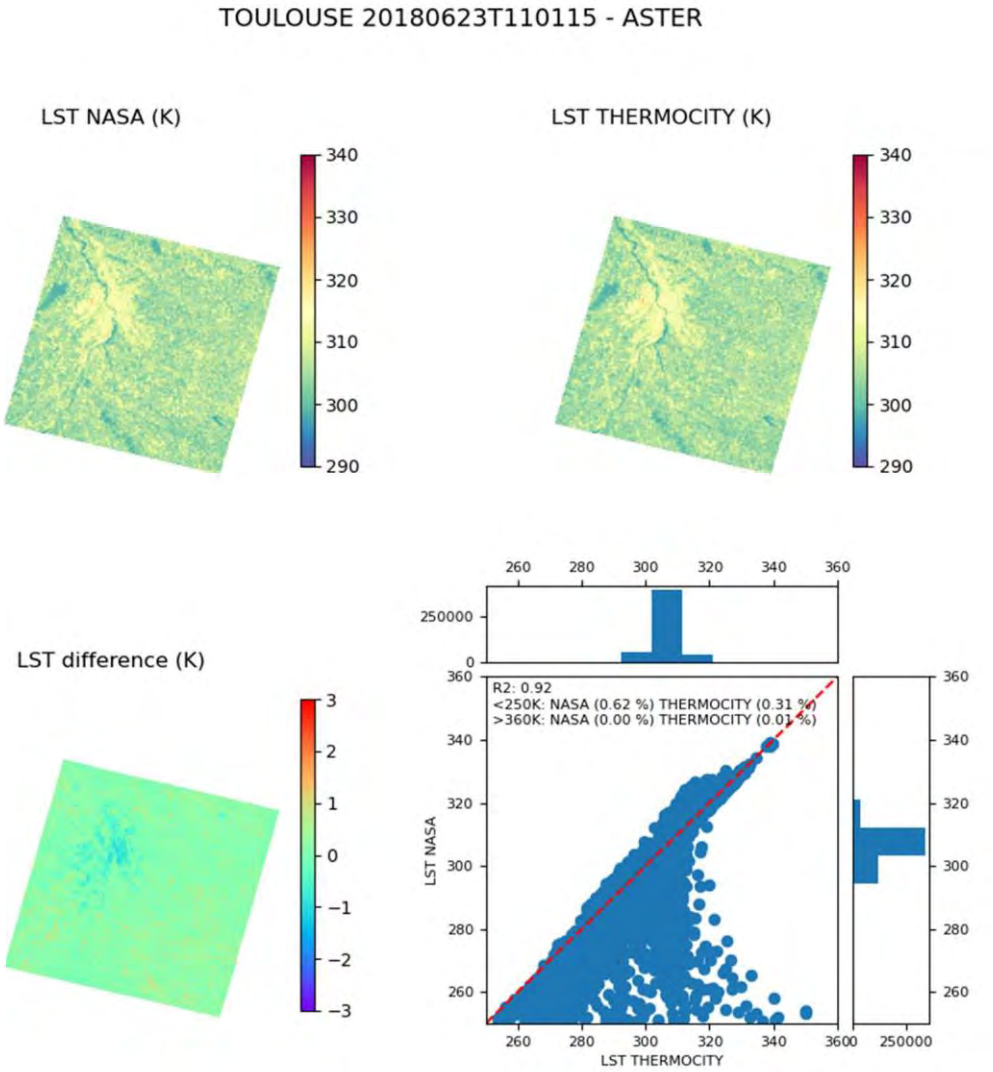

The retrieved temperatures are coherent between the two products. Higher temperatures are observed in the THERMOCITY map, as confirmed by the statistics in Table 18 with 1.22 K. These higher temperatures are mainly located on build-up areas and bare ground.

7.2. Appendix B: ASTER LST maps disaggregated at 30 m and 15 m

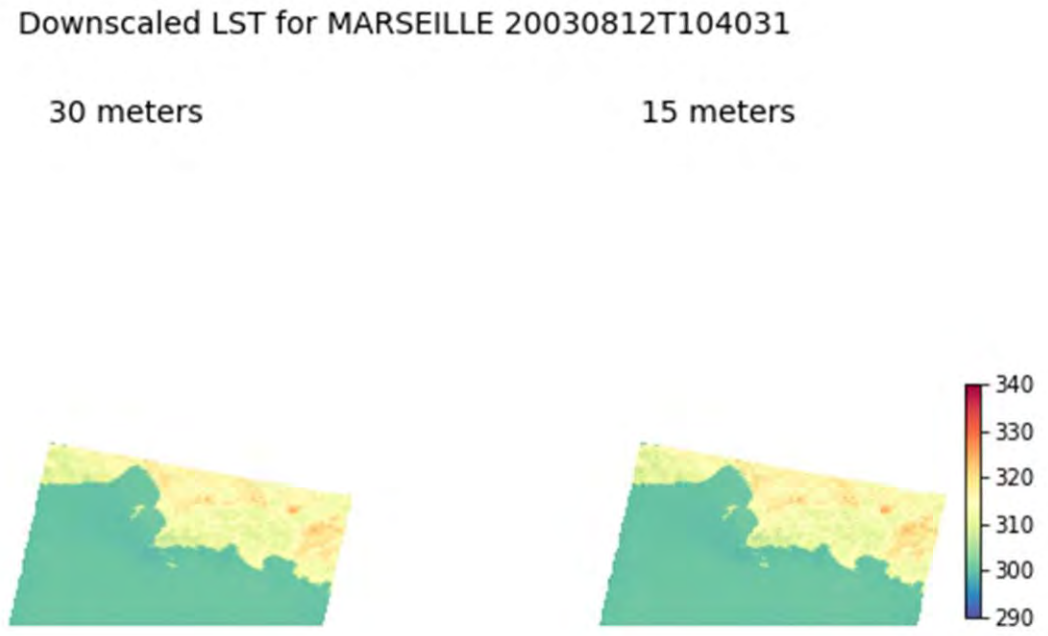

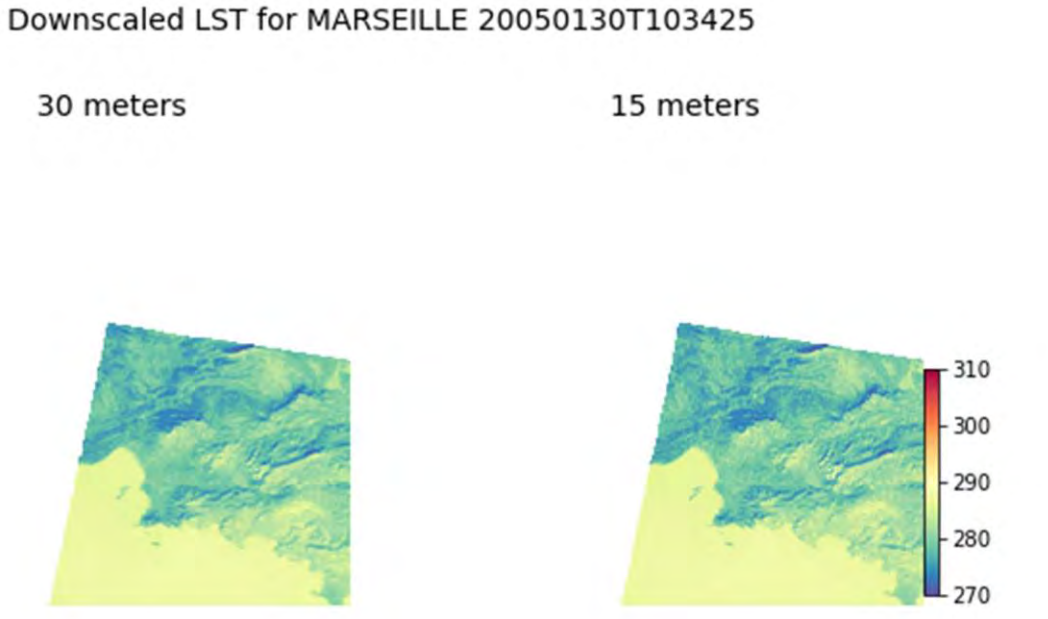

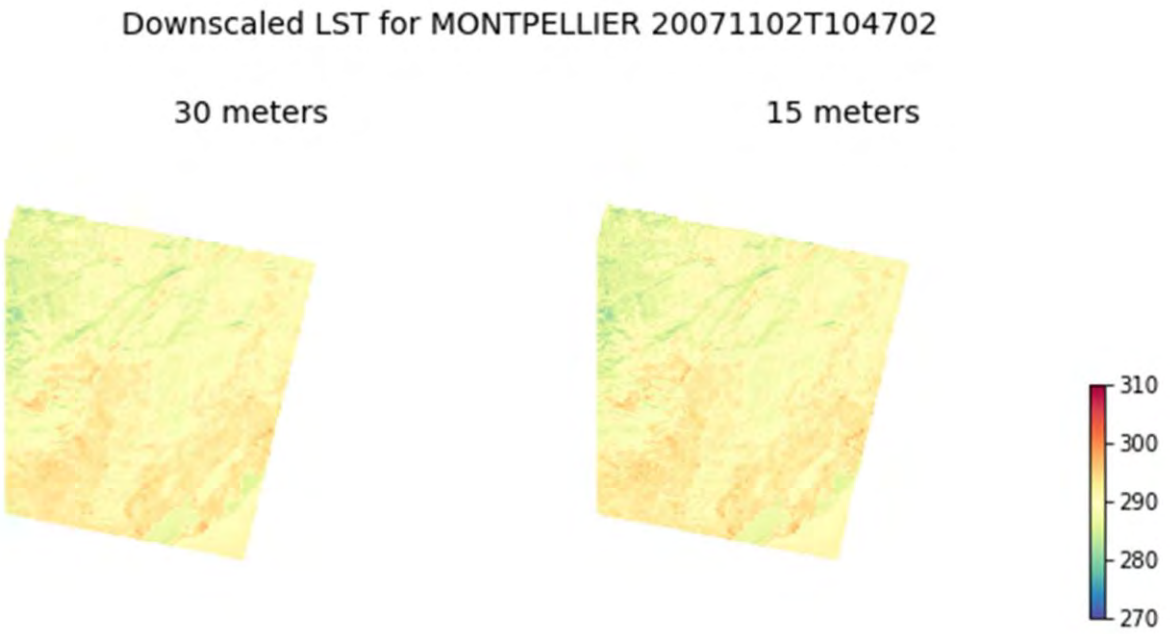
Downscaled LST for MONTPELLIER 20071102T104702
30 meters
15 meters
310
300
290
280
270

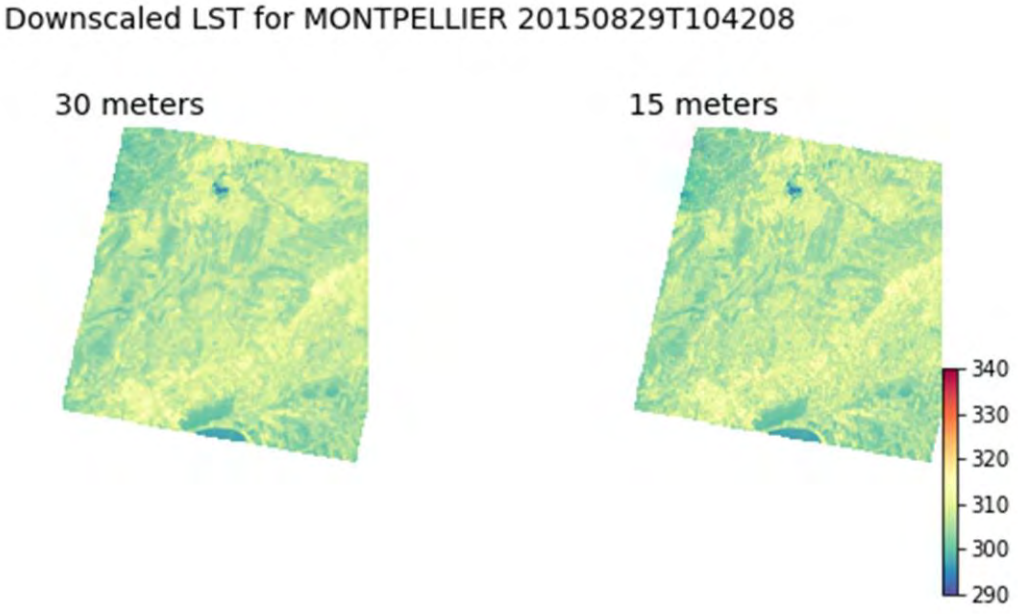
Downscaled LST for MONTPELLIER 20150829T104208
30 meters
15 meters
340
330
320
310
300
290

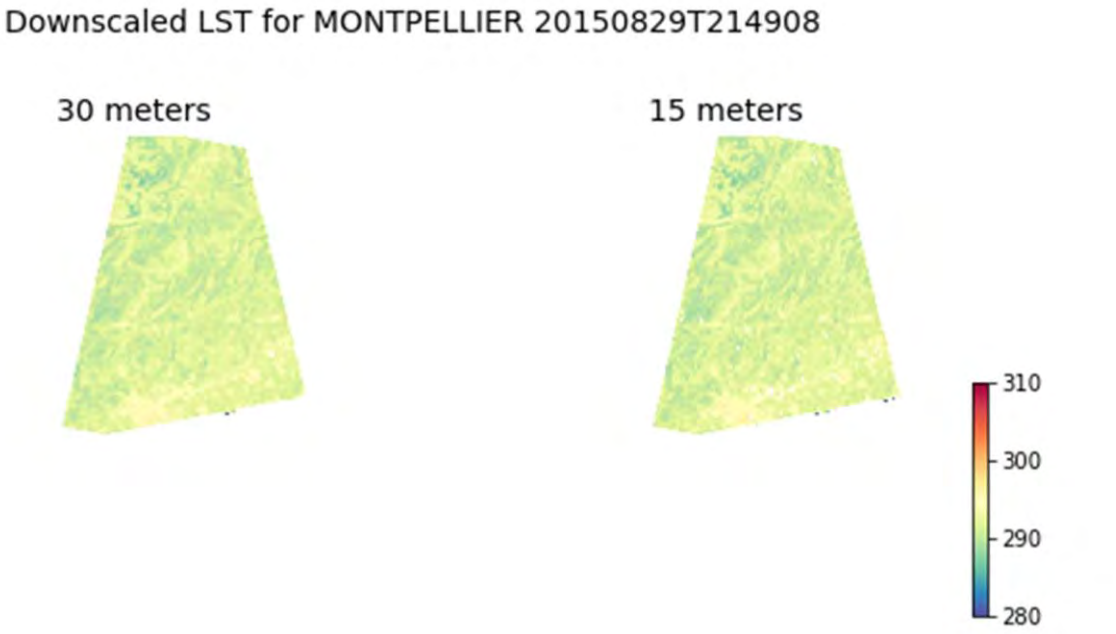
Downscaled LST for MONTPELLIER 20150829T214908
30 meters
15 meters
310
300
290
280

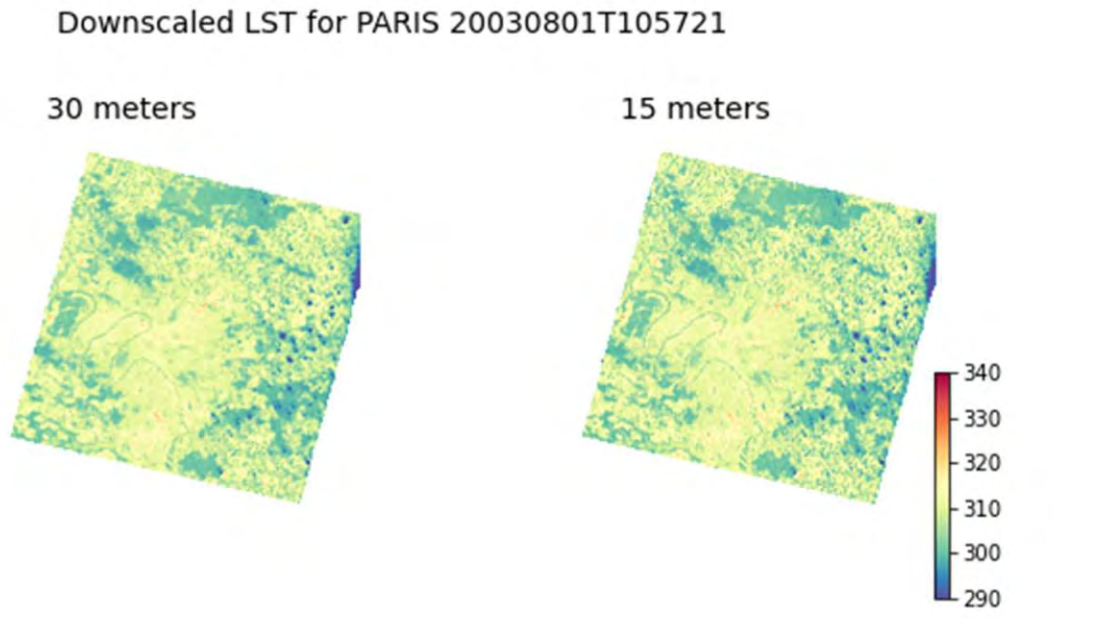
Downscaled LST for PARIS 20030801T105721
30 meters
15 meters
340
330
320
310
300
290

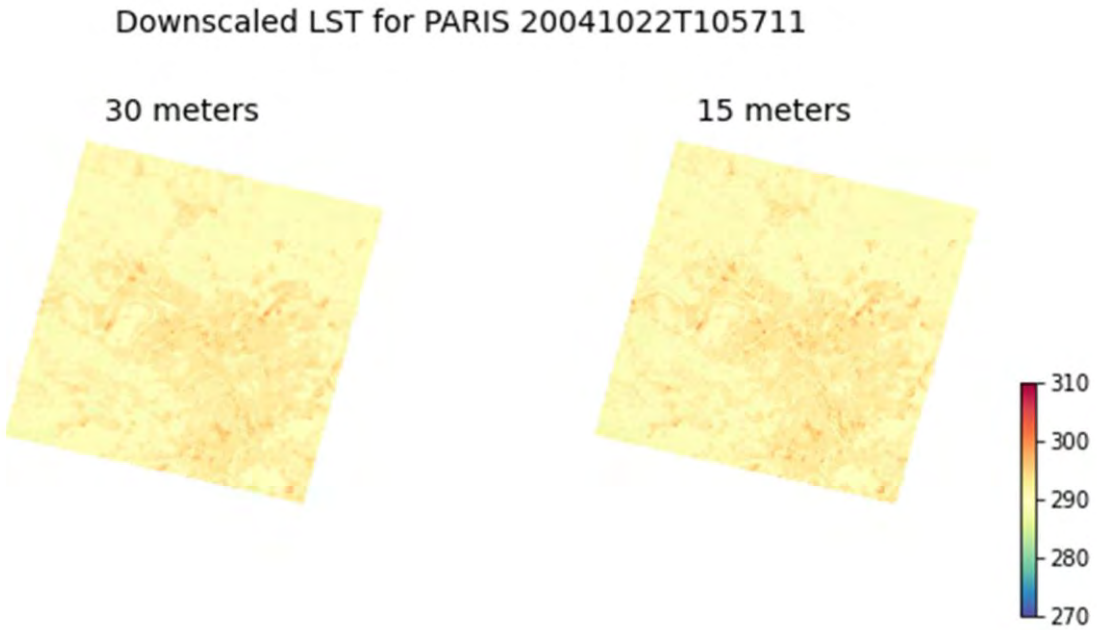
Downscaled LST for PARIS 20041022T105711
30 meters
15 meters
310
300
290
280
270

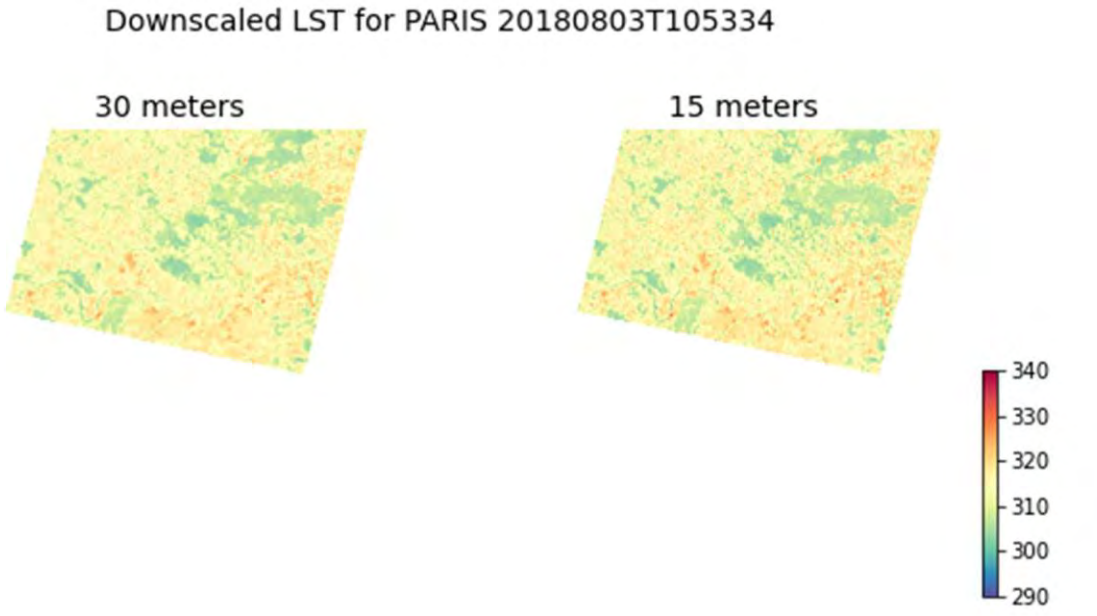
Downscaled LST for PARIS 20180803T105334
30 meters
15 meters
340
330
320
310
300
290

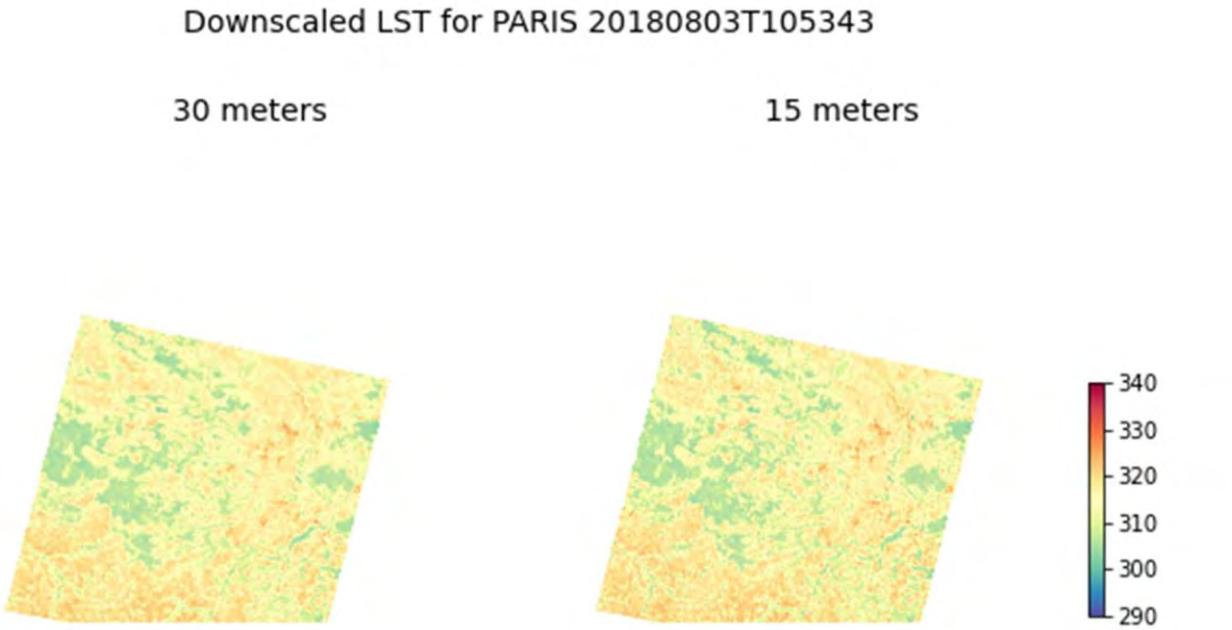
Downscaled LST for PARIS 20180803T105343
30 meters
15 meters
340
330
320
310
300
290

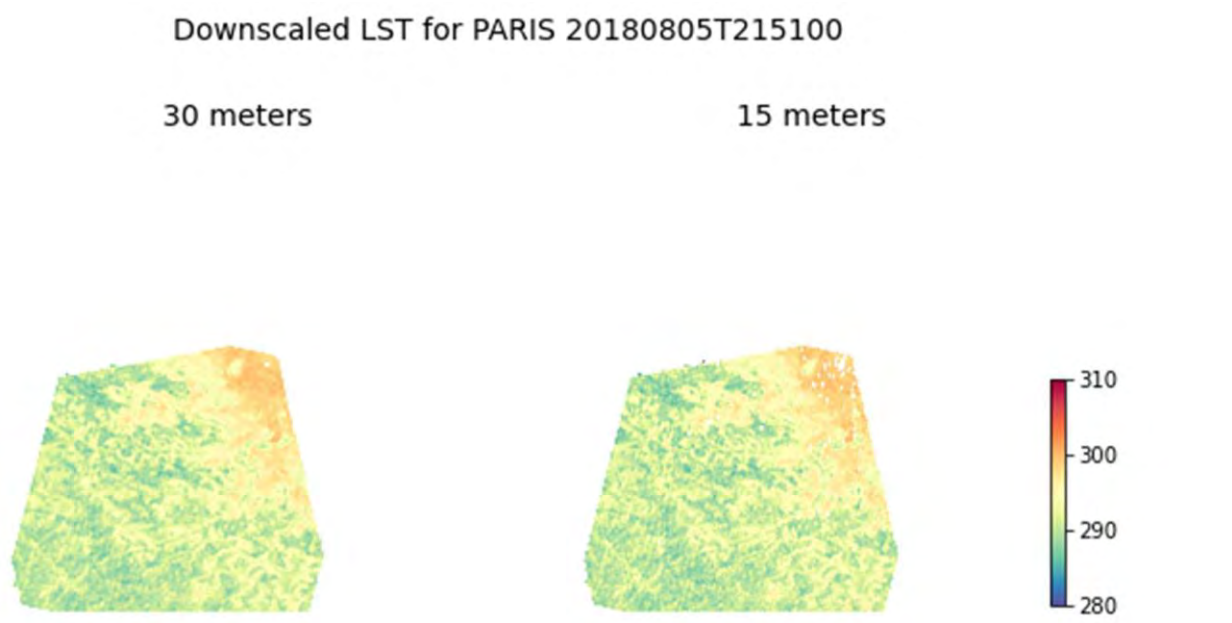
Downscaled LST for PARIS 20180805T215100
30 meters
15 meters
310
300
290
280

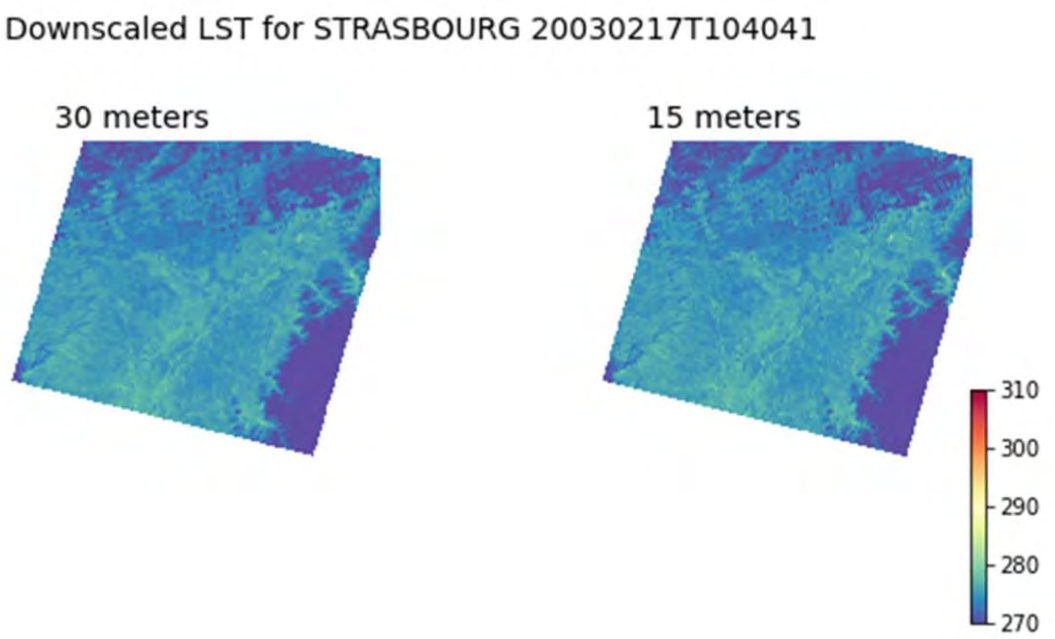
Downscaled LST for STRASBOURG 20030217T104041
30 meters
15 meters
310
300
290
280
270

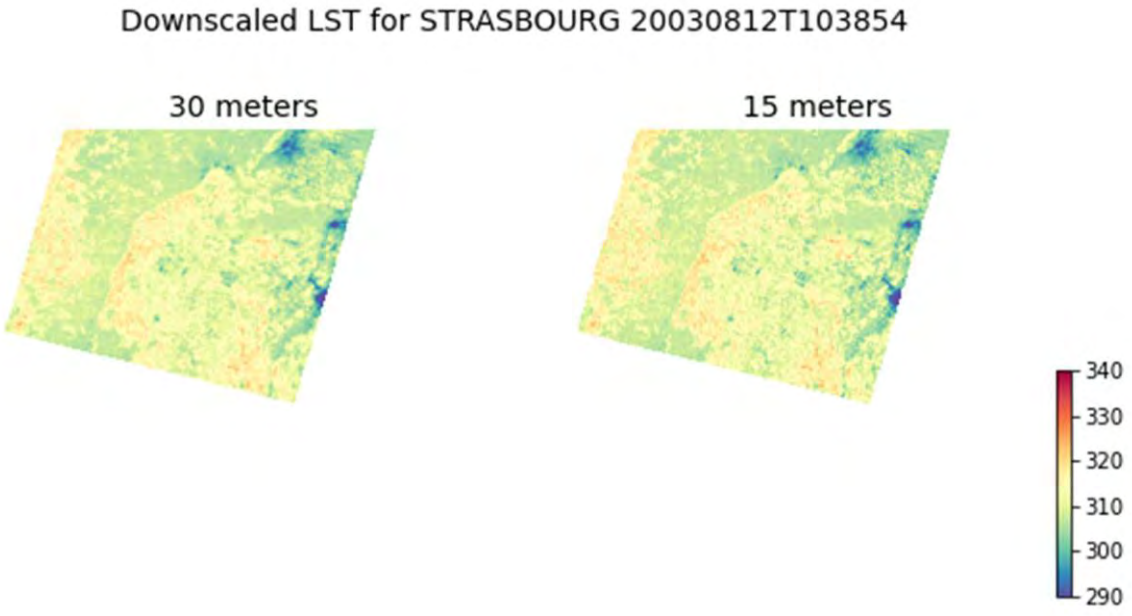
Downscaled LST for STRASBOURG 20030812T103854
30 meters
15 meters
340
330
320
310
300
290

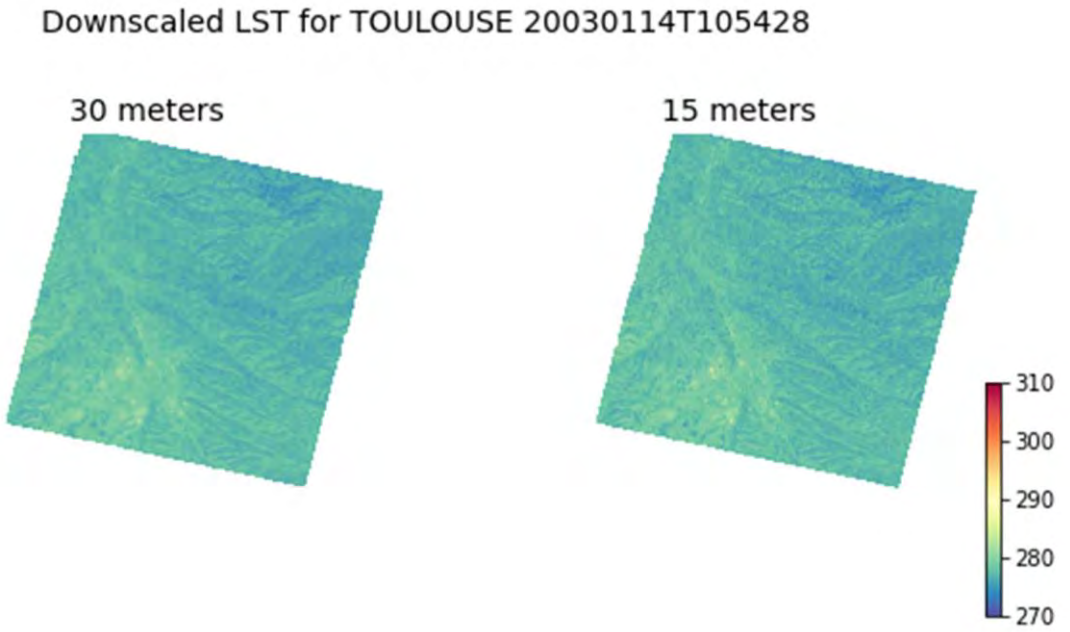
Downscaled LST for TOULOUSE 20030114T105428
30 meters
15 meters
310
300
290
280
270

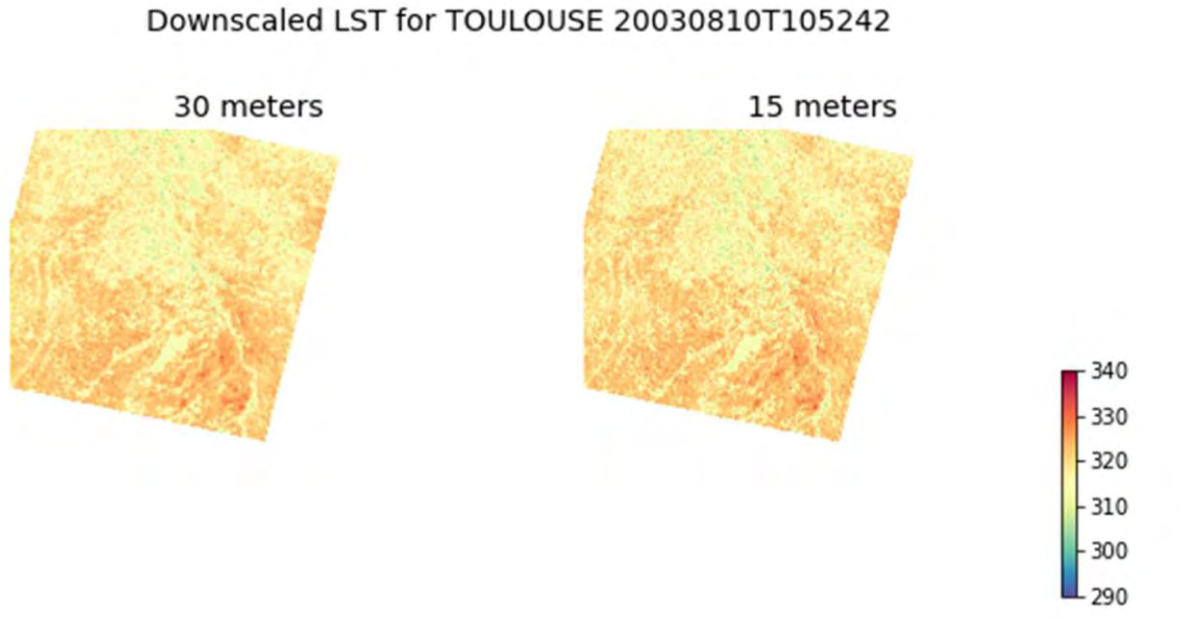
Downscaled LST for TOULOUSE 20030810T105242
30 meters
15 meters
340
330
320
310
300
290

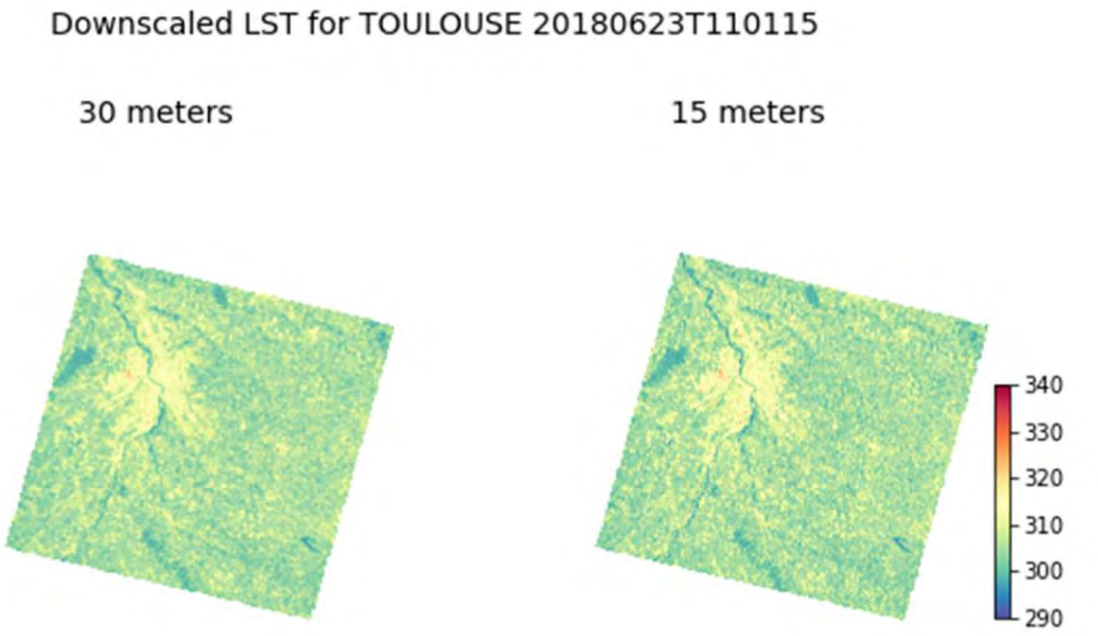
Downscaled LST for TOULOUSE 20180623T110115
30 meters
15 meters
340
330
320
310
300
290

7.3. Appendix C: Comparison of ECOSTRESS LST maps at 70 m with the NASA standard products

Difference maps could not be computed for all the dates due to geometric correction issues with the ECOSTRESS data (refer to [4] for more information).

When available, the difference map is computed as LST NASA - LST THERMOCITY. The scatterplot on the bottom right is surrounded by histograms showing the distribution of each product and provides three metrics:

- Pearson linear correlation coefficient (R^2),
- Percentage of pixel below 250 K for each product (extreme values outside of the scatterplot range),
- Percentage of pixel above 360 K for each product (extreme values outside of the scatterplot range).

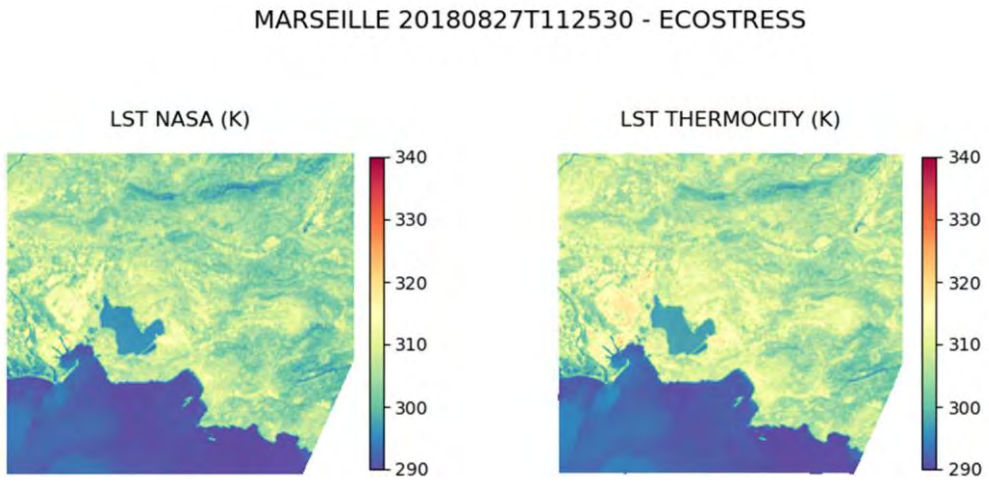

No difference map available for this date.

The retrieved temperatures are coherent between the two products. Globally higher temperatures are observed in the THERMOCITY map, as confirmed by the statistics in Table 18 with +1.61 K in average. These higher temperatures are mainly located on build-up areas and bare ground.

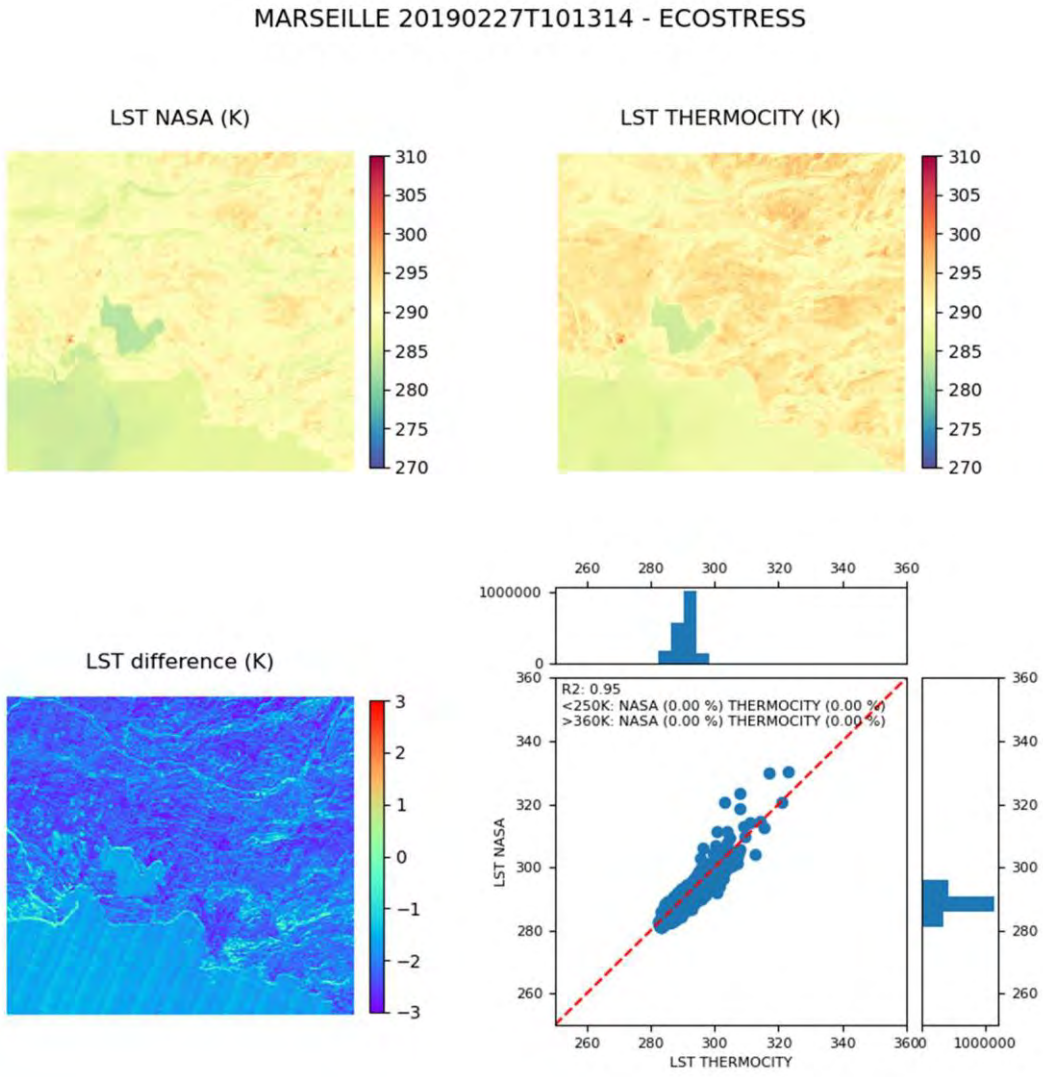

The retrieved temperatures are coherent between the two products. Globally higher temperatures are observed in the THERMOCITY map, as confirmed by the statistics in Table 18 with +1.97 K in average. These higher temperatures are mainly located on build-up areas and bare ground.

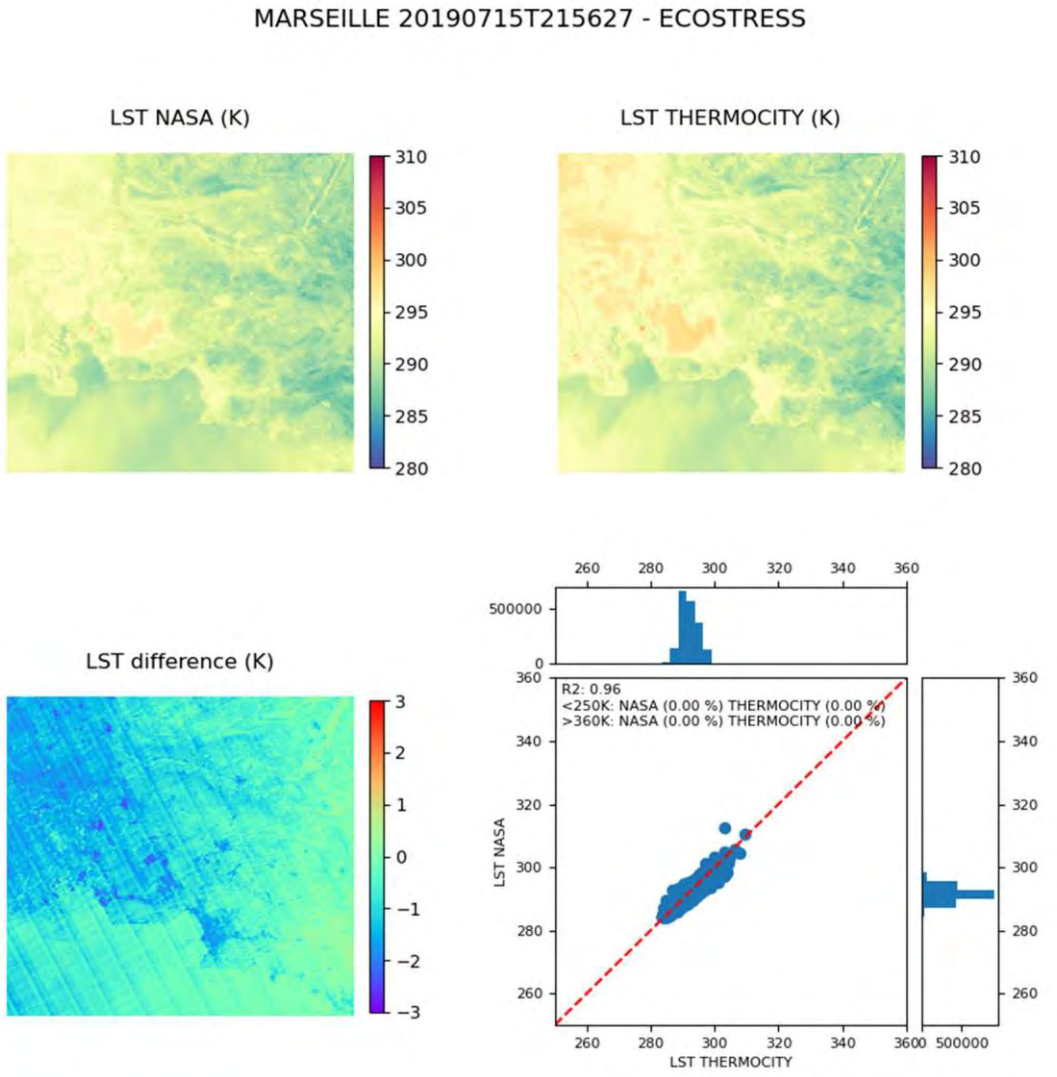

The retrieved temperatures are coherent between the two products. The average temperature difference is low for this date (0.76 K, see Table 18). Higher temperatures are observed in the THERMOCITY map, mostly on build-up areas. The difference map also highlights radiometric issues in the ECOSTRESS data.

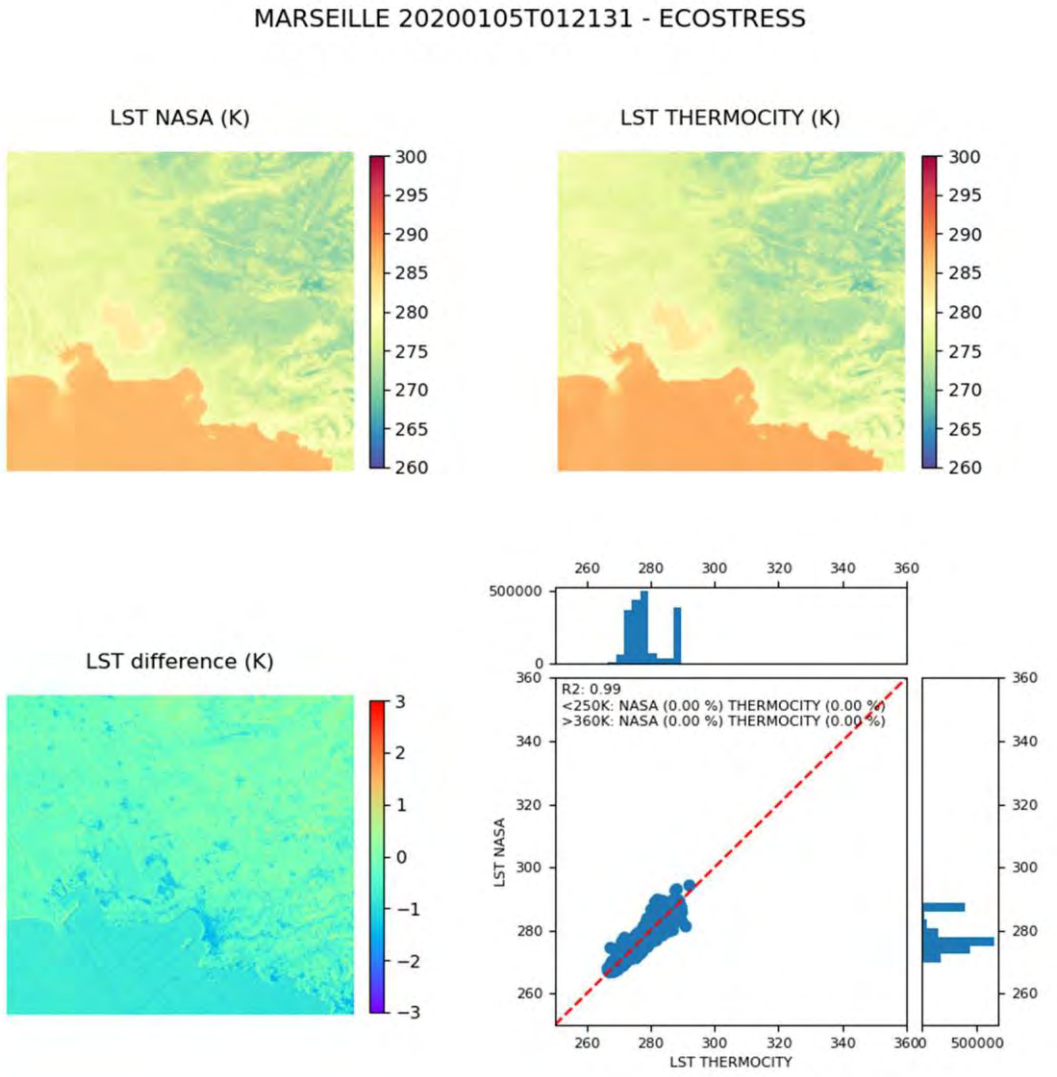

The retrieved temperatures are coherent between the two products. The average temperature difference is low for this date (0.39 K, see Table 18). Higher temperatures are observed in the THERMOCITY map only over the build-up areas.

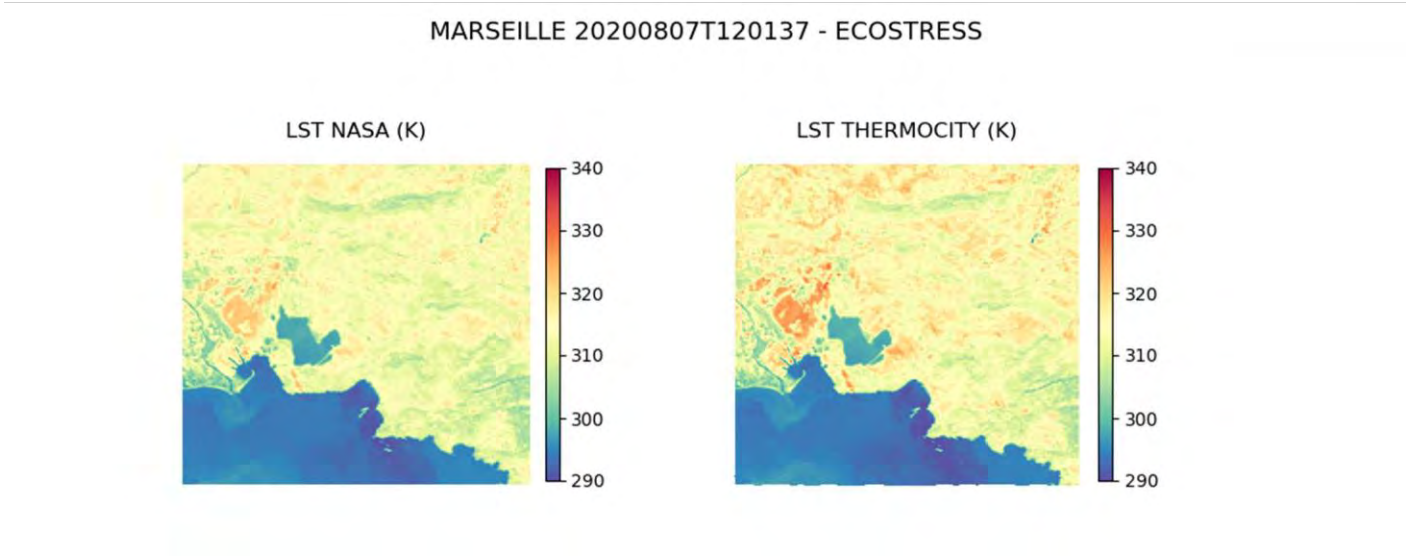

No difference map available for this date.

The retrieved temperatures are coherent between the two products. Globally higher temperatures are observed in the THERMOCITY map, as confirmed by the statistics in Table 18 with +1.22 K in average. These higher temperatures are mainly located on build-up areas and bare ground.

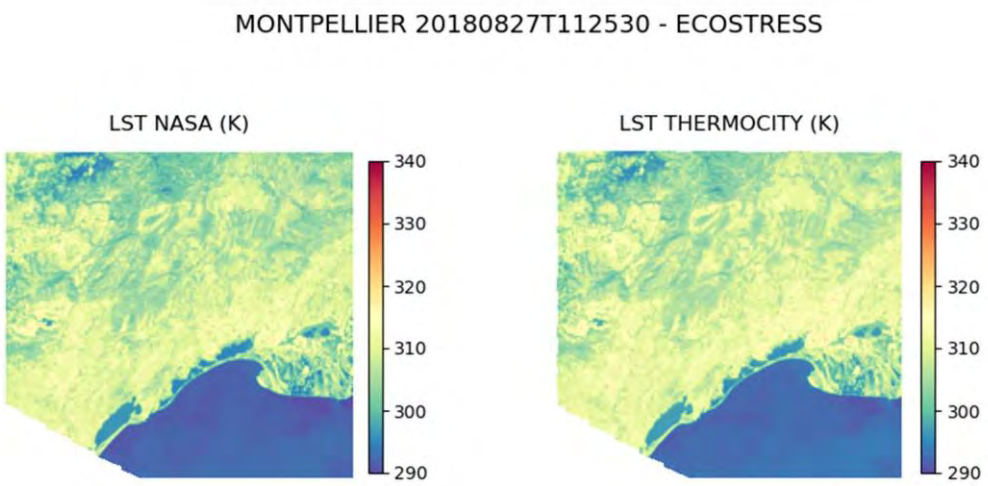

No difference map available for this date.

The retrieved temperatures are coherent between the two products. The average temperature difference is low for this date (0.88 K, see Table 18).

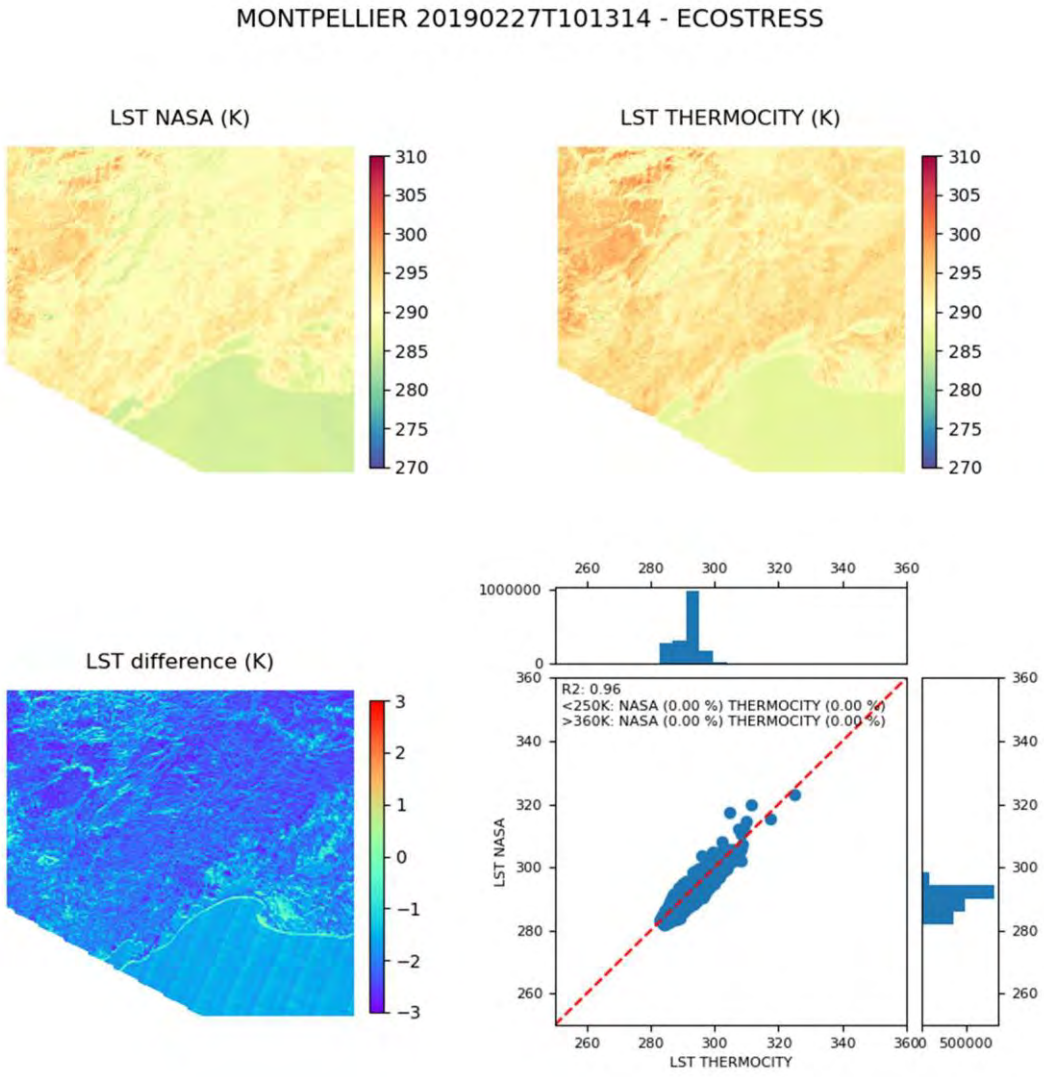

The retrieved temperatures are coherent between the two products. Globally higher temperatures are observed in the THERMOCITY map, as confirmed by the statistics in Table 18 with +1.92 K in average.

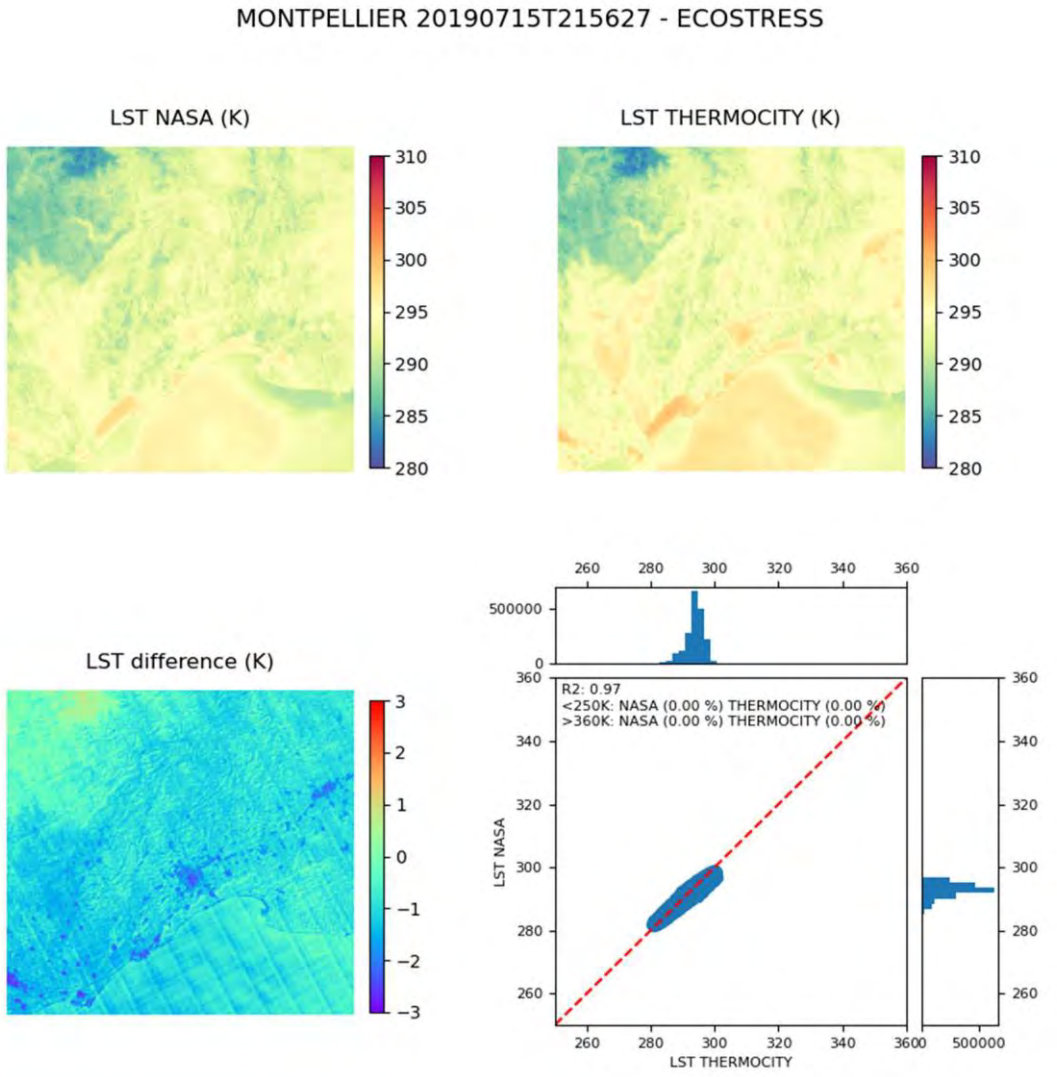

The retrieved temperatures are coherent between the two products. The average temperature of the THERMOCITY map is a bit higher, 0.93 K (see Table 18) than in the NASA product. Those higher temperatures are observed mostly on build-up areas. The difference map also highlight radiometric issues in the ECOSTRESS data.

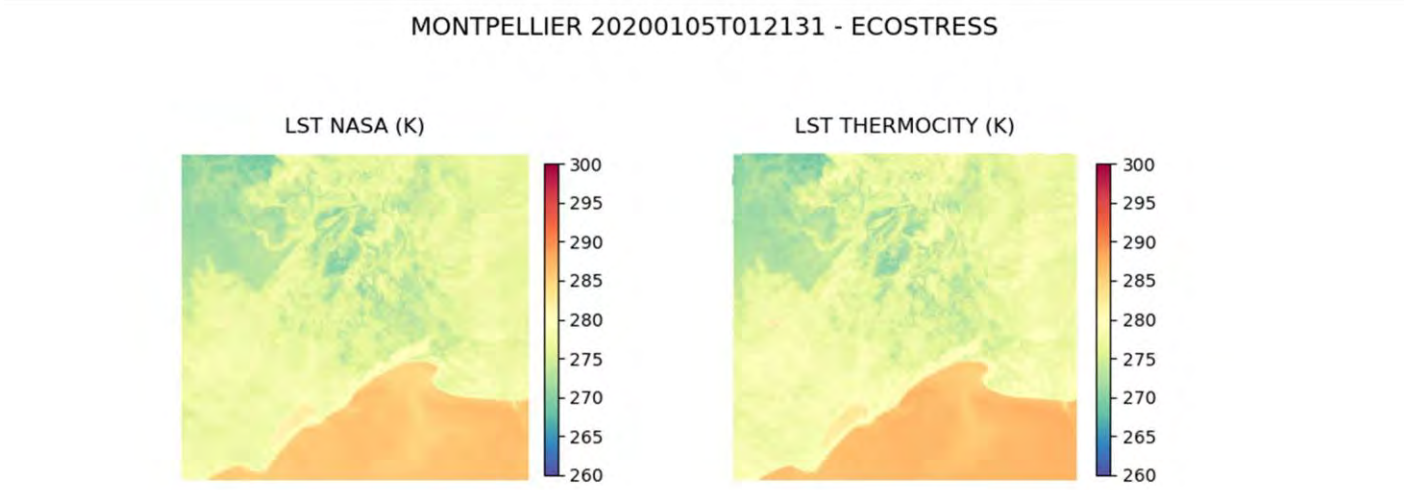

No difference map available for this date.

The retrieved temperatures are coherent between the two products. The average temperature difference is low for this date (0.56 K, see Table 18).

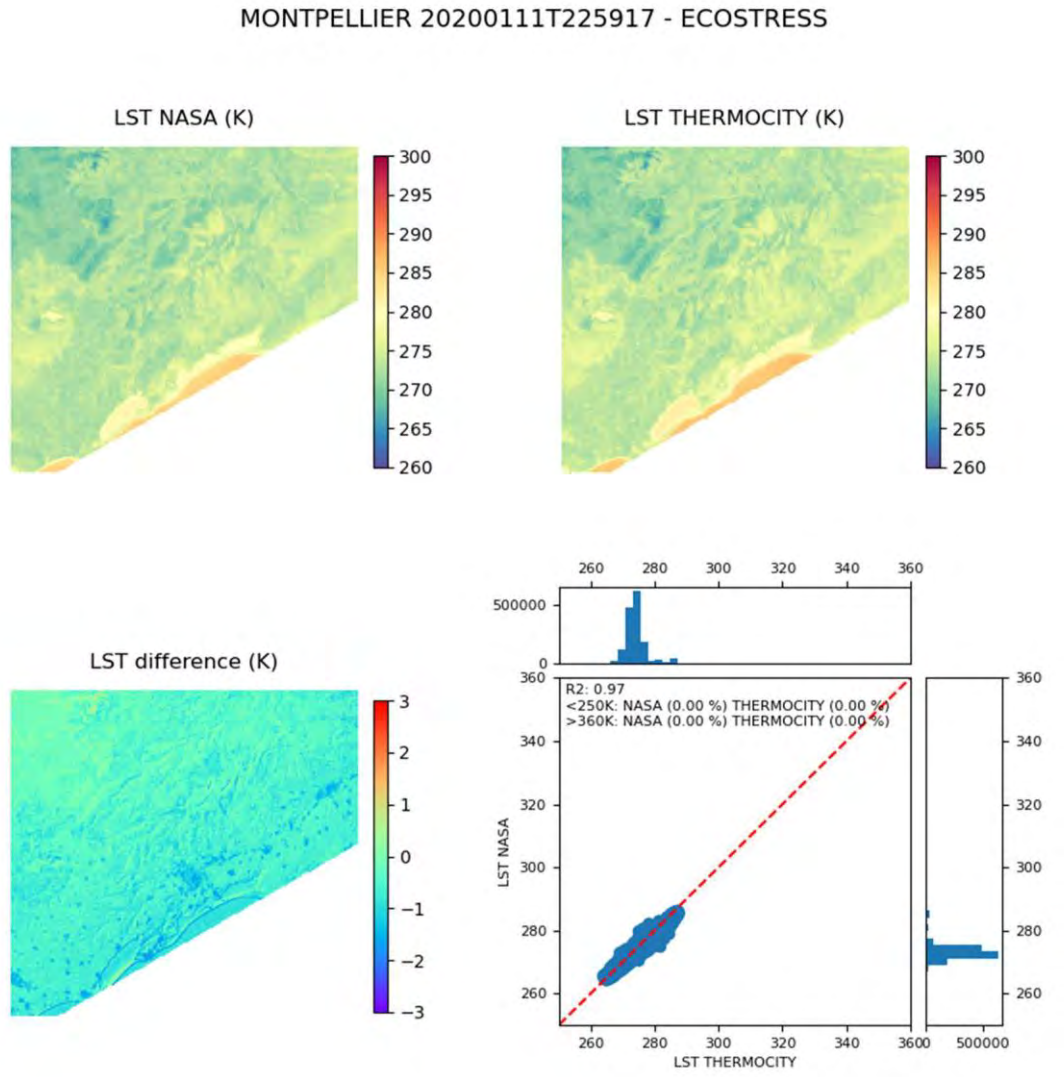

The retrieved temperatures are coherent between the two products. The average temperature difference is low for this date (0.56 K, see Table 18). Higher temperatures are observed in the THERMOCITY map only over the build-up areas.

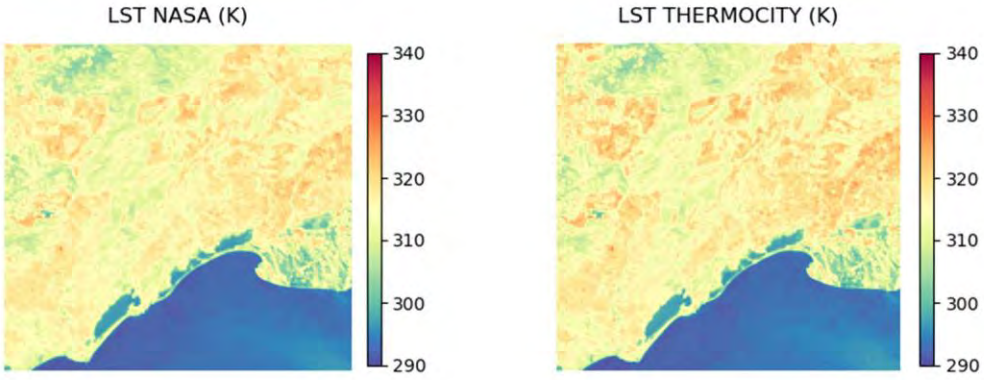

No difference map available for this date.

The retrieved temperatures are coherent between the two products. The average temperature difference is low for this date (0.54 K, see Table 18).

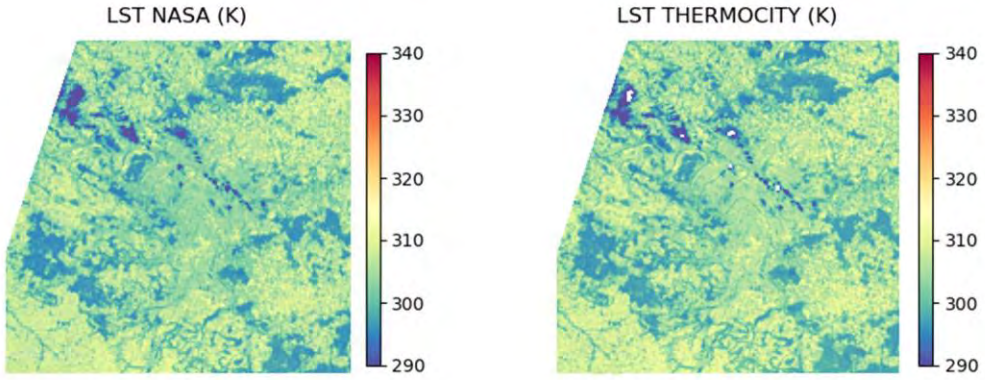

No difference map available for this date.

The retrieved temperatures are coherent between the two products. We can notice the presence of some clouds, crossing the image from the North-West to the South-East. The average temperature difference is low for this date (0.4 K, see Table 18).

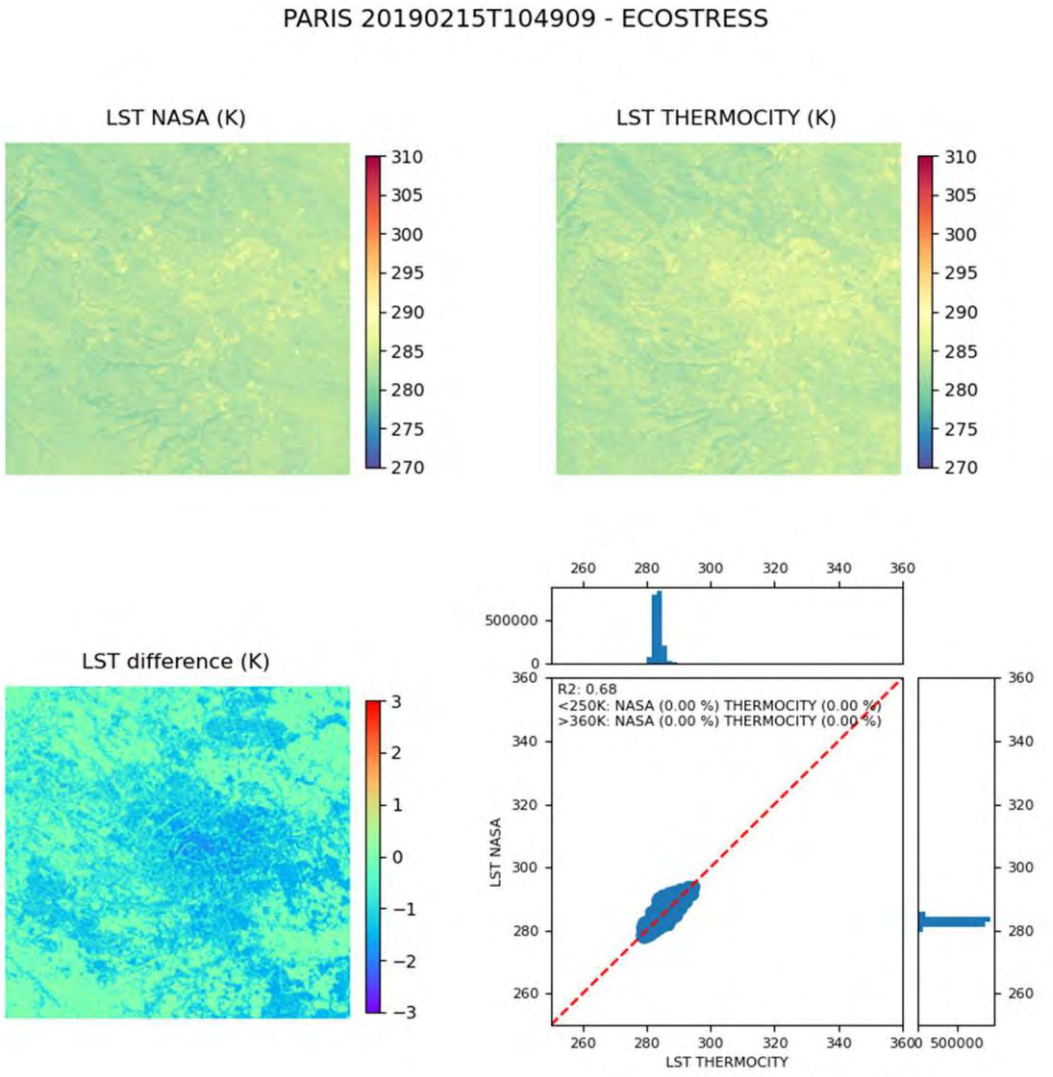

The retrieved temperatures are coherent between the two products. The R^2 value is a bit weak but the low temperature dynamic range observed on this date explains this. The average temperature difference is low for this date (0.67 K, see Table 18). These differences can be observed with higher temperatures in the THERMOCITY map over the build-up and forested areas.

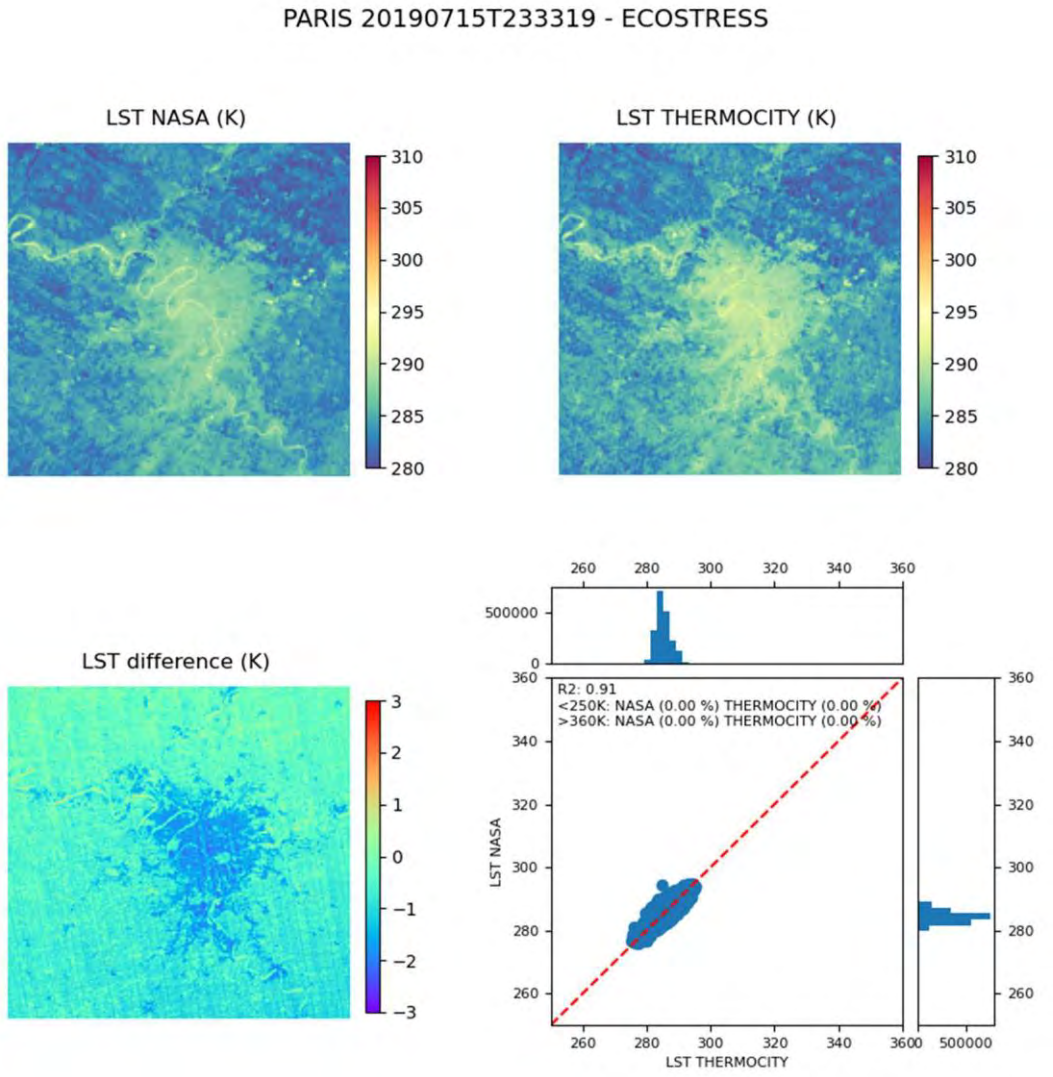

The retrieved temperatures are coherent between the two products. The average temperature difference is low for this date (0.68 K, see Table 18). Higher temperatures are observed in the THERMOCITY map only over the build-up areas.

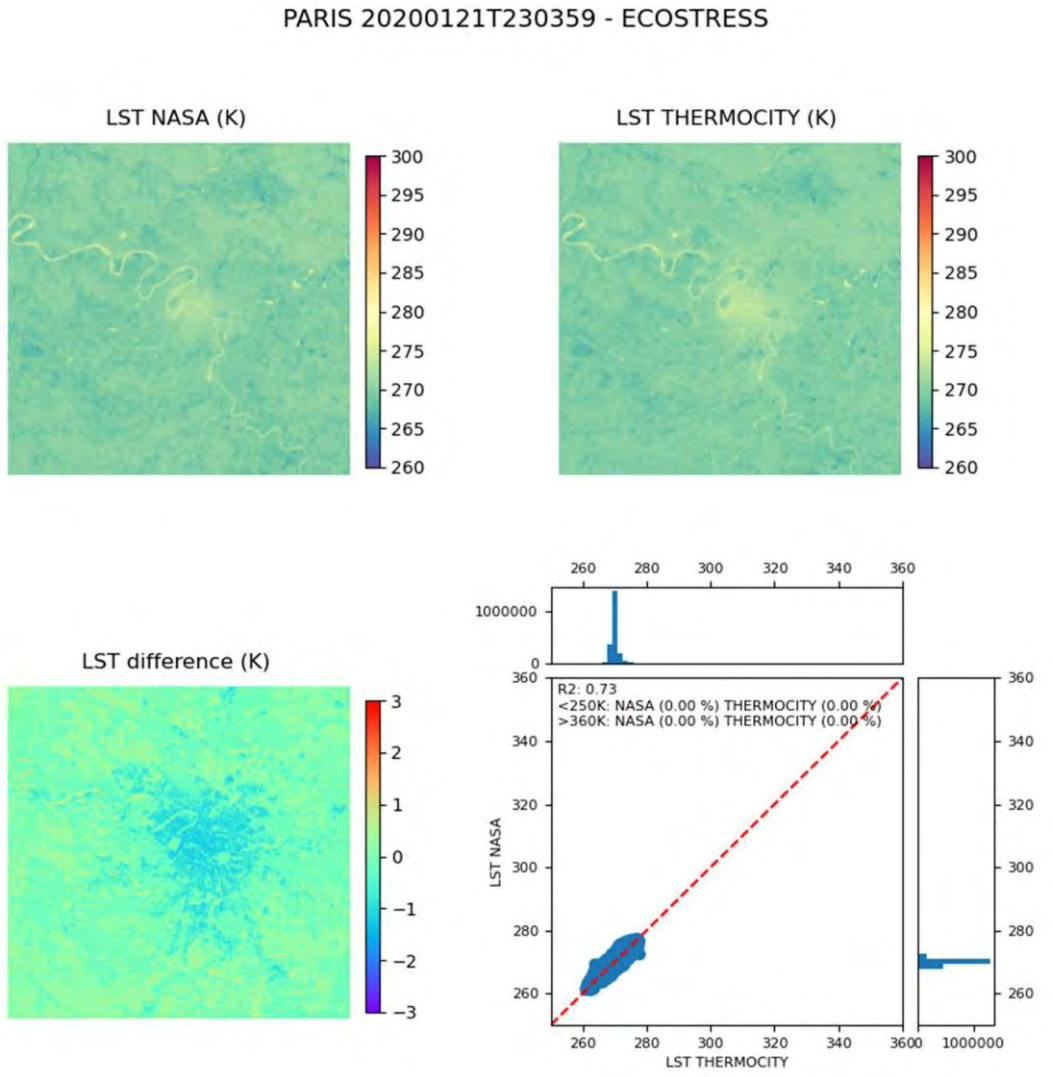

The retrieved temperatures are coherent between the two products. The R^2 value is a bit weak but the low temperature dynamic range observed on this date explains this. There is almost no average temperature difference between the two products (0.09 K, see Table 18). However, the difference map highlights slightly higher temperatures over build-up areas and lower temperatures over agricultural lands in the THERMOCITY map.

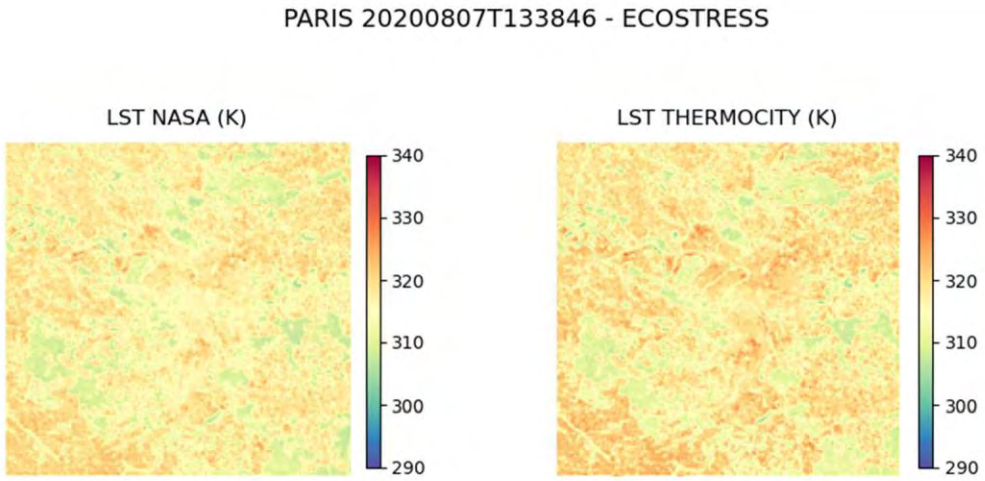

No difference map available for this date.

The retrieved temperatures are coherent between the two products. The average temperature of the THERMOCITY map is 0.97 K higher than in the NASA product (see Table 18). Those higher temperatures are observed mostly on build-up areas.

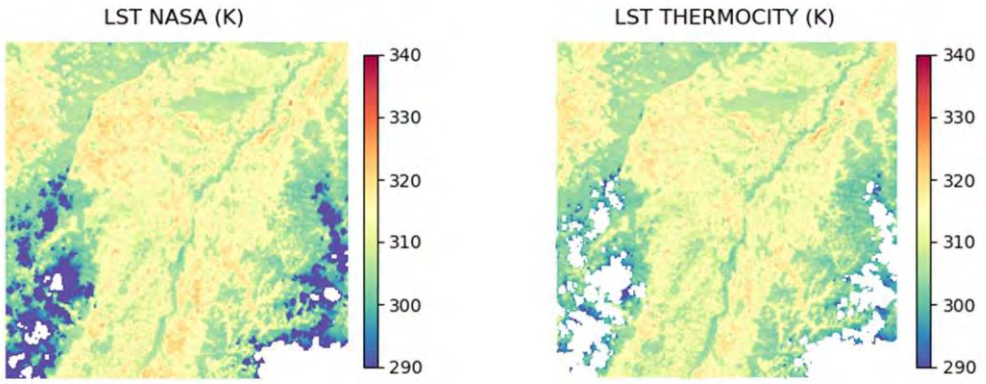

No difference map available for this date.

The retrieved temperatures are coherent between the two products. The average temperature of the THERMOCITY map is 0.93 K lower than in the NASA product (see Table 18). This value is impacted by the large presence of cloud on the bottom left and right sides of the image.

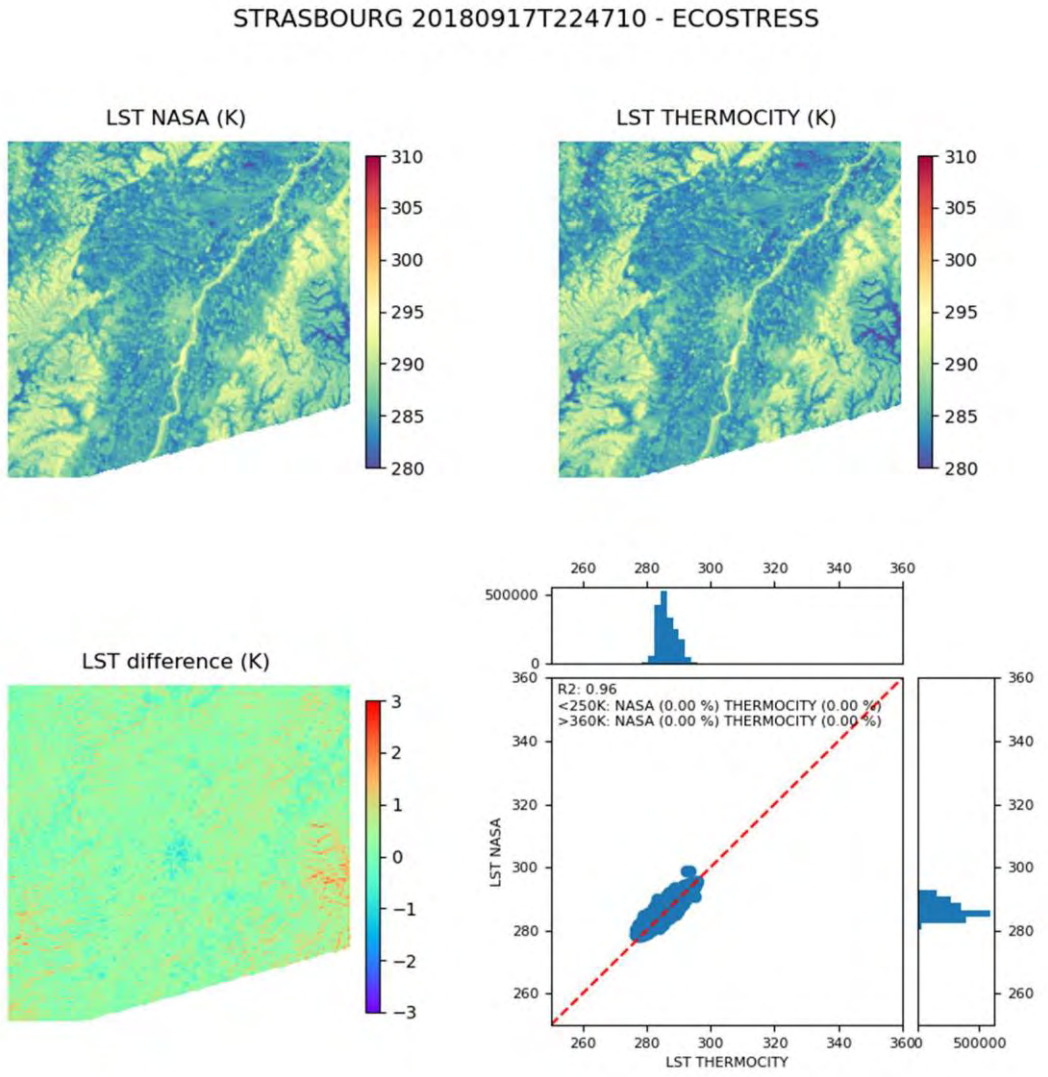

The retrieved temperatures are coherent between the two products. The average temperature difference is low for this date (0.31 K, see Table 18). However, the difference map highlights slightly higher temperatures over build-up areas in the THERMOCITY map and an impact of the topography in the mountainous areas.

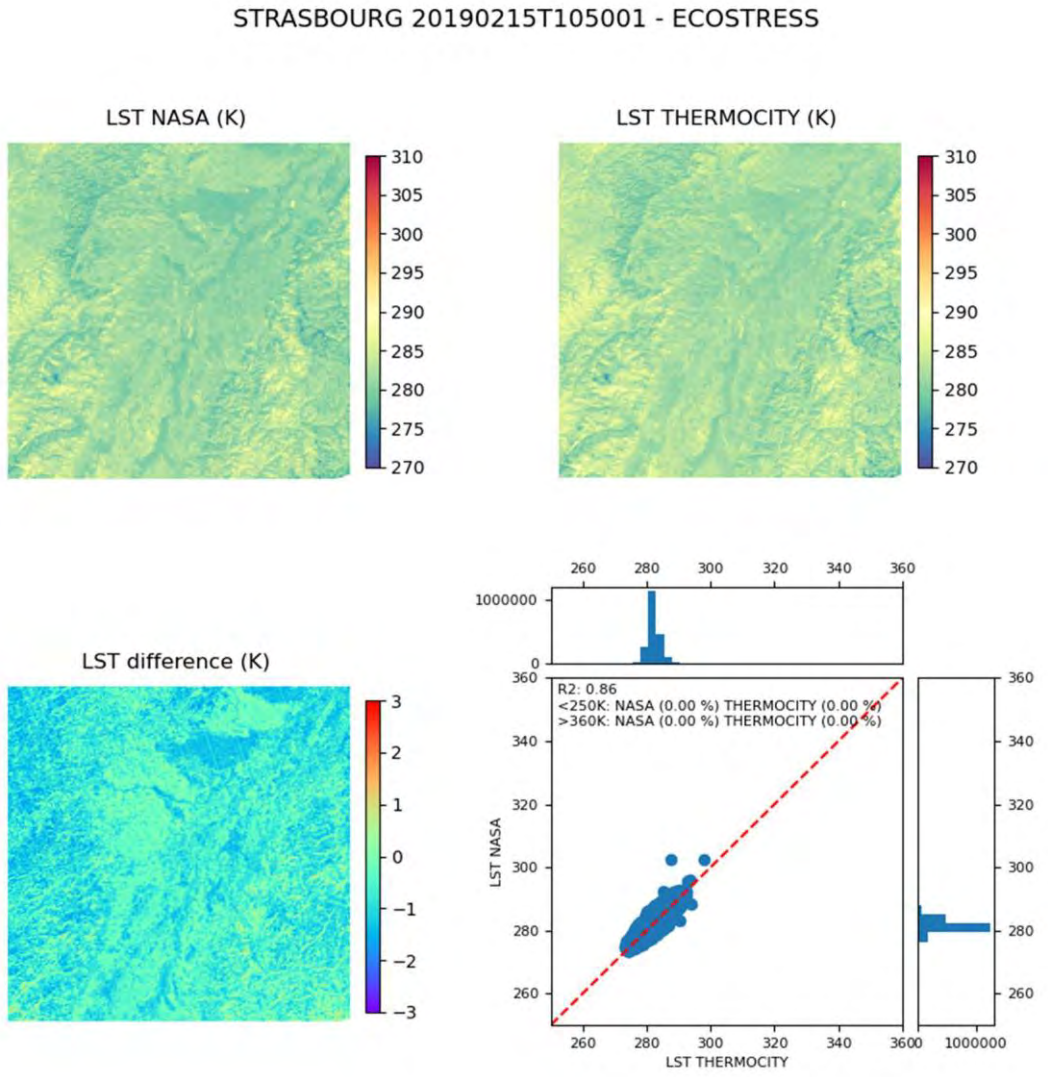

The retrieved temperatures are coherent between the two products. The average temperature difference is low for this date (0.71 K, see Table 18), with temperature differences mainly located over forested areas where there is higher values in the THERMOCITY map.

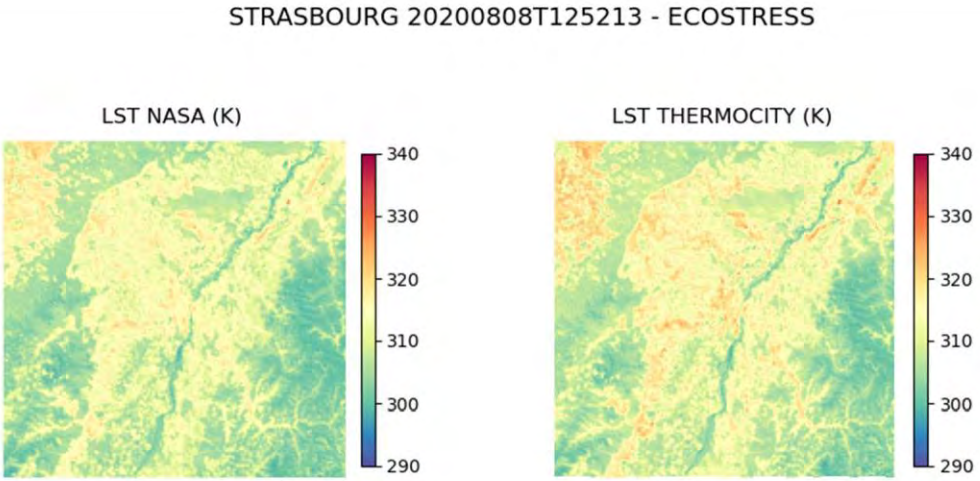

No difference map available for this date.

The retrieved temperatures are coherent between the two products. The average temperature of the THERMOCITY map is 1.35 K higher than in the NASA product (see Table 18), with temperature differences observed mainly on the build-up and agricultural areas.

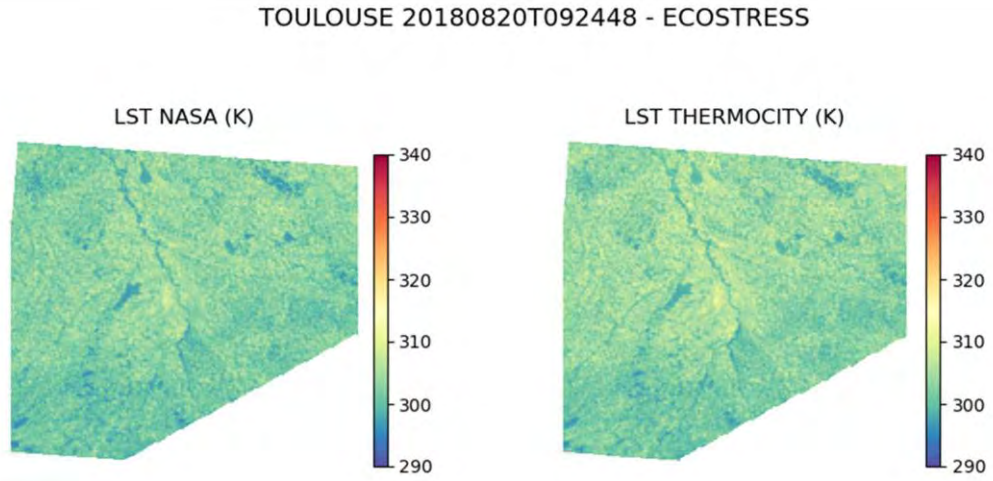

No difference map available for this date.

The retrieved temperatures are coherent between the two products. The average temperature of the THERMOCITY map is 0.88 K higher than in the NASA product (see Table 18), with temperature differences which seems mainly located over build-up areas.

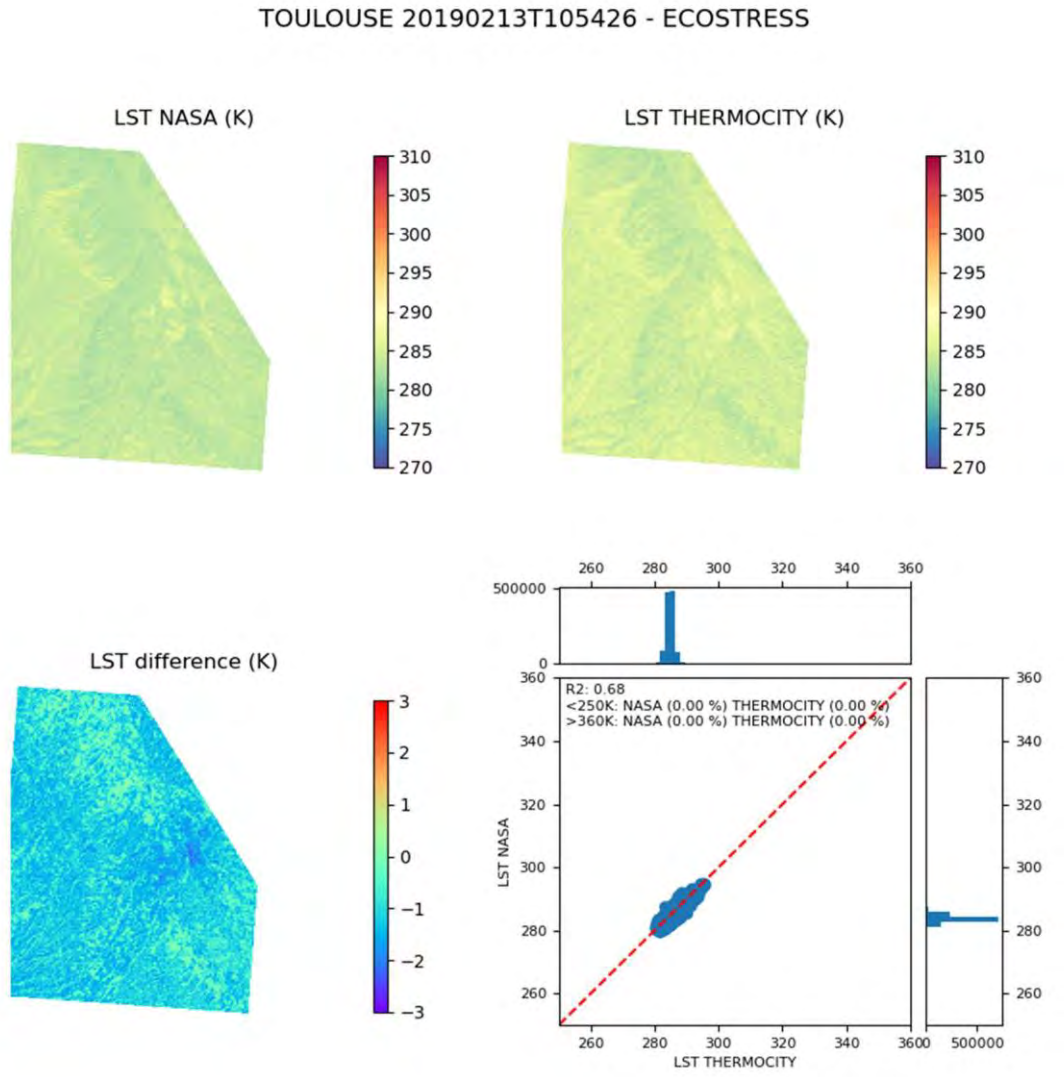

The retrieved temperatures are coherent between the two products. The R^2 value is a bit weak but the low temperature dynamic range observed on this date explains this. The average temperature of the THERMOCITY map is 1.08 K higher than in the NASA product (see Table 18), with temperature differences mostly located over build-up areas.

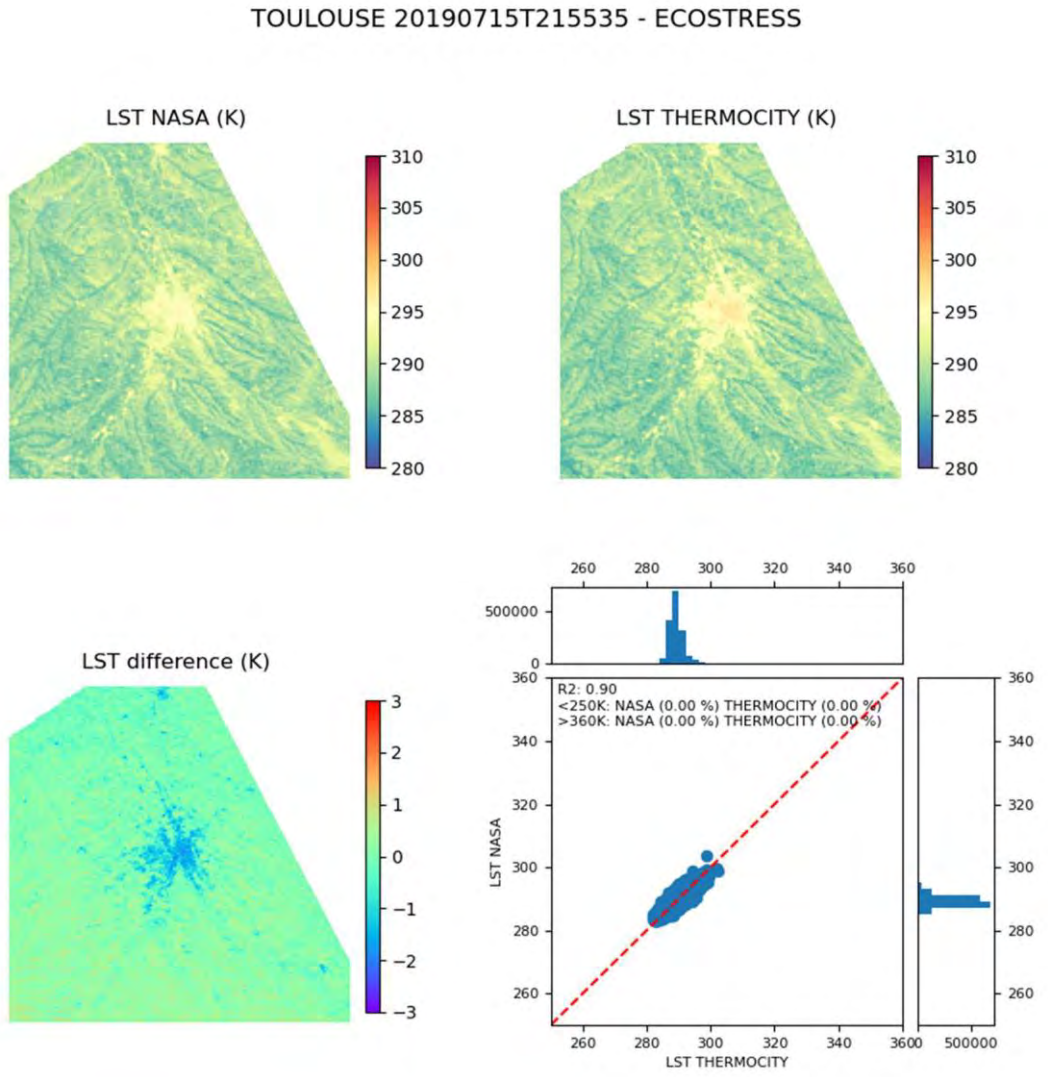

The retrieved temperatures are coherent between the two products. There is almost no average temperature difference between the two products (0.04 K, see Table 18). However, the difference map highlights significantly higher temperatures over build-up areas in the THERMOCITY map as well as a slight impact of the topography.

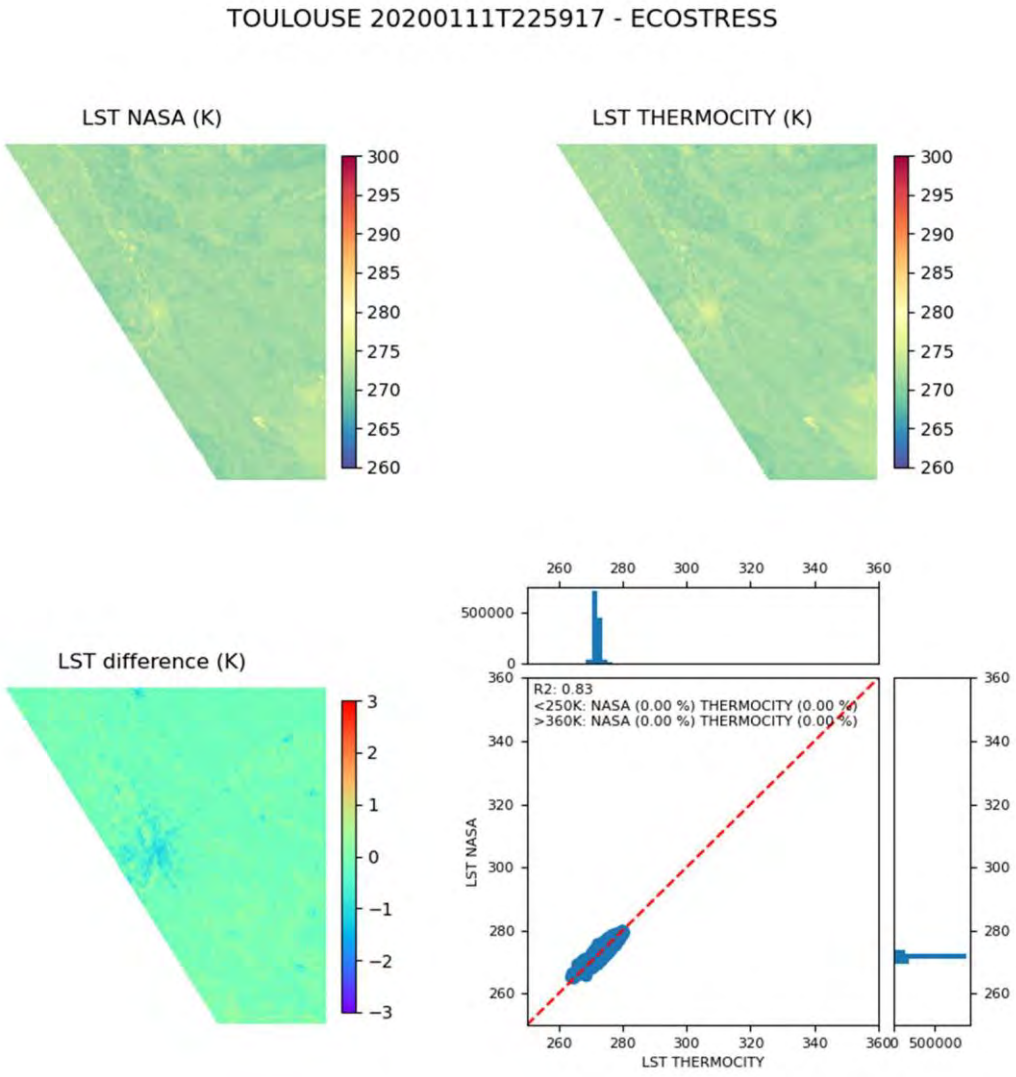

The retrieved temperatures are coherent between the two products. There is almost no average temperature difference between the two products (0.11 K, see Table 18). However, the difference map highlights higher temperatures over build-up areas in the THERMOCITY map.

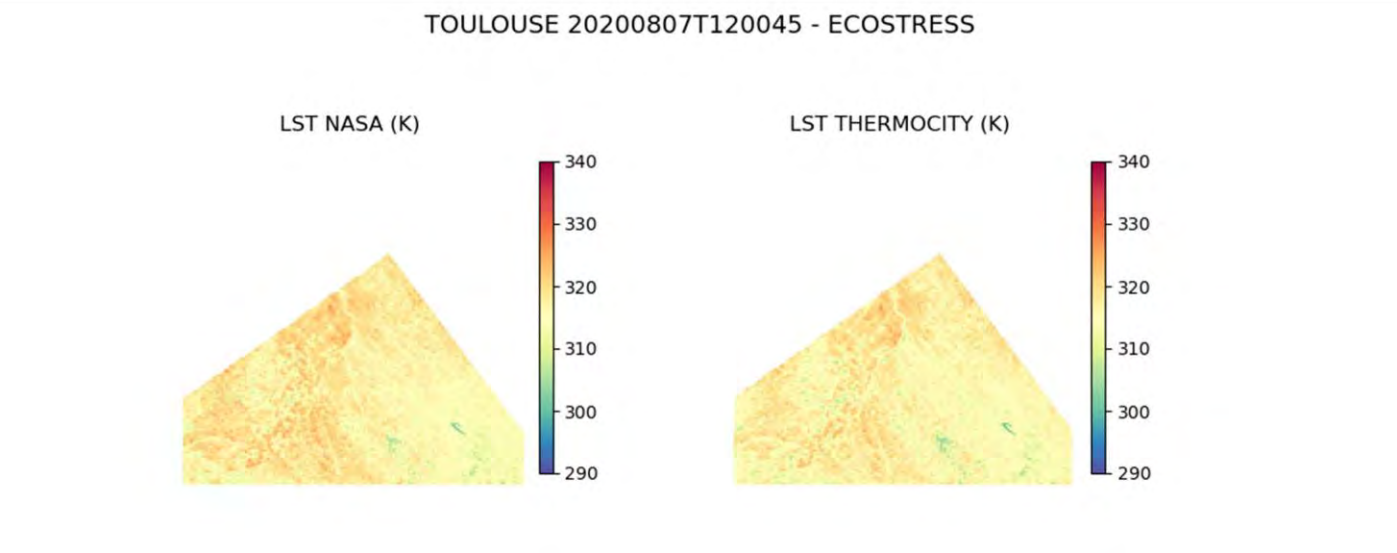

No difference map available for this date.

The retrieved temperatures are coherent between the two products. The average temperature of the THERMOCITY map is 0.86 K lower than in the NASA product (see Table 18).